RADIO RESOURCE AND INTERFERENCE MANAGEMENT IN UPLINK MU-MIMO SYSTEMS WITH ZF POST-PROCESSING

by

Aasem N. Alyahya

Submitted in partial fulfillment of the
requirements for the degree of Doctor of Philosophy

at

Dalhousie University
Halifax, Nova Scotia
August 2016

To My Parents & Family

Table of Contents

List of Figures

Abstract

This dissertation investigates cross-layer designs in spatial division multiplexing (SDM) for multiuser multiple-input multiple-output (MU-MIMO) transmissions on the uplink. The MU systems which allow simultaneous transmissions on the downlink offer various improvements, such as an increase in total system throughput, and have already been standardized in IEEE 802.11ac wireless local area networks (WLANs) and cellular networks. However, the implementation of MU-MIMO SDM on the uplink is still considered to be an open problem. The challenges include radio resource management and low complexity decoding designs. Motivated by these considerations, this dissertation presents four main contributions.

First, this research focuses on the physical layer MU-MIMO issues by proposing an uplink approach that employs a design with low complexity, while maintaining an acceptable sum rate performance. This is done by utilizing zero forcing (ZF) cancellation, and by assuming that channel state information (CSI) is required only at the base station (BS). In addition, spatial coordination is applied to improve the total system performance by giving medium access to a limited number of transmitters.

Secondly, two resource management algorithms are developed with the objective of maximizing the total system sum rate by considering the impact of multiple access noise enhancement on the spatial stream capacity. An additional scheme is then proposed to maximize the weighted sum capacity of all admitted users, where the weights are chosen based on the state of user buffers. The proposed resource allocation and scheduling algorithms operate in a reduced search space for sub-optimum configurations targeting lower overall complexity.

Thirdly, two-layer decoding is proposed in a multi-cell environment for MU-MIMO systems. The first layer of decoding handles multiple access interference (MAI) by applying the ZF approach, where this process is executed at the BS level. The second layer utilizes a diversity combining technique on a selected number of mobile stations (MS), with the aim of reducing inter-cell interference (ICI).

Finally, an interference-aware joint scheduling algorithm is presented for the multi-cell MU-MIMO system. This algorithm focuses on selecting users/antennas, and utilizes power allocation to improve the total system performance. Spatial coordination is executed in a distributive manner with full independence from the power allocation, in order to reduce the search time. Moreover, Newton's method of optimization is included to find the optimum power level for all transmitting users.

This dissertation advances MU-MIMO system designs for the uplink by contributing to the development of interference and radio resource management algorithms. The motivation of this work is to propose a low complexity design that reduces the level of interference while providing good overall system performance as measured by the total sum rate. The results presented in this work are applicable to wireless networks such as WLANs that can operate with a single autonomous access point (AP) as well as coordinated APs that are managed by centralized controllers.

List of Abbreviations and Symbols Used

The following abbreviations and acronyms are used in this dissertation.

AWGN	additive white Gaussian noise
BER	bit error rate
BPSK	binary phase shift keying
BS	base station
CoMP	coordinated multi point
CR	cooperative reception
CSI	channel state information
CSIT	channel state information at the transmitter
EGC	equal gain combining
ICI	inter-cell interference
ISI	inter-symbol interference
MAC	medium access control
MAI	multiple access interference
MIMO	multiple-input multiple-output
MLD	maximum likelihood decoding
MMSE	minimum mean square error
MRC	maximum ratio combining
MS	mobile station
MU	multiuser
OFDM	orthogonal frequency division multiplexing
PSD	power spectral density
RRM	radio resource management
RSSI	received signal strength indicator

SIC	successive interference canceler
SIMO	single-input multiple-output
SISO	single-input single-output
SNIR	signal-to-interference-to-noise ratio
SNR	signal-to-noise ratio
SU	single user
SVD	singular value decomposition
WC	wireless controller
WLAN	wireless local area networks
ZF	zero forcing

The following symbols are used in this dissertation. Vector scalar variables are denoted by lower-case letters, and matrices by bold-face letters.

K	number of active MSs
k	index of active MSs
$\ddot{K}$	number of available MSs
$\bar{k}$	index of MSs causing intra-cell interference
$\hat{k}$	index of MSs causing ICI
B	number of BSs
R	number of receiving antennas at the BS
M_k	number of active antenna(s) that are enabled for MS k
$\ddot{M}_k$	number of available antenna(s) for MS k
Ω_b	a data set that holds all active users that are associated with BS b
$\mathbf{s}_k$	the symbols sent from MS k
$\mathbf{y}$	received signal at the BS
$\mathbf{H}_k$	the flat fading channel between MS k and the BS
$\mathbf{h}_{km}$	the channel conditions between the mth antenna of MS k and the BS
λ	diversity spatial gain
D_{bk}	the macro-scale signal attenuation between MS k and BS b

d_{bk}	the distance between MS k and BS b
α	the signal wave propagation factor
Ψ_b	the ICI and AWGN affecting signals received by BS b
$\mathbf{T}_k$	ZF decoding matrix for MS k
w_{bi}	MRC coefficient
$\mathbb{I}$	the identity matrix
$(^{\mathcal{H}})$	the Hermitian transpose operator
$(^*)$	complex conjugate operator
null	the kernel function
Inv	the pseudo-inverse function
$\binom{n}{k}$	the binomial coefficient
γ_{kj}	the SNR on the jth stream for user k
$\hat{\gamma}_k$	the SNR cut of value for user k
$\overrightarrow{p}_k$	the power allocation vector for MS k
L_k	MS k current buffer size
ν	average arrival rate
ρ	average dispatch rate

Acknowledgments

I wish to express my sincere gratitude to Professor Jacek Ilow for his guidance and support throughout the duration of my study at Dalhousie University. I admire and appreciate the technical knowledge and personal experiences that he has shared with me.

I would like to acknowledge the major scholarship I received to pursue my PhD degree from the government of Saudi Arabia (SA) represented at King Saud University, Riyadh, SA.

I wish to thank Dr. Octavia A. Dobre for serving on my supervisory committee as the external examiner. I am grateful to Dr. William Phillips, and Dr. Zhizhang Chen for serving on my PhD. supervisory committee.

I wish to extend my thanks to all the members of my research group for their assistance, specifically Fadhel Alhumaidi, Rashed Alsakarnah, Zichao Zhou and Scott Melvin.

Finally, I am very grateful to my family, whose continued love, understanding, and patience made this dissertation possible.

Chapter 1

Introduction

Multiple-input multiple-output (MIMO) technology represents a disruptive paradigm shift in wireless communication systems, enabling high capacity transmissions with the use of multiple-transmit multiple-receive antennas [1, 2]. New developments in this area consider multiuser MIMO (MU-MIMO) operations, to allow simultaneous transmissions between multiple hosts and a base station, where the spatial dimension is utilized to serve many users in parallel [3, 4, 5]. In particular, IEEE 802.11ac wireless local area network (WLAN) standardization and long-term evolution (LTE) cellular systems consider this approach on a downlink from the base station to the hosts [6, 7], because of the feasible implementation of channel estimation and the accessibility of channel state information from the base station to any of the hosts. However, designing integrated medium access control (MAC) and baseband processing for MU-MIMO on the uplink, from users to the base station, is still an open problem, and is the main focus of this work [8].

Initially, MIMO was deployed only in point-to-point communication between two terminals, either to provide higher transmission rates by increasing bandwidth efficiency or to improve reliability with space-time coding [9, 10]. In recent years, network MIMO and cooperative MIMO approaches have emerged, where simultaneous MIMO

transmissions (to and from users) are coordinated to control the level of multiple access interference (MAI) [1]. The MAI is a result of mutual inter-user interference, where users share frequency, time and spatial streams, and power in wireless channels with broadcast characteristics and a limited spectrum [11]. Coordination for the utilization of radio resources is realized via significant data and channel state information (CSI) sharing across cooperating BSs over the backhaul links [12]. Under ideal conditions, the gains achieved by employing multiple antennas to exploit the spatial dimension in the downlink and uplink are well recognized, and theoretically similar strategies could be deployed. However, because of practical constraints such as (i) insufficient channel knowledge, (ii) asymmetry in the computational capabilities of user terminals and BSs, (iii) backhaul capacity, and (iv) the constrained level of coordination among users, the signal processing strategies pursued for uplink MU-MIMO transmissions differ from those developed for downlink MU-MIMO [13].

Scheduled transmissions to and from users distributed in space are generally referred to as space division multiplexing (SDM). This has been investigated primarily in the context of single-user (SU) transmissions [1, 11, 13]. The SDM for MU-MIMO is based on minimum mean square error (MMSE), zero forcing (ZF) or beamforming methods of signal detection, to allow parallel communications in the same time-frequency plane [1]. The major disadvantage of MMSE is that its performance suffers from intra-cell interference, whereas the other two methods mitigate the effects of MAI. The MMSE method can be developed together with a successive interference canceler (SIC) to reduce the effects of MAI and achieve optimum capacity, however, this results in a considerable increase in decoding complexity. The ZF and beamforming methods differ from one another in terms of the requirement for channel state information (CSI) availability: The ZF approach requires CSI only at the receiver end [14, 15], while the beamforming approach requires CSI at both ends [16]. Consequently, this work adopts the ZF approach due to its low complexity and the

fact that the limited coordination among users in practical systems does not permit global CSI knowledge for every user.

Infrastructure-based wireless systems with a base station (BS) serving an area referred to as a cell can operate in a single-cell or multi-cell mode. Depending upon the level of coordination among the BSs, these deployments are classified either as autonomous (with no coordination) or coordinated multi-cell systems. The performance of both types of system depends upon resource allocation, i.e., how time, power, frequency, and spatial resources are divided among users [13]. This work characterizes the problems of resource allocation with ZF detection at the BSs, and develops signal processing algorithms to solve these problems in the case of autonomous (single-cell) as well as multi-cell systems. This is accomplished for single carrier transmissions within the framework of coordinated multipoint transmission/reception (CoMP) [17], where user interference is managed through the scheduling of transmissions and resource allocation in order to enhance overall system performance [11]. The challenge is to maximize the aggregate system throughput, while maintaining user fairness, for instance with a comparable bit error rate (BER) performance.

In MU-MIMO SDM, multiple users share spatial channels which can be modeled as parallel links affected by MAI. From a theoretical point of view, parallel channels in the spatial, frequency or time domains could be handled in a similar way, however in practice this is not the case. Considerable research has been done on resource allocation and scheduling for orthogonal frequency domain multiplexing access (OFDMA) and single user systems [18, 19, 20, 21]. Scheduling algorithms in OFDMA assign active MSs a subset of all subcarriers, based on their channel gain conditions [22]. In the case of MU systems where user transmissions are separated in the frequency domain, the capacity of a subcarrier allocated to a particular user does not depend upon the choices of other MSs (in terms of their subcarrier gains and power). This is because the subcarriers are orthogonal, and processing at the receiver does not allow

inter-carrier interference [23]. In uplink MU-MIMO with ZF decoding, the capacity of spatial streams allocated to a particular user depends upon the set of active users and their decoding vectors and joint power control [1, 15]. As a result, spatial coordination is more difficult to solve than OFDMA. Although parallel transmissions in OFDMA and MU-MIMO differ with regard to noise modeling, nevertheless there are a number of OFDMA methods that could prove beneficial for the design of algorithms for MU-MIMO [24, 25, 26].

As wireless networks develop to a multi-cell environment, it is envisioned that wireless controller (WC) management of access points (APs) for wireless local area networks (WLANs), as already deployed in cellular networks, will not be limited to the data link and higher layers, but will also affect the radio front end. In these systems, the WCs are referred to as WLAN controllers (WLCs) [27] and mobile switching centers (MSCs). In multi-cell networks, inter-cell interference (ICI) from devices re-using the same frequency channel is a major factor that affects overall performance. Initial investigations of MU-MIMO proposed the use of coordinated multi-point (CoMP) systems to cancel ICI [28, 29]. In CoMP systems, all BSs receive the same signals from all active transmissions, though with different channel gains. The signals received are then forwarded to the WC for processing [30]. Therefore, the whole system depends upon a central unit to perform decoding processes and resource management, resulting in more robust system performance than that of stand-alone BSs.

Another ICI coordination solution to address ICI problems is the implementation of radio resource management, which helps to minimize the effects of ICI and improve the total system sum rate [13, 11, 31]. This method is important for controlling interference levels encountered especially by users that are located at the edges of cells [32, 33]. A few algorithms have already been proposed in this field, including [34, 31, 35, 36, 37]. However, most of these studies propose solutions for multi-cell systems

using MMSE decoders at the BS, or address OFDMA systems without considering the effects specific to MU-MIMO with ZF decoding.

The major contributions of this work involve the integration of spatial coordination and power allocation for MU-MIMO systems, where ZF is utilized to perform the SDM. To this end, joint scheduling algorithms are developed to mitigate the noise enhancement and interference caused by the system, in order to maximize the total system sum rate. Special consideration of decoding complexity is included in the proposed designs, to offer a system that is applicable to real-time applications.

1.1 Dissertation Objectives, Contributions and Organization

1.1.1 Objectives

This dissertation proposes interference-aware resource management algorithms for single-cell and multi-cell networks. The primary aim is to increase the total system sum rate by allocating system resources among the available MSs. This thesis has four main objectives.

The first objective is to analyze MAI and noise enhancement when working with a ZF decoder, and then to implement a low complexity SDM for MU-MIMO to limit MAI on the uplink. This is achieved by considering two decoding strategies that are both based on ZF equalizer principles for nulling undesired signals. The two decoders utilize the ZF method with and without precoding vectors at the MSs, based on singular value decomposition (SVD). Applying SVD within the system requires additional processing at the MSs and may be suitable in cases where user terminals or MSs have strong processing capabilities.

The second objective involves the design of a scheduling algorithm that is applicable for a single-cell wireless network. The scheme considers channel gain as the main parameter for making spatial coordination decisions. In addition, noise enhancement, which is a result of ZF processing, is included in the selection process to improve system performance. A load-adaptive algorithm is also integrated with the proposed algorithm in order to increase system throughput and fairness.

The third objective is to apply the cooperative reception (CR) method to a few active users in a multi-cell system. Utilizing this method helps to achieve some of the advantages provided by CoMP, while still keeping system complexity as low as possible. Transmitted signals that are received cooperatively are subject to fewer interference effects. In general, system performance as a whole improves as ICI levels are reduced.

The fourth and final objective is to design a distributed scheduler, where spatial coordination and power allocation are performed for multi-cell systems. Newton's method of optimization is utilized to help find the optimum power allocation and temporarily disable transmitting antennas that are contributing to deterioration of the total system performance.

1.1.2 Contributions

Results of the research described in this thesis have been published in the form of conference papers [38, 39, 40, 41]. In addition, one journal article has been submitted and another is in preparation [42, 43]. The details of these publications are outlined below.

Refereed Conference Proceeding Publications

[C-1] A. Alyahya and J. Ilow, "*Zero-forcing assisted spatial stream allocation in uplink multiuser MIMO systems*," in 2015 IEEE 28th Canadian Conference on

Electrical and Computer Engineering (CCECE), 3-6 May 2015, pp.1030-1035.

[C-2] **A. Alyahya** and J. Ilow, "*Spatial stream scheduling in uplink multiuser MIMO systems with zero-forcing post-processing*," in 2015 IEEE 14th Canadian Workshop in Information Theory (CWIT), 6-9 Jul 2015, pp.101-105.

[C-3] **A. Alyahya** and J. Ilow, "*Uplink scheduling in multi-cell MU-MIMO systems with ZF post-processing and diversity combining*," in 2015 IEEE 14th Canadian Workshop in Information Theory (CWIT), 6-9 Jul 2015, pp.83-87.

[C-4] **A. Alyahya** and J. Ilow, "*Short paper: Radio resource and interference management in uplink multi-cell MU-MIMO systems with ZF post-processing*," in 2015 IEEE in Vehicular Technology Conference (VTC Fall), 6-9 Sep 2015.

Papers Submitted to Refereed Journals or in Preparation

[IPJ-1] **A. Alyahya** and J. Ilow, "*Spatial coordination and resource management for uplink MU-MIMO systems*," In Preparation.

[SJ-1] **A. Alyahya** and J. Ilow, "*Multi-cell Coordination of radio resources in MU-MIMO systems with ZF post-processing*," Computer Communications, submitted in July 2016.

The research in each of the papers cited above was initiated and carried out by the principal author of the papers, who is also the author of this dissertation.

The research contributions of this thesis can be classified into four areas, which correspond to the four main chapters of the dissertation. The specific papers and the chapters that relate to them are listed below.

Chapter 2: **Spatial Coordination and ZF in Uplink MU-MIMO**

A design for a low complexity ZF post-processing uplink MU-MIMO is proposed and compared with conventional systems. Two methods are illustrated in this

chapter, a stand-alone ZF post-processing approach and a ZF-SVD method [C-1] and [IPJ-1].

Chapter 3: **Resource Allocation and Noise Enhancement in an Uplink MU-MIMO Single-Cell System**

An interference-aware user selection and resource allocation algorithm is introduced for an uplink MU-MIMO system with a ZF-SVD process. Antenna/spatial coordination algorithms are proposed with the aim of either increasing the total system sum rate or improving overall user fairness [C-2] and [IPJ-1].

Chapter 4: **Spatial Coordination Algorithm and CR Method in a Double-Cell Environment**

A double-cell MU-MIMO uplink system model is analyzed with the aid of the ZF stand-alone post-processing approach. A user/antenna selection algorithm is described where the possibility of cooperative reception (CR) is considered with the aim of countering the ICI [C-3] and [SJ-1].

Chapter 5: **Resource Management for Multi-Cell Networks**

Distributed resource management algorithms are proposed for a multi-cell topology, where spatial coordination and power allocation are considered. The two resource allocation algorithms perform independently to provide the system with lower complexity [C-3], [C-4] and [SJ-1].

1.1.3 Thesis Organization

Below is a brief outline of the organization of the chapters of this dissertation.

Chapter 1

In Section 1.1 the objectives, contributions and organization of the dissertation

are outlined. The remainder of this chapter reviews the general concepts and elements employed throughout the dissertation. Section 1.2 presents an overview of the wireless channel model, while Section 1.3 reviews the concepts related to diversity in wireless communications. The MIMO system model is described in Section 1.4, and an analysis of its capacity is presented in Section 1.5. Next, a brief description of the MU-MIMO model is provided in Section 1.6, followed by an elaboration of SDM in Section 1.7. Finally, the chapter concludes with a summary in Section 1.8.

Chapter 2

The MU-MIMO model and the ZF decoder are introduced in Section 2.1 and Section 2.2, respectively. In addition, a preliminary spatial coordination algorithm is implemented in Section 2.3 to highlight the advantages that can be gained from the system. The simulation results are presented in Section 2.4, and the chapter concludes with Section 2.5.

Chapter 3

The chapter begins with a system model description in Section 3.1. Power, capacity and buffer state are analyzed in Section 3.2. Two rate adaptive scheduling algorithms are introduced in Section 3.3, with the simulation results for their performance. In addition, a hybrid (rate- and load-adaptive) algorithm is described in Section 3.4, which also presents the simulation results. Finally, Section 3.5 concludes the chapter.

Chapter 4

In Section 4.1, a double-cell system model for the MU-MIMO uplink system is presented. A two-layer decoder to perform MU detection and CR is described in Section 4.2. In addition, a successive interference canceler (SIC) is also utilized to improve the total system performance. A low-complexity scheduling

algorithm is presented in Section 4.3, and the simulation results are provided in Section 4.4. Section 4.5 summarizes the chapter.

Chapter 5

In Section 5.1 a multi-cell system model is presented, and a generalized total system capacity formula is introduced in Section 5.2. Newton's method for optimization of the cost function in hand is derived in Section 5.3, which also includes simulation results for finding the best parameters for the model. A resource allocation algorithm is proposed in Section 5.4, while the simulation results are presented in Section 5.5. Section 5.6 summarizes the chapter.

Chapter 6

The concluding chapter summarizes this dissertation and outlines its contributions. In addition, suggestions for future work are presented.

1.2 Modeling Wireless Communication Channels

This dissertation contributes to the theoretical development of signal processing algorithms for MU-MIMO systems and the results are verified through simulations. This is the first step, which precedes practical implementation and is an acceptable methodology in the field of communication system design, as not all physical layer wireless communication proposals go into the implementation stage. Sound modeling of wireless channels plays an essential role in analyzing and studying large wireless communication systems. In essence, transmitted signals are subject to detrimental effects such as noise and signal attenuation. This section reviews some of the wireless communication channel models used in this dissertation.

1.2.1 Additive White Gaussian Noise

Additive white Gaussian noise (AWGN) is a channel model that includes numerous effects of wideband noise omnipresent in the RF front end of wireless receivers [44]. According to the central limit theorem, the summation of many random variables (RVs) results in a Gaussian distribution which has a probability density function (pdf):

$$pdf(n) = \frac{1}{\sqrt{2\pi\sigma_0^2}} \exp^{\frac{-(n-\mu)^2}{2\sigma_0^2}} \tag{1.1}$$

with a zero mean ($\mu = 0$) and a noise variance (σ_0^2) that represents the power spectral density ($\frac{N_0}{2}$ [W/Hz]). This dissertation deals with received signals after downconverting and matched filtering, and noise is represented as a RV rather than as a stochastic process.

1.2.2 Rayleigh Fading Channel

When a signal is transmitted in a radio channel, it arrives at the receiver via different paths due to atmospheric or object refractions and reflections. Therefore, various copies of the original message are combined at the receiver at the output of matched filtering, but with different attenuation effects and time delays. This condition is recognized as fading, where the replicas of the original signal from all multipaths when combined represent the multiplicative effect of the received signal. The most common type of fading is flat, slow fading where the multiplicative factor is given by a random variable denoted as h. Here h is a complex variable with real and imaginary components considered as Gaussian RVs, being independently and identically distributed (i.i.d.). Therefore, the random gain of the fading channel is: $|h| = \sqrt{\Re(h)^2 + \Im(h)^2}$, where $\Re(h)$ and $\Im(h)$ denote the real and imaginary values of h, respectively, where h is a complex normal RV: $h \sim \mathcal{CN}(0, \sigma_h^2)$. Therefore $|h|$ has a

pdf of

$$pdf(|h|) = \frac{2|h|}{2\sigma_h^2} \exp^{\frac{|h|^2}{2\sigma_h^2}} \tag{1.2}$$

where σ_h^2 is a power scaling parameter. Hence, $|h|$ has a Rayleigh distribution. This applies only when there is no line-of-sight (LOS) path and (1.2) represents the most adverse type of fading.

1.2.3 Large-Scale Attenuation

The signal power level decays when the signal propagate through a channel over distance. This phenomenon is known as signal attenuation or deterministic path loss. To capture this effect, different mathematical models are proposed for different radio propagation conditions [45]. This work adopts a generalized formula which links the attenuation to the traveled distance $d > 1$ as follows:

$$p_r(d) = \frac{p_t}{d^\alpha} \tag{1.3}$$

where $p_r(d)$ and p_t represent the power of the received and transmitted signals, respectively. The α parameter corresponds to the propagation condition; normally this value ranges from 2 in free-space conditions to 6 in a dense urban area.

1.3 Diversity Schemes

As transmitted signals travel through a channel, they encounter various obstacles which cause them to scatter and to arrive at the receiver with different delays, resulting in multipath fading. Multipath fading significantly degrades wireless system performance in terms of BERs. This problem is usually solved by increasing the transmission power. However, increasing the transmission power is not always a practical solution, particularly for mobile applications with limited energy resources. Diversity techniques are therefore used to restore the data by creating multiple replicas of the

original signal. Diversity is exploited in either the time, frequency or space domains. It is also possible to work with combinations of diversity types, referred to as hybrid models. For example, the Alamouti scheme, which was developed to increase the reliability of MIMO transceivers, uses both time and spatial diversity [46]. The present research focuses primarily on spatial diversity, by exploiting available antennas. Thus, bandwidth expansion is not imposed, as required by frequency diversity, nor are extra time slots needed, as is the case with time diversity [9, 10].

1.4 Multi-Input Multi-Output Systems

In Figure 1.1, three basic spatial diversity models are presented. First the single-input multi-output (SIMO) model is shown, where a single antenna is located at the transmitter and multiple antennas are used at the receiver. Next, the multi-input single-output (MISO) system is illustrated, where there are multiple antennas at the transmitter and only one antenna at the receiver. The last model shows the multi-output multi-input (MIMO) system, where both the transmitter and the receiver have multiple antennas. All of these models are considered as single-user (SU) models, with one transmitter occupying all spatial dimensions created between the transmitter and the receiver in this peer-to-peer type of communication.

A more detailed representation of the SU-MIMO model is shown in Figure 1.2, where M and R represent the total number of antennas for the transmitter and the receiver, respectively. For the case where channel state information (CSI) is not available at the transmitter, the total transmission power is divided equally among

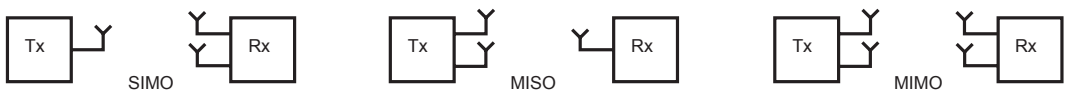

Figure 1.1: Antenna configurations for different spatial diversity models.

all the antennas (P/M), where P is the total transmitted power. Two types of noise that affect signal transmission are considered. The first is additive Gaussian noise, represented as the vector $\mathbf{n}$, with size $R \times 1$. The n_r element of the matrix $\mathbf{n}$, where $r = 1, .., R$, represents the AWGN that affects the rth antenna of the receiver. The standard assumption here is that $\mathbf{n}$ is an independently identically distributed (i.i.d) Gaussian random column vector. Secondly, Rayleigh multipath fading is represented as the $\mathbf{H}$ channel gain matrix with size $R \times M$. The coefficient h_{rm} in $\mathbf{H}$ represents the fading coefficient (random channel gain) occurring from the mth antenna of the transmitter to the rth antenna of the receiver, where $r = 1, \cdots, R$ and $m = 1, \cdots, M$. Finally, the vector of the received signal is represented in matrix notation as:

$$\mathbf{y} = \mathbf{Hs} + \mathbf{n} \tag{1.4}$$

and in an expanded version as:

$$\begin{bmatrix} y_1 \\ \vdots \\ y_R \end{bmatrix} = \begin{bmatrix} h_{11} & \cdots & h_{1M} \\ \vdots & \ddots & \vdots \\ h_{R1} & \cdots & h_{RM} \end{bmatrix} \begin{bmatrix} s_1 \\ \vdots \\ s_M \end{bmatrix} + \begin{bmatrix} n_1 \\ \vdots \\ n_R \end{bmatrix} \tag{1.5}$$

where the $\mathbf{s}$ and $\mathbf{y}$ vectors represent the signals sent and received, respectively.

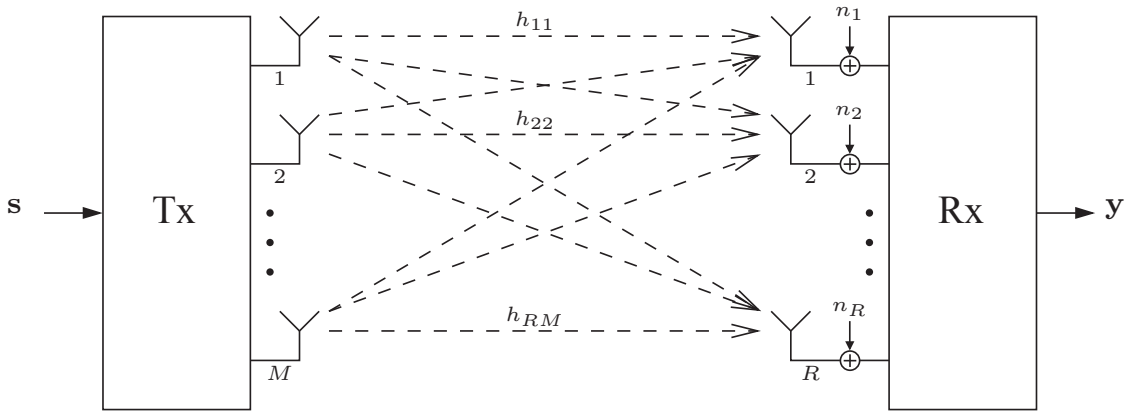

Figure 1.2: The basic MIMO model.

1.5 MIMO Capacity

System capacity is defined as the maximum transmission rate in bits per second which is accommodated in one hertz of bandwidth with an acceptable BER. For a SISO model with an additive white Gaussian channel, the capacity is given by Shannon's channel capacity formula:

$$C = \log_2 (1 + SNR) \qquad [bps/Hz] \tag{1.6}$$

To extend this formula in order to calculate the total channel capacity for the MIMO system, (1.4) is considered. The channel matrix can be decomposed by using singular value decomposition (SVD):

$$\mathbf{H} = U\Lambda V^{\mathcal{H}} \tag{1.7}$$

where U and V are both unitary matrices, i.e., $U \cdot U^{\mathcal{H}} = \mathbb{I}$ and $V \cdot V^{\mathcal{H}} = \mathbb{I}$. The $(^{\mathcal{H}})$ notation refers to the Hermitian operator, and $\mathbb{I}$ is the identity matrix. Λ is a diagonal matrix which holds the singular values of H, i.e., the square roots of the eigenvalues of $HH^{\mathcal{H}}$. The consideration of $\mathbf{S} = V\mathbf{s}$, $\widehat{\mathbf{y}} = U^{\mathcal{H}}\mathbf{y}$ and $\widehat{\mathbf{n}} = U^{\mathcal{H}}\mathbf{n}$, and substitution of (1.7) into (1.4) yields:

$$\widehat{\mathbf{y}} = \mathbf{\Lambda S} + \widehat{\mathbf{n}} \tag{1.8}$$

where $\mathbf{s}$ represents the pre-processed (precoded) version at the transmitter of the original data $\mathbf{S}$ to be sent, and $\widehat{\mathbf{y}}$ represents the post-processed version of the received signal vector $\mathbf{y}$. The pre- and post-processing depend upon knowledge of the channel matrix $\mathbf{H}$, or knowledge of the V and U matrices at the transmitter and the receiver, respectively. The matrix V (pre-processing matrix) is employed as a beamforming matrix that adjust the elements of transmitted signal in amplitude and phase. From (1.8), the MIMO model can be represented as parallel Gaussian channels, as shown in Figure 1.3, where X available channels correspond to the size of the Λ matrix. The number of available channels is given by $X = min(M, R)$, and λ_x is

the singular value associated with the xth parallel ("logical" or "virtual") path, that characterizes the equivalent multipath fading factor.

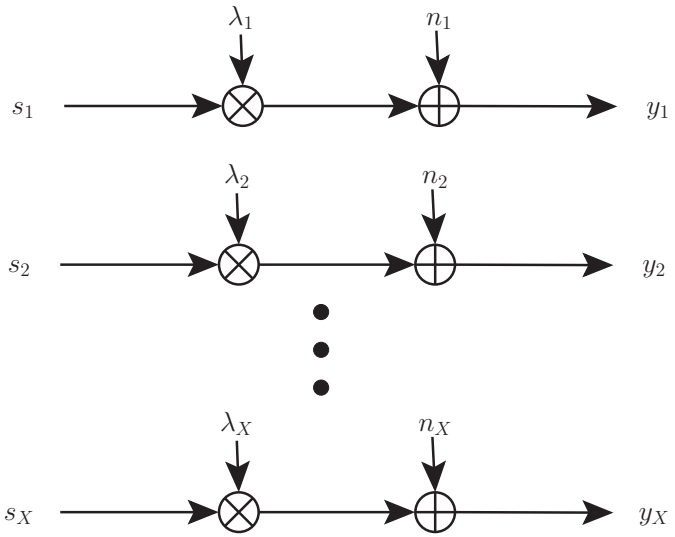

Figure 1.3: SVD-equivalent MIMO model.

The total capacity for MIMO systems is therefore given by the sum of the capacities of individual parallel channels in the spatial domain. From (1.6), the total MIMO link capacity can be written as:

$$C = \sum_{x=1}^{X} \log_2 \left(1 + \frac{\lambda_x^2 p_x}{2n_x}\right) \tag{1.9}$$

where p_x is the total energy invested in the xth channel.

Two cases related to the availability of CSI are represented in this discussion. The first case includes access to CSI at both sides of the transceiver as discussed above, i.e., at the transmitter and at the receiver. In this case the transmitter is able to distribute the power bias among the transmission antennas to take advantage of less faded channels, in order to achieve maximum capacity by using water-filling algorithms [23].

However, in some applications it is difficult to obtain the CSI at the transmitter side. In this case, with different signal processing in the MIMO transceiver, the total

available power P is equally distributed among all the M antennas. Hence, (1.9) is written as:

$$C = \sum_{x=1}^{X} \log_2 \left(1 + \frac{\lambda_x^2 E_s}{2M n_x}\right) \tag{1.10}$$

1.6 Multiuser MIMO Model

In multiuser MIMO (MU-MIMO) systems with BSs, a set of terminals equipped with multiple antennas transmit to (or receive from) the BSs at the same time and frequency, and their transmissions are separated using some kind of spatial signature. This contrasts with single-user MIMO (SU-MIMO), where a single multi-antenna transmitter communicates with a single multi-antenna receiver in a given time slot. The MU-MIMO system is a type of one-to-many and many-to-one model, whereas the SU-MIMO system is a one-to-one model [47].

Figure 1.4 shows an example of a MU-MIMO model with one base station (BS) and four mobile stations (MSs). Every MS is equipped with at least one antenna,

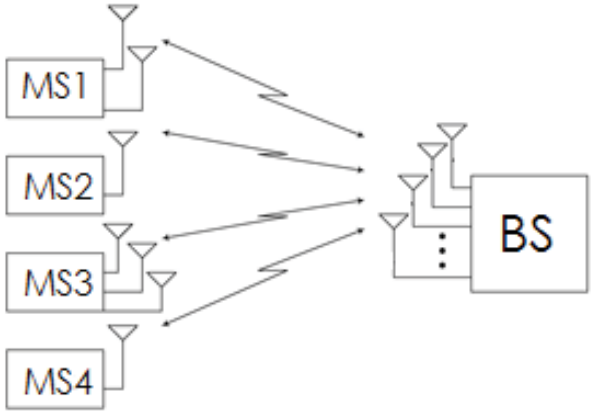

Figure 1.4: MU-MIMO model with 4 mobile stations.

and the BS always has multiple antennas for receiving and transmitting. The MU-MIMO model offers a number of multiple channel streams that are equal to the

number of antennas at the BS. The MSs compete among themselves in order to gain access to the spatial streams, and each MS may obtain access to a number of spatial streams equal to but not exceeding the number of its antennas. Thus, the more channel streams provided by the BS, the more MSs can be accommodated for parallel transmissions, where different MSs communicate with the BS using the same spectrum at the same time. MU-MIMO systems offer flexibility in assigning spatial channels to MSs with advantageous channel conditions, and in this regard are much more beneficial than SU-MIMO systems. This flexibility is achieved by taking advantage of the distributed communications and channel diversity that occur with MU-MIMO, where multiple MSs communicate with a single device. Specifically, in MU-MIMO systems as compared to SU-MIMO systems, when wireless channel conditions vary, the total system capacity is not dramatically degraded when one of the MSs experiences poor channel conditions, because some of its spatial streams can be reallocated to other users [4].

The physical layer of the MU-MIMO model is characterized as one of two types, according to the direction of transmissions: The downlink and the uplink. The downlink refers to sending information from the BS to the MSs. Because the BS is the only node that is using the channel, downlink transmissions are usually considered to be easier to implement in terms of multiple access control. The uplink refers to information flow in the opposite direction, involving transmission from the MSs to the BS. The design of communication strategies is more complex for the uplink than it is for the downlink, because the MSs do not have the advantage of having the same CSI, and there may be a need to implement a CSI sharing protocol in order to organize the access of MSs to the shared channel. Also, the MSs do not have access to the data transmitted from other MSs to the BS. In contrast, for a downlink transmission, the BS has access to data transmitted to all MSs, and usually also has access to the CSI for the individual links to all MSs.

1.7 Space-Division Multiplexing

In the MU-MIMO model for a downlink, parallel communications using spatial streams between the BS and MSs require specialized processing of the transmitted data. The processing overhead is biased toward the BS, due to the higher computational processing capabilities of the BS, and because the BS is able to obtain all of the CSI for the whole system (the global CSI). However, some processing approaches require processing to be executed at both the BS and MSs. This is usually considered to be a complex design, because the MSs then require full knowledge of the MU-MIMO system CSI, or at least a feedback channel from the BS. The ZF technique, which is a low-complexity method that permits parallel communications in the MU-MIMO setting, is summarized next, as this approach is an important aspect in this dissertation.

The ZF method was originally introduced in the context of a linear equalization algorithm which cancels inter-symbol interference (ISI) by inverting the channel frequency response. A modified version of the ZF equalizer is used for ISI cancellation in the SU-MIMO model, and for removing the effects of MAI in the MU-MIMO model [48]. Most research investigations consider this approach for the downlink flow, with processing overhead added only at the BS [14].

Figure 1.5 illustrates the general signal processing model for downlink MU-MIMO in single-cell systems that take advantage of the ZF method. As shown in the figure, R antennas are available at the BS, and M_k antennas are available for the kth user, where $R > 1$, $M_k \geq 1$ and $k \in \{1, 2, \ldots, K\}$. Encoding (signal pre-preprocessing) is applied only at the BS, hence the MSs do not require any CSI to decode messages. There are K signals, $\mathbf{s}_k$, to be transmitted to K MSs. Before being sent, the signals are multiplied by their designated encoding matrices $\mathbf{T}_k$ implying liner signal processing. Due to the broadcast characteristics of the wireless channel, the signal received at

user k is:

$$\mathbf{y}_k = \mathbf{H}_k \left(\sum_{i=1}^{K} \mathbf{T}_i \mathbf{s}_i \right) + \mathbf{n}_k \tag{1.11}$$

where $\mathbf{H}_k$ and $\mathbf{n}_k$ are the channel gain matrix between the BS and the kth MS and the Gaussian noise, respectively. Although user k is interested only in its own transmitted signal, represented by the term $\mathbf{H}_k \mathbf{T}_k \mathbf{s}_k$, a summation of all signals multiplied by their corresponding encoding matrices is received. Hence, at the BS, from the perspective of user k, the encoding matrices $\mathbf{T}_i,\ i \neq k$ and $i \in \{1, \cdots, K\}$ associated with the other $K-1$ users should be chosen such that the impact of undesired signals $\mathbf{s}_i$ is nulled, i.e., $\mathbf{H}_k \cdot \mathbf{T}_i \cdot \mathbf{s}_i = 0$ for a fixed k and $i \neq k$ and $i \in \{1, \cdots, K\}$. When these requirements are combined for all users, the encoding matrices $\mathbf{T}_k$ at the BS should be selected so that [14]:

$$\mathbf{T}_k = \arg_{1<i<K, i \neq k} \left(\mathbf{H}_i \mathbf{T}_k = 0 \right) \tag{1.12}$$

subject to power constraints on the encoded signal. In (1.12), $\mathbf{T}_k$ does not depend upon $\mathbf{s}_k$ as in the earlier discussion, because it is considered as a random vector

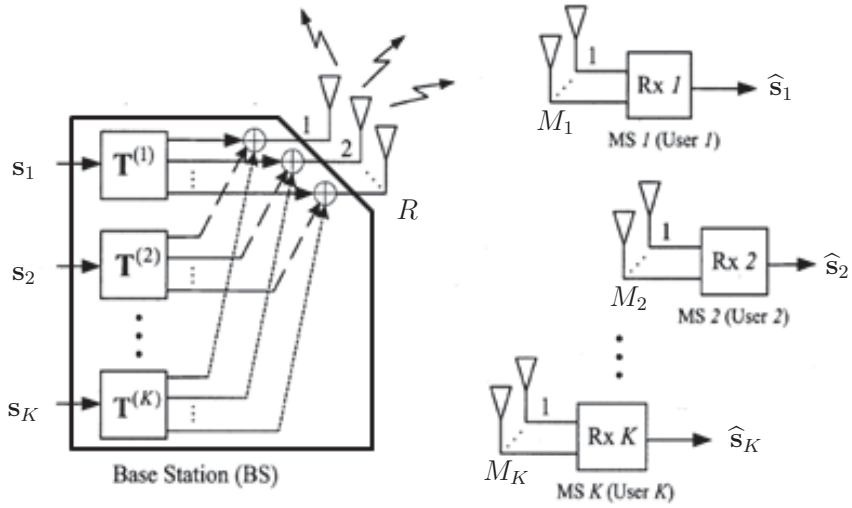

Figure 1.5: ZF approach for downlink flow.

representing user data from a finite alphabet set. On the other hand, $\mathbf{H}_i$ is assumed to be known from the channel estimation process: Channel gain matrices $\mathbf{H}_i$ are varying, but with the assumption of slow fading they are assumed to be fixed over the block of transmitted data. From linear algebra, encoding matrices $\mathbf{T}_k$ can be solved in (1.12), with the condition that $R > \sum_{i=1,i\neq k}^{K} M_i$. Hence, with this nulling or ZF approach, every MS would receive only the information intended for it.

Although there are some published works which use a ZF analytical approach similar to that proposed in [49] for the uplink flow, their methods assume additional processing overhead at the MSs and BS, and they result in considerably more complex designs than those pursued in this dissertation.

Another SDM technique for MU-MIMO is the beamforming approach. This technique is based on applying the beam-space beamforming model, where the transmitted signal is combined with orthogonal parameters [50]. The design of the orthogonal parameters is usually similar to code division multiple access, as described in [51]. Most publications consider this strategy for the uplink data flow [16], although it could be generalized for full duplex communication, where encoding and decoding are required at both the BS and the MSs.

1.8 Summary

This chapter has presented an overview of the research area considered in this dissertation, and has outlined the objectives, contributions, and organization of the dissertation. In addition, a review of the relevant concepts used throughout this dissertation is included, with the main topics: Wireless channel modeling, MIMO system capacity, MU-MIMO schemes, and SDM with ZF processing on the downlink.

Chapter 2

Spatial Coordination and ZF in Uplink MU-MIMO

Multiple access systems with multiple antennas allow several users to communicate simultaneously in the same frequency band with an access point (AP) or a base station (BS), by spatially multiplexing several data streams onto the MU-MIMO channel [1]. In these systems, the objective for MU-MIMO decoding is to resolve mixed signals from different users in the spatial domain and thus decompose a MU-MIMO channel into multiple parallel SU-MIMO channels.

This chapter analyzes two MU linear decoders based on the ZF approach for the uplink connection. At a common BS, ZF processing performs the spatial demultiplexing of user signals, with the low computational complexity of the developed algorithms. Moreover, global CSI is required only at the BS, and there is no need to distribute the global CSI to MSs. In addition, an antenna-based spatial coordination algorithm is developed with the aim of improving the overall system performance, by reducing the noise enhancement effects that result from deploying ZF decoders.

The chapter is structured as follows. Section 2.1 first presents the underlying

system model. The two MU-MIMO uplink schemes, one based exclusively on ZF post-processing at the AP and the other being an improvement incorporating SVD pre-processing at the hosts, are introduced in Section 2.2. The antenna/user scheduling algorithm is proposed in Section 2.3, while the performance analysis and simulation results are presented in Section 2.4. Finally, Section 2.5 summarizes the chapter.

2.1 ZF System Model for MU-MIMO

Figure 2.1 illustrates the general model for the uplink transmissions in a single-cell MU-MIMO system, where K potentially active MSs send data to a common BS. The kth MS is equipped with M_k omnidirectional transmitting antennas, while the BS has R omnidirectional receiving antennas. Simultaneously, in one time slot, each MS propagates its own signal ($\mathbf{s}_k$) toward the BS, where $\mathbf{s}_k$ is the $M_k \times 1$ column vector representing the kth user data at the baseband equivalent.

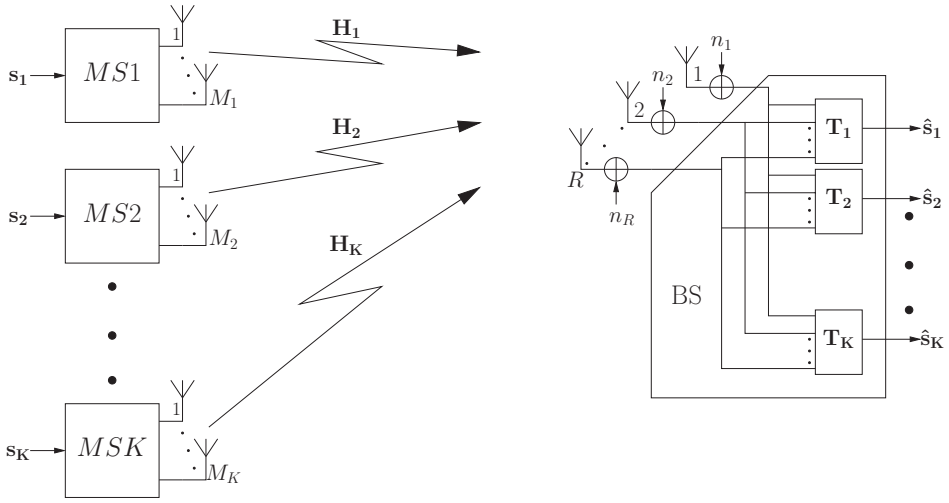

Figure 2.1: The ZF uplink MU-MIMO system model.

When the signals are transmitted over a common broadcast wireless medium, it is assumed that they are affected by flat fading. The channel gain (coefficients) matrix

of the MIMO channel between user k and the BS is denoted by $\mathbf{H_k}$, representing a $R \times M_k$ matrix. The (r, m)th element in $\mathbf{H}_k$ represents a complex channel gain from the mth antenna of the kth MS to the rth antenna of the BS. Assuming Rayleigh fading, all of the elements in $\mathbf{H}_k$ $(k \in 1, 2, \cdots, K)$ are i.i.d. zero-mean complex Gaussian RVs with a unit variance $(\mathbf{H}_k(r, m) \sim \mathcal{CN}(0, 1))$.

The signal received at the BS through over-the-air signal summation is a combination of all transmitted signals. It is then decoded/processed by the BS to retrieve all of the users' information. These operations at the BS receiver are referred to as post-processing reception. In linear processing, the decoding matrix $\mathbf{T}_k$ is deployed at the BS to recover the transmitted data from user k, where $\mathbf{T_k}$ is a $M_k \times R$ matrix. Here the kth user's decoded data can be represented as:

$$\hat{\mathbf{s}}_k = \mathbf{T}_k \left(\sum_{i=1}^{K} \mathbf{H}_i \mathbf{s}_i + \mathbf{n} \right) \tag{2.1}$$

where $\mathbf{n}$ is a $R \times 1$ column vector representing the AWGN with the n_r – rth element of vector $\mathbf{n}$ – being complex Gaussian noise which affects the rth receiving antenna of the base station, as shown in Figure 2.1.

The post-processing with $\mathbf{T}_k$ at the BS on the uplink in (2.1) and the pre-processing with $\mathbf{T}_k$ at the BS on the downlink in (1.11) have a common interpretation of canceling other users' interference. However, the major difference is that in (2.1) for uplink transmissions, the post-processing with $\mathbf{T}_k$ modifies (enhances) the original AWGN noise $\mathbf{n}$ from the RF front end at the BS. This observation is a cornerstone for many new results in this thesis.

2.2 ZF Post-Processing in Uplink MU-MIMO

The primary aim of this section is to present and analyze the effects of signal processing at the BS. The objective of this decoding process is to convert the MU-MIMO

model presented in Section 2.1 into a set of conventional single-user (SU)-MIMO systems from the perspective of the MSs. This is to be accomplished with low-complexity linear decoding for all K users. This decoding, as represented by matrices $\mathbf{T}_1, \mathbf{T}_2, \ldots, \mathbf{T}_K$, operates as a MU interference canceler. In addition, it must be ensured that the decoding matrices, $\mathbf{T}_k$, retrieve the original data sent from MS k with acceptable reliability. To this end, two approaches are investigated: The first is based on implementing only a zero forcing (ZF) technique, to retrieve the original data at the BS only; and the second approach focuses on designing the ZF technique at the BS so as to incorporate the advantages of the singular value decomposition (SVD) method at the MSs.

2.2.1 The ZF Approach

In the ZF approach, the decoding matrix for user k, $\mathbf{T}_k$, is calculated so that it satisfies the following matrix relation:

$$\mathbf{T}_k \left(\sum_{i=1, i\neq k}^{K} \mathbf{H}_i \mathbf{s}_i \right) = \mathbf{0} \tag{2.2}$$

where $\mathbf{T}_k$ should not be the zero matrix solution, and $\mathbf{T}_k$ should be such that (2.2) holds for any possible data $\mathbf{s}_i$, which are essentially RV vectors from a finite set representing the modulated symbols. To exclude the impact of $\mathbf{s}_i$ in (2.2), the condition is enforced that $\mathbf{T}_k \mathbf{H}_i = \mathbf{0}$ where $i \in \{1, 2, \cdots, k-1, k+1, \cdots n\}$ (in the present instance the size of the zero matrix is $M_k \times M_i$). The existence of a viable solution for $\mathbf{T}_k$ ($k \in 1, \cdots, K$) is verified later. In addition, the decoding matrix should also consider the retrieval of the original data without scaling. Hence,

$$\mathbf{T}_k \mathbf{H}_k = \mathbb{I} \tag{2.3}$$

where $\mathbb{I}$ is the identity matrix (in this case, with size $M_k \times M_k$). From (2.2) and (2.3), it can be seen that $\mathbf{T}_k$ should satisfy:

$$\mathbf{T}_k = \arg_{\mathbf{T}_k \neq \mathbf{0}} \begin{pmatrix} \mathbf{T}_k\mathbf{H}_1 = \mathbf{0} \\ \vdots \\ \mathbf{T}_k\mathbf{H}_{k-1} = \mathbf{0} \\ \mathbf{T}_k\mathbf{H}_k = \mathbb{I} \\ \mathbf{T}_k\mathbf{H}_{k+1} = \mathbf{0} \\ \vdots \\ \mathbf{T}_k\mathbf{H}_K = \mathbf{0} \end{pmatrix} \tag{2.4}$$

In this dissertation, it is assumed that at the BS accurate information is available regarding the channel gain matrices $\mathbf{H}_k$ ($k \in 1, \cdots, K$), also referred to as global CSI.

The technique employed in this work for deriving the system of matrix equations constraining the decoding/post-processing matrices $\mathbf{T}_k$ may be viewed as an approach that is complementary to deriving the system of matrix equations constraining the pre-coding matrices in the uplink MU-MIMO scenario originally proposed in [14]. However, a careful examination of the constraints presented in relation (1) in [14] and the constraints indicated in (2.2) should show a clear differentiation between these two approaches which actually result in very similar final solutions for $\mathbf{T}_k$ matrices.

From (2.4), $\mathbf{T}_k$ can be found, as an algebraic solution to:

$$\mathbf{T}_k \begin{bmatrix} \mathbf{H}_1 & \dots & \mathbf{H}_{k-1} & \mathbf{H}_k & \mathbf{H}_{k+1} & \dots & \mathbf{H}_K \end{bmatrix} = \mathbf{Y} \tag{2.5}$$

where matrix $\mathbf{Y}$ is designed to hold the values of 1(s) from a diagonal of the identity matrix (2.3), starting from row $\sum_{i=1}^{k-1} M_i$ and column $\sum_{i=1}^{k} M_i$, with zero values everywhere else. It should be noted here that a non-zero solution for $\mathbf{T}_k$ ($k \in \{1, 2, \cdots, K\}$) in (2.5) can be found for all $\mathbf{T}_k$(s) only if

$$R \geq \sum_{k=1}^{K} M_k \tag{2.6}$$

From (2.1) and the constraints in (2.5), it can be seen that the recovered data for the kth user is:

$$\hat{\mathbf{s}}_k = \mathbf{s}_k + \mathbf{T}_k\mathbf{n} \tag{2.7}$$

where $\mathbf{T}_k\mathbf{n}$ represents the enhanced noise (through matrix $\mathbf{T}_k$) that resulted from MU post-processing at the BS. This noise is dependent only on the channel matrices, and is not affected by the transmitted power utilized at the MSs.

2.2.2 Integrated ZF and SVD Approaches

The adoption of SVD pre-processing at the MSs to aid in MU-MIMO detection serves the purpose of reducing the impact of AWGN noise enhancement as shown in (2.7) when deploying ZF alone, and takes advantage of the known local channel gain matrix $\mathbf{H}_k$ at the kth MS. With this integrated ZF-SVD approach, it is possible to achieve additional performance gains for the MU-MIMO, as already demonstrated for downlink transmissions [14, 15]. The SVD permits the fading channel matrix to be represented as $\mathbf{H}_k = \mathbf{U}_k\mathbf{\Lambda}_k\mathbf{V}_k^{\mathcal{H}}$, where the $(\cdot)^{\mathcal{H}}$ operator denotes the Hermitian transpose and $\mathbf{\Lambda}_k$ is a diagonal matrix that always holds the positive singular values. Consequently, (2.1) can be rewritten as:

$$\hat{s}_k = \mathbf{T}_k\left(\sum_{i=1}^{K}\mathbf{U}_i\mathbf{\Lambda}_i\mathbf{V}_i^{\mathcal{H}}\mathbf{S}_i + \mathbf{n}\right) \tag{2.8}$$

The original data $\mathbf{s}_k$ sent from the kth user are adjusted via a linear transform $\mathbf{V}_k$, so that the transmitted data are $\mathbf{S}_k = \mathbf{V}_k\mathbf{s}_k$. This additional local pre-processing procedure at the user side requires the MS to have access to its channel gain matrix relative to the BS ($\mathbf{H}_k$, known as the local CSI) and to calculate the SVD. Access to $\mathbf{H}_k$ can be accomplished via the reverse channel from the BS to the MS or, with the assumption of channel reciprocity, it can be estimated by using the transmission of pilot signals. The latter approach is similar to the procedure for SU-MIMO systems

where the uplink and downlink channels are assumed to be the same and a data training is performed for local CSI estimation. On the other hand, the BS needs to acquire the complete CSI ($\mathbf{H}_k$ for any $k \in \{1, \cdots, K\}$), so as to be able to cancel all of the MU interference and to recover the data for all users.

From equivalent relations as in (2.2) leading to (2.3), with $\mathbf{H}_i$ now replaced by $\mathbf{U}_i\mathbf{\Lambda}_i$ and $\mathbf{s}_i$ replaced by $\mathbf{S}_i$, at the receiver, to remove the MAI, first the initial post-processing matrices $\mathbf{G}_k$ (equivalent to $\mathbf{T}_k$ in the ZF-only approach) can be found such that:

$$\mathbf{G}_k = \text{null}\left(\begin{bmatrix} \mathbf{U}_1\mathbf{\Lambda}_1 \\ \vdots \\ \mathbf{U}_{k-1}\mathbf{\Lambda}_{k-1} \\ \mathbf{U}_{k+1}\mathbf{\Lambda}_{k+1} \\ \vdots \\ \mathbf{U}_K\mathbf{\Lambda}_K \end{bmatrix}\right) \tag{2.9}$$

where null($\mathbf{X}$) is used to derive the kernel or null space of matrix $\mathbf{X}$, and where (2.6) should be met so as to find a non-zero solution for $\mathbf{G}_k$ ($k \in \{1, 2, \cdots, K\}$). In addition, in order to retrieve the original information, the BS needs to perform additional processing for the kth MS, because the post-processed signal is now a transformed version of the original vector $\mathbf{s}_k$:

$$\zeta_k = \mathbf{G}_k\mathbf{U}_k \tag{2.10}$$

where ζ_k is a matrix of size $M_k \times R$. Hence, there is no left inverse for ζ_k as $M_k < R$, and, as a consequence, there is no straightforward solution to this problem. Therefore, a matrix $\hat{\zeta}_k$ is created that contains the first $M_k \times M_k$ values found in ζ_k. From this the de-mixing matrix $\mathbf{A}_k$ for the original data is derived as:

$$\mathbf{A}_k = \text{Inv}(\hat{\zeta}_k) \tag{2.11}$$

where Inv($\mathbf{X}$) is the pseudo-inverse of $\mathbf{X}$. Hence, from (2.9) and (2.11) the decoding matrix for user k can be calculated as:

$$\mathbf{T}_k = \mathbf{A}_k \mathbf{G}_k \tag{2.12}$$

The columns that are not included in $\hat{\zeta}$ are not relevant, because they are multiplied by zeros from $\mathbf{\Lambda}_k$. As a result, (2.8) can be rewritten as:

$$\hat{s}_k = \mathbf{\Lambda}_k \mathbf{s}_k + \mathbf{A}_k \mathbf{G}_k \mathbf{n} \tag{2.13}$$

where the enhanced noise ($\mathbf{A}_k \mathbf{G}_k \mathbf{n}$) is similar to that described in the previous section, as it depends only on the channel matrices. Henceforth, all active MSs could transmit at their maximum transmission power without affecting each other's performance.

2.3 Antenna Selection Algorithm

A significant drawback evident in the system model presented above is that noise is modified (and potentially amplified) during the decoding procedure, which could degrade the signal-to-noise ratio (SNR) used when determining the BER for individual users after spatial stream decoupling. For this reason, a rate-adaptive algorithm and spatial coordination are proposed here to take advantage of the antennas associated with channel gains, thus resulting in lower BERs and contributing less to MU noise enhancement in the ZF-type algorithms at the BS receiver.

The user/antenna admission decision is made with the aid of a central controller unit that should first acquire the full CSI of the whole MU-MIMO system, which is usually available at the BS. The system model is now extended to $\ddot{K}$ available users where the kth user ($k \in 1, 2, \cdots, \ddot{K}$) has $\ddot{M}_k$ antennas. The scheduler has to limit the number of active MSs to K, and must meet the condition in (2.6) in order to control the number of enabled (transmitting) antennas. In general, the scheduling is done at

the BS, where the central unit can select any of the $\left(\begin{smallmatrix}\sum_{i=1}^{\ddot{K}} \ddot{M}_i \\ R\end{smallmatrix}\right)$ available combinations of transmit antennas ($\binom{n}{k}$ represents the binomial coefficient). Selected antennas that are associated with one or different users are allowed to transmit in a specific time slot, while the others are temporary disabled. There are two approaches for selecting the best combination of antennas to maximize the capacity on the parallel channels as in (1.9). One is based on reducing the effects of noise enhancement, whereas the other aims at increasing the effective signal gain after post-processing so as to overcome noise.

The first approach, which considers reducing the noise, is more appropriate for deployment with the ZF-only decoding method, because in this case the decoding matrix normalizes the effective gain after processing, as in (2.3). In light of (2.7), where $\mathbf{T}_k$ controls the noise variance after post-processing, the decoding matrix ($\mathbf{T}_k$) average gain values should be as low as possible, where $\mathbf{T}_k$ is the pseudo-inverse of $\mathbf{H}_k$ as discussed in (2.3). In general, the greater the fading channel gains, the lower the decoding matrix magnitude values. This in turn reduces the noise enhancement effects.

Table 2.1 presents the proposed algorithm to reduce MU noise enhancement, where the impact of all antennas is analyzed separately as a function of $\mathbf{h}_{km}$, where m denotes the mth antenna for user k; i.e., $\mathbf{h}_{km}$ is described as the mth column of $\mathbf{H}_k$. Hence, the channel gain per path is calculated and averaged over all R available spatial streams/paths. Finally, the antennas with the highest average path gain are selected for transmissions. The reduced complexity of the proposed algorithm is due to the fact that after ranking the channel gains, the algorithm selects for transmission only antennas with the highest gains, rather than processing all possible combinations of antennas.

When ZF is adopted in combination with SVD, the model takes advantage of added gains from the positive singular values in $\mathbf{\Lambda}_k$ resulting from the SVD. As in

Table 2.1: A rate-adaptive algorithm for the ZF approach.

Input
R: number of antennas for the BS
$\ddot{M}_k$: number of antennas per MS
$\ddot{K}$: number of available MSs
H_k: the channel matrix between the MSs and the BS
Algorithm
Begin
For k=1:$\ddot{K}$
  For m=1:$\ddot{M}_k$
    Calculate: the average channel path gain for $\mathbf{h}_{km}$
    Store: the value in $AvgGain(k, m)$
  end
end
Select: the maximum R value from $AvgGain$
      that corresponds to a specific user's antenna

the case of the ZF-only algorithm, a simplified algorithm is proposed in Table 2.2 to calculate the available spatial stream gain per antenna. The algorithm then finds the R antennas that are associated with the greatest added gain. This is done with the objective of increasing overall system capacity.

2.4 Simulation Results

In this section, the results of computer simulations are presented in order to analyze and investigate the performance of the proposed MU-MIMO ZF decoding strategies. The two approaches implemented are the stand-alone ZF approach, and the ZF approach integrated with SVD. These approaches are identified below as ZF and ZF-SVD, respectively. In the simulations, binary phase shift keying (BPSK) is adopted with the flat fading MIMO channels corrupted by omnipresent complex AWGN at the BS receive antennas. A single BS with four antennas is always used, and $\ddot{K}$ users are always available in the cell covered by this BS. Every user has $\ddot{M}$ antennas that

Table 2.2: A rate-adaptive algorithm for the ZF approach with SVD.

Input
R: number of antennas for the BS
$\ddot{M}_k$: number of antennas per MS
$\ddot{K}$: number of available MSs
H_k: the channel matrix between the MSs and the BS
Algorithm
Begin
For k=1:$\ddot{K}$
  For i=m:$\ddot{M}_k$
    Calculate: the Euclidean norm for H_{km}
    Store: the value in $ChannelGain(k, m)$
  end
end
Select: the maximum R value from $ChannelGain$
      that corresponds to a specific user's antenna
end

could be activated. The active configuration of MS antennas is usually written as (4, $[\ddot{M}_1,\ddot{M}_2,\ldots,\ddot{M}_K]$), where 4 represents the number of antennas at the BS. Moreover, a $R \times M$ SU-MIMO system with a maximum likelihood decoder with and without SVD is also implemented as a benchmark for comparisons, and is represented as (R,M). The two approaches were tested in simulations in terms of their performance as measured through the BER and system throughput, as a function of the SNR per receive antenna. System throughput is defined in this section as the number of correctly received bits at the BS per time slot from all active users considering that all transmissions are BPSK. This throughput could be considered as the measure for the total system sum rate though the latter one is going to be evaluated in other chapters using semi-analytical results based on (1.9) or (1.10).

Figure 2.2 provides the initial results for the BER as a function of the SNR, where the simulated strategies do not consider the proposed spatial coordination method and there are up to four (4) available MSs. Thus, the data streams are divided evenly

among the MSs, even if some users are experiencing a high level of distortion. The two MU-MIMO systems under consideration are a model with four MSs ($\ddot{K} = K = 4$), where every station is equipped with a single antenna ($\ddot{M} = M = 1$), and a model with two MSs ($\ddot{K} = K = 2$), with two antennas per MS ($\ddot{M} = M = 2$). Moreover, a 4×4 SU-MIMO system is implemented that utilizes the SVD. A comparison of the resulting curves shows that at a low SNR the 4×4 SU-MIMO systems exhibit better results. This is due to the fact that Gaussian noise at low SNRs can overwhelm the received signals when the data are decoded at the BS after post-processing. However, for SNR values of 15 dB or above, the MU-MIMO systems achieve BER values that are comparable to those of SU-MIMO systems.

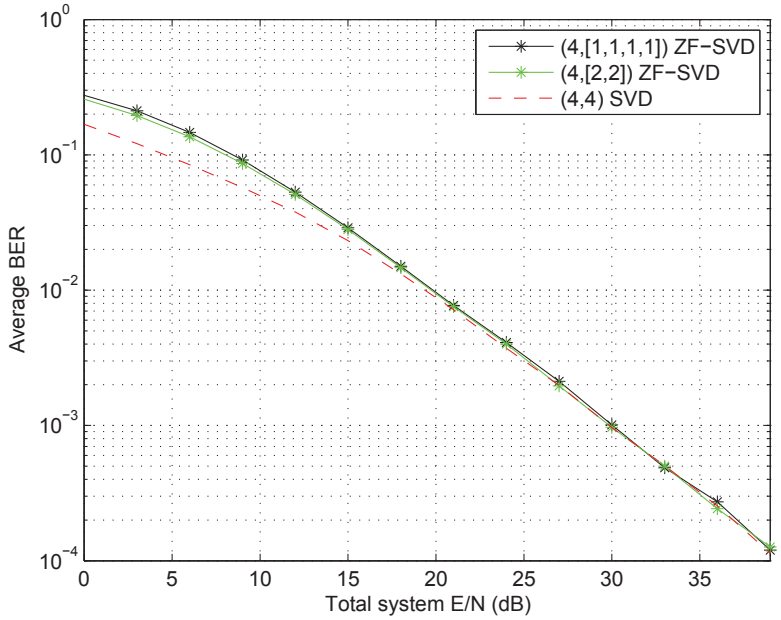

Figure 2.2: A comparison of SU-MIMO and MU-MIMO system BERs.

Figure 2.3 shows the BER as a function of the SNR for the enhanced signal processing algorithms proposed in this chapter. From five available MSs ($\ddot{K} = 5$), up to four "best" users ($K \leq 4$) with their corresponding antennas are selected for transmissions, to take advantage of user diversity. The two MU-MIMO systems implemented

use the ZF approach with and without SVD, based on rate adaptation. Both models consider five users, and every MS is equipped with four antennas ($\ddot{M} = 4$). Because the total number of MS antennas is greater than the number of BS antennas, a scheduling algorithm is applied here. Since users with the best channel conditions are to be selected, for a fair comparison, two SU-MIMO systems are adjusted, with five users from which to select. The results show that both of the systems investigated exhibit better BER values throughout the whole simulation, with savings equal to 1 dB at a BER of 10^{-3}.

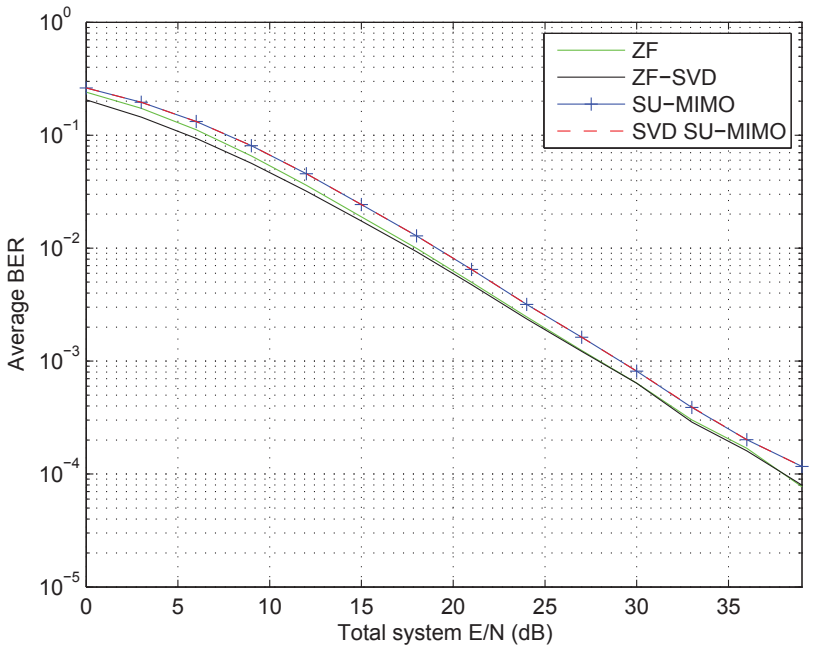

Figure 2.3: Comparison of BERs for a SU-MIMO system and a MU-MIMO system with spatial allocation.

The proposed ZF and ZF-SVD schemes were tested further by using Monte-Carlo simulations for the averaged system throughput as a function of SNR by averaging the results over random realization of channel gain matrices. This was compared with the throughput of the SU-MIMO approach. The results of these simulations

are shown in Figure 2.4. The models used are the same as those described for the previous test setups. It was found that the SU-MIMO systems achieve a better data rate at a low SNR, however with an increasing SNR the system throughput levels off at 3.7 bits/transmission. In contrast, the MU-MIMO systems with ZF alone exhibit low data rates at a low SNR, and with an increasing SNR the data rate increases to achieve the maximum possible value of 4 bits/transmission. It should be noted that the ZF-SVD approach represents the optimal solution, with the best competitive results at a low and high SNR.

Moreover, when ZF alone is compared with ZF-SVD at a low BER, it can be seen in Figures 2.3 and 2.4 that ZF-SVD achieves better results. This is due to the spatial gain obtained when using the SVD that increases the post-processed signal energy; this has a higher impact when transmitting with low power. From a statistical

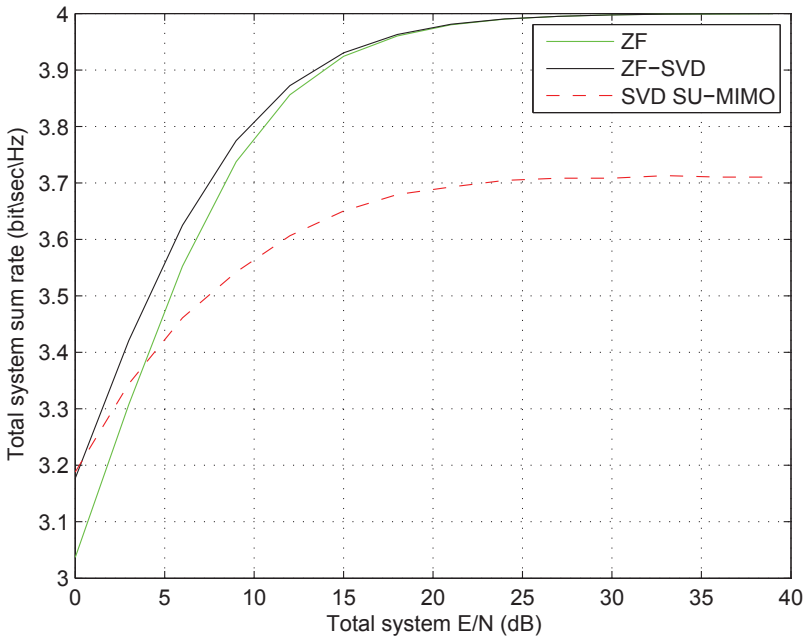

Figure 2.4: Comparison of system throughput for a SU-MIMO system and a MU-MIMO system with spatial allocation.

characterization of the antenna selection process for the two proposed algorithms, it was found that although they resulted in different selection combinations, this did not affect the system performance. Hence, it is concluded that the first algorithm is preferable due to its low complexity for calculating channel gains, as it can be applied to both system models.

In summary, Figure 2.2 shows that results for the multi-user approach are similar to those for the single-user approach, but with the advantage of allowing simultaneous user transmissions, i.e., with better fairness regarding MIMO channel access and no transmission delays. Furthermore, with the application of spatial coordination, the MU model achieved improved BER performance in comparison to the SU systems. This is also confirmed by the results of data rate tests shown in Figure 2.4. In this chapter, our investigation were focused on a small number of available MSs ($\ddot{M} = 5$), and we increase this parameter in the following chapters.

2.5 Summary

This chapter introduced an uplink ZF post-processing approach for MU-MIMO systems. Through decoupling the user streams at the BS, this technique could be adapted to allow simultaneous SU-MIMO transmissions of any kind, not necessarily limited to BPSK (provided that limitations on the number of antennas are met, and assuming access to global CSI at the BS). The available spatial streams are allocated centrally through antenna/user spatial coordination. The proposed approach ensures processing with low complexity, because no additional MU coding is required on the MS side. This provides the opportunity to build a cross-layer multiple access control protocol for MU-MIMO systems. Simulation results are also presented in order to compare the BER with that of corresponding currently used conventional systems. Furthermore, the throughput simulation results demonstrate the increased data rates that can be achieved.

Chapter 3

Resource Allocation and Noise Enhancement in an Uplink MU-MIMO Single-Cell System

As demonstrated in the previous chapter, MU-MIMO networks allow several users to utilize a common bandwidth simultaneously in the spatial dimension. In real wireless systems, MSs that are competing to access the channel must be coordinated in order to satisfy overall performance goals. As elaborated in this chapter, in the context of ZF post-processing at the BS, this is accomplished by developing centralized radio resource management (RRM) strategies that provide two basic functions. First, they limit the number of active antennas/users to comply with ZF decoding requirements. Secondly, in order to maximize the system sum rate, they implement power allocation based on the water-filling principle, to counter interference and noise enhancement effects. When users are admitted to send data, the state of the buffers at the MSs is also considered.

The purpose of this chapter is to analyze the noise in spatial streams on the uplink, when ZF-type post-processing is deployed with power allocation to decouple

user data [14]. The MSs use linear pre-processing based on SVD/beamforming in order to reduce noise and to allow basic power water-filling for their own spatial streams. As described in the general observation in [16], without beamforming at the MSs, power allocation maximizing the sum rate with ZF at the BS alone is not practically feasible, due to the complexity of the optimization algorithm.

Section 3.1 explains the analyzed system model, while Section 3.2 derives analytical representations for the power allocation algorithm, the capacity and the buffer conditions. The proposed schedulers for user/antenna and power selections are presented in Sections 3.3 and 3.4, where the corresponding simulation results are also provided. Finally, the chapter is summarized in Section 3.5

3.1 Single-Cell MU-MIMO System Model

The single-cell MU-MIMO model under study is illustrated in Figure 3.1. The number of MSs that are requesting access to the channel is given by $\ddot{K}$, while K represents the number of MSs that are considered as potentially active users. The BS is equipped with an array of R antennas, and all MSs have $\ddot{M}$ antenna(s). The green block represents the state of buffers at the MSs which initially is not taken into account, i.e., the buffers are always backlogged.

Every MS has unique flat fading channel gains, from its M_k active antenna(s) to the R antennas at the BS. For the kth user, this is represented by the channel matrix $\mathbf{H}_k$ with $R \times M_k$ dimensions. Throughout the encoding/beamforming at the MS and the decoding at the BS it is assumed that (i) every MS has full knowledge of the local channel state information at the transmitter (CSIT) between itself and the BS only, i.e., $\mathbf{H}_k$ for the kth user, and (ii) the central controller/scheduler at the BS is aware of all channel matrices $\mathbf{H}_k$, i.e., global CSI. A discussion concerning the distribution and "learning" of local and global CSI at the MSs and the BS and about the sending

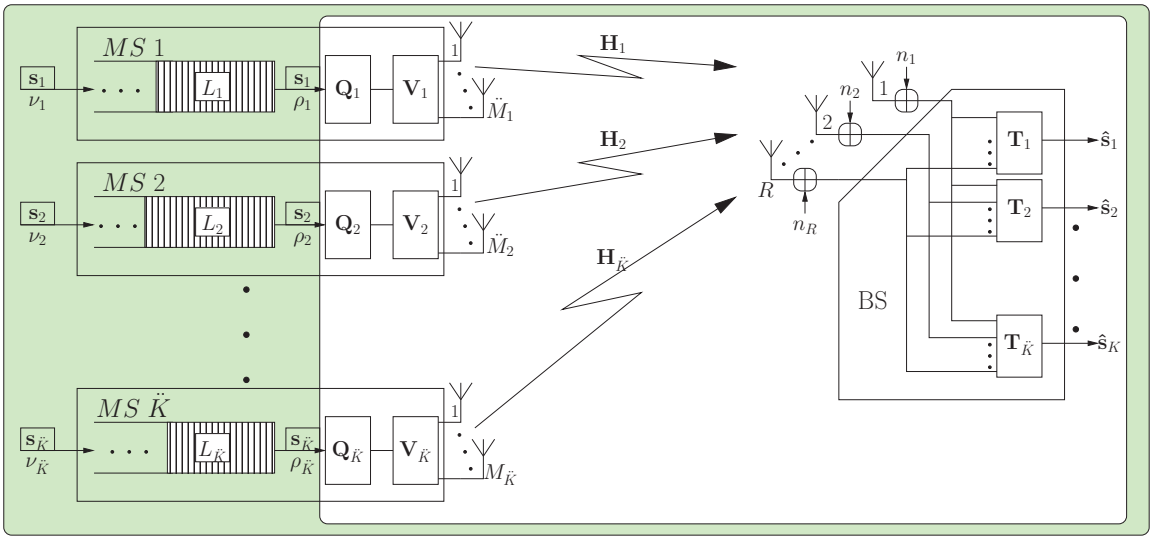

Figure 3.1: The uplink MU-MIMO system model.

of limited control information regarding user/antenna selection (feedback) is beyond the scope of this work. Since only local CSIT is assumed, the precoders at the MSs cannot be designed jointly. When mitigating the noise effects on their own spatial streams, the MSs will utilize the SVD of $\mathbf{H}_k$, where the fading channel matrix is represented as:

$$\mathbf{H}_k = \mathbf{U}_k \mathbf{\Lambda}_k \mathbf{V}_k^{\mathcal{H}} \tag{3.1}$$

and the $(^{\mathcal{H}})$ operator denotes the Hermitian transpose, while $\mathbf{U}_k$ and $\mathbf{V}_k$ are unitary matrices with size $R \times R$ and $M_k \times M_k$, respectively. $\mathbf{\Lambda}_k$ is a diagonal matrix that always holds the non-negative singular values (λ_{kx}) of $\mathbf{H}_k$. These values could also be described as the root mean square of the diversity spatial gain for the xth spatial channel allocated to the kth user .

3.2 Problem Formulation

3.2.1 Power Considerations

Prior to the pre-processing/multiplication of the transmitted signal at the MS by $\mathbf{V}_k$, it is also amplified with the power constraint:

$$P_k \geq \sum_{x=1}^{M_k} p_{kx} \tag{3.2}$$

where P_k is the constrained power for the kth MS and p_{kx} is the invested power at the xth spatial stream for the kth MS. The kth MS has access to a number of spatial streams, equal to the number of its active antenna (M_k). In the case where the channel between the kth MS and the BS is unknown, the power could be apportioned equally between transmit streams. However, when the local CSIT is available, a more efficient approach to distributing the power is to use the water-filling principle as described in [23, 9, 10]. From the perspective of a single user, the objective of using the water-filling approach is to bias the power distribution for certain spatial streams to increase the capacity C_k of user k, calculated in the presence of i.i.d. AWGN (with the variance σ_{kx}^2 for the xth spatial stream) as:

$$C_k = \max_{P_k \geq \sum_{x=1}^{M_k} p_{kx}} \sum_{x=1}^{M_k} \log_2 \left(1 + \frac{\lambda_{kx}^2 p_{kx}}{2\sigma_{kx}^2}\right) \tag{3.3}$$

Here, $\gamma_{kx} = \frac{\lambda_{kx}^2 p_{kx}}{2\sigma_{kx}^2}$ is the signal-to-noise ratio (SNR) for the xth spatial stream for user k, accounting for all processing at the MIMO transceiver(s). A water-filling solution for the power allocation in (3.3) is:

$$p_{kx} = \begin{cases} \frac{P_k}{\hat{\gamma}_k} - \frac{2\sigma_{kx}^2}{\lambda_{kx}^2} & \frac{\lambda_{kx}^2 P_k}{2\sigma_{kx}^2} \geq \hat{\gamma}_k \\ 0 & \frac{\lambda_{kx}^2 P_k}{2\sigma_{kx}^2} < \hat{\gamma}_k \end{cases} \tag{3.4}$$

where $\hat{\gamma}_k$ is the cutoff value for the kth MS.

3.2.2 Capacity Analysis

The signal transmitted from the kth MS is:

$$\mathbf{S}_k = \mathbf{V}_k \mathbf{Q}_k \mathbf{s}_k \tag{3.5}$$

with $\mathbf{Q}_k = \text{diag}\left(\sqrt{p_{k1}} \cdots \sqrt{p_{kM_k}}\right)$ being the diagonal gain scaling matrix and $\mathbf{Q}_k^2$ defining the $\overrightarrow{\mathbf{p}}_k = [p_{k1} \cdots p_{kM_k}]$ power allocation vector. In the wireless channel, the signals from K users are summed together, and at the BS the received signal is:

$$\mathbf{y} = \sum_{i=1}^{K} \mathbf{U}_i \mathbf{\Lambda}_i \mathbf{V}_i^{\mathcal{H}} \mathbf{S}_i + \mathbf{n} \tag{3.6}$$

where $\mathbf{y}$ and $\mathbf{n}$ are $R \times 1$ column vectors, and the rth elements from both vectors represent the signal at the rth receiving antenna and the corresponding AWGN, respectively.

To retrieve the original data $\mathbf{s}_k$ transmitted from the kth MS, at the BS the received signal in (3.6) is passed through the ZF decoding matrix $\mathbf{T}_k$, in order to cancel the MAI. The decoded data of the kth user is thus:

$$\hat{\mathbf{s}}_k = \mathbf{T}_k \left(\sum_{i=1}^{K} \mathbf{U}_i \mathbf{\Lambda}_i \mathbf{V}_i^{\mathcal{H}} \mathbf{S}_i + \mathbf{n} \right) \tag{3.7}$$

The decoding matrix $\mathbf{T}_k$ is calculated on the basis of representing it as a product of two matrices: $\mathbf{T}_k = \mathbf{A}_k \mathbf{G}_k$ as described in (2.12). The derivation of G_k is based on the null operator as shown in (2.9), where null($\mathbf{X}$) calculates the orthonormal basis for the null space of $\mathbf{X}$, and $\mathbf{G}_k$ thus cancels all of the multiuser interference. When $\mathbf{Q}$ is diagonal (more generally invertible), null($\mathbf{XQ}$) = null($\mathbf{X}$), and there is no need to consider power matrices when calculating $\mathbf{G}_k$.

From (2.12), the post-processed signal at the BS in (3.7) can be rewritten as:

$$\hat{\mathbf{s}}_k = \mathbf{\Lambda}_k \mathbf{Q}_k \mathbf{s}_k + \mathbf{A}_k \mathbf{G}_k \mathbf{n} \tag{3.8}$$

The noise affecting data recovery for the kth MS is:

$$\widetilde{\mathbf{n}}_k = \begin{bmatrix} \widetilde{n}_{k1} \\ \vdots \\ \widetilde{n}_{kM_k} \end{bmatrix} = \mathbf{A}_k \mathbf{G}_k \mathbf{n} \tag{3.9}$$

where $\widetilde{n}_{kx}$ shows on the xth spatial stream for the kth MS. The post-processed, or enhanced, noise $\widetilde{\mathbf{n}}_k$ is caused by the MU-MIMO decoding matrix, $\mathbf{A}_k\mathbf{G}_k$, multiplying AWGN vector $\mathbf{n}$ at the R antennas of the BS. The latter is common when decoding all K users. Thus $\widetilde{\mathbf{n}}_k$ depends only upon channel matrices related to the other transmitting MSs, i.e., $\mathbf{U}_l$ and $\mathbf{\Lambda}_l$ with $l \neq k$. As a result, power allocation vectors $\overrightarrow{\mathbf{p}}_k$ from any of the k MSs do not affect the post-processed noise $\widetilde{\mathbf{n}}_k$. Hence, with the assumption of independent components in $\widetilde{\mathbf{n}}_k$, (3.3) can now be rewritten as:

$$C_k = \max_{P_k \geq \sum_{x=1}^{M_k} p_{kx}} \sum_{x=1}^{M_k} \log_2 \left(1 + \frac{\lambda_{kx}^2 p_{kx}}{2\hat{n}_{kx}^2}\right) \tag{3.10}$$

where $\hat{n}_{kx}^2$ is the variance of the post-processed noise on the xth spatial stream when decoding user k, and is given by the xth diagonal element of $\mathbf{A}_k\mathbf{G}_k(\mathbf{A}_k\mathbf{G}_k)^{\mathcal{H}}$. It was later verified when simulating the algorithms that the assumption of independence did not affect the results significantly. In the case when the noise is dependent, deterioration in performance has been demonstrated in [52].

In (3.10), the capacity optimization is expressed from the perspective of a single user. The eventual objective of a system is to optimize power allocation (and antenna selection) so as to maximize the system capacity given by the sum rate of all active users. Therefore, the total system sum rate optimization is expressed as:

$$C_{system} = \max_{\Omega} \sum_{k \in \Omega} C_k \tag{3.11}$$

where Ω is a set with K elements, that indexes the selected MSs and their associated antennas/power.

3.2.3 Buffer Analysis

In addition to the sum rate analysis with resource allocation at the physical link layer, this dissertation also considers user scheduling based the state of user buffers. When data buffers are considered in order to decide on user transmissions, this becomes a MAC layer issue, which in this case is integrated with RRM.

Figure 3.1 illustrates in green that every MS is regarded as having its own buffer of infinite capacity, containing data of size L_k for user k, where working with finite buffer size is beyond the scope of this work. The arrival and dispatch rate are represented by ν and ρ, respectively. At a specified time (t), the current buffer size for MS k is calculated by using Little's law, $L_k(t) = (\nu_k - \rho_k(t))t$, where $\nu_k = \nu$ is considered a constant value for Poisson traffic (with the same load for all users), while ρ_k changes through the time slots, as it is dependent upon the multiuser scheduling algorithm and the MS channel conditions (resource allocation and spatial channel capacity).

3.3 Best Channel Scheduling Algorithms

The primary aim of this chapter is to design resource allocation and scheduling algorithms for a single-cell network, in light of the noise and capacity analysis in the previous section. The proposed schemes maximize the overall system sum rate by selecting preferential antennas (and corresponding power allocations) associated with the admitted MSs. The desgined schemes are refered to as best channels schuduling algorithems because we select the antennas and corosponing transmission power from the finite set of potential solutions but beccuase of limited search space we do not guarantee the optimal solution. To take advantage of user diversity, a distinction is made between the K potentially active users and the total number of users in the system $\ddot{K}$. The algorithm design is based on selecting R antennas to transmit, from

all of the available MS antennas, while temporarily disabling the rest. The general flow of all of the algorithms developed in this section is presented in Figure 3.2.

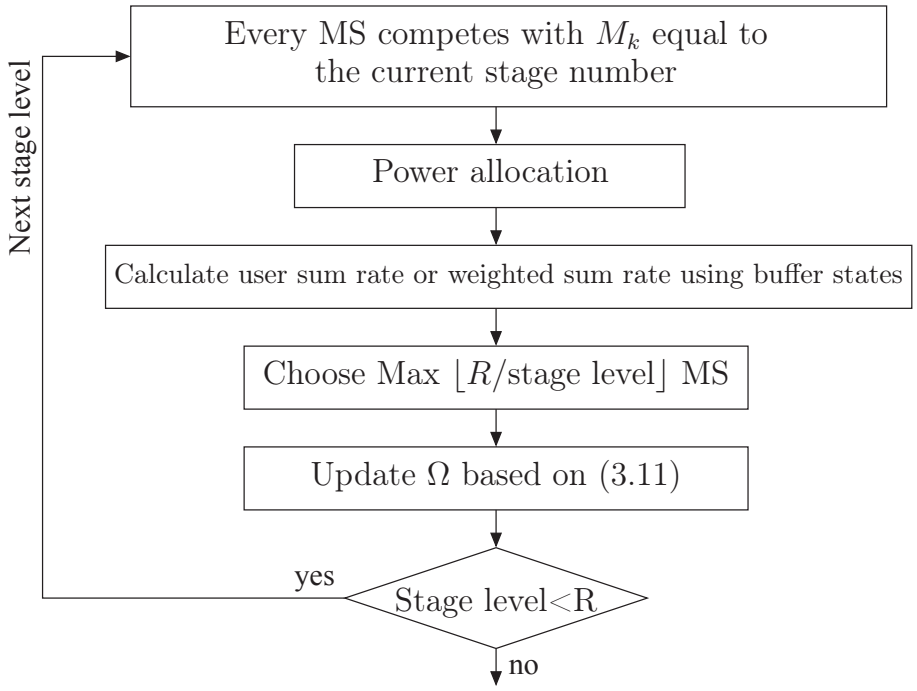

Figure 3.2: General flow of proposed algorithms for the single-cell system.

Initially all antennas of all MSs individually compete to gain access to the MU-MIMO channel, regardless of the state of the MS buffers. All of the following designs are based on the total system sum rate optimization presented in (3.11) and (3.10), and the consideration that at most only R MSs can be selected from the available $\ddot{K}$, in order to comply with condition (2.6).

To this end, without yet considering buffers, two antenna selection algorithms are proposed. The first algorithm, presented in Section 3.3.1, utilizes diversity spatial gain information alone in order to assess different available antenna combinations that could offer the best sum rate performance, i.e., assuming fixed noise levels independent of other users in making the evaluation (3.10). This scheme results in a very low-complexity algorithm. The second algorithm, presented in Section 3.3.2, includes

multiuser noise enhancement effects and spatial gain in its calculations when deciding on the R MS antennas, hence there is a higher level of complexity. The resulting trade-off between the two proposed algorithms is improved system capacity with more accurate user/antenna selection, versus increased complexity.

3.3.1 Best Channels Based on Spatial Gains

In this algorithm, to maximize the sum rate given in (3.11), the selection of users and their antennas is based exclusively on λ_{kj} values, assuming that $\hat{n}_{kj}^2 = \sigma^2$ on all spatial streams. This would ensure an increased value of the numerator in (3.10), that in turn increases the SNR on the assigned spatial streams in a suboptimal way. Also, this approach does not require feedback from the BS to the MSs concerning the power allocation vectors $\overrightarrow{\mathbf{p}}_k$, as users could calculate $\overrightarrow{\mathbf{p}}_k$ based on their local CSIT.

The algorithm is divided into R stages: The first stage considers allowing only one spatial stream per MS, the second stage allows two spatial streams, and so on. Dividing the algorithm into stages yields a less complex design and a more flexible algorithm, as will be seen below. Before beginning the first stage, it is important to organize and sort the antennas from best to worst, based on the spatial channel diversity gain for every MS. The antenna with the highest gain for MS k is indexed as J_{k1}, and the gain value is represented as $\lambda_{kJ_{k1}}$. Similarly, the mth best antenna is represented as J_{km}, with gain value $\lambda_{kJ_{km}}$. Hence, when stage one starts it considers only the best antenna J_{k1} for all MSs, and discards the remaining $\ddot{M}_k - 1$ antenna(s). This reduces the number of processed antenna combinations. The initially selected candidates are stored in Ω, where they represent the best R MSs that would satisfy (3.11), with a maximum of one spatial stream per MS.

The second stage, where a MS could occupy two spatial streams, would then select $\lfloor R/2 \rfloor$ stations, where $\lfloor \cdot \rfloor$ represents the floor operation. For this stage, the two best antennas are selected for every MS (J_{k1} and J_{k2}). However, the channel gains must

be recalculated, as their values are adjusted when enabling another antenna on the same device. The water-filling process is now considered, as it assists in dividing the available power efficiently between the two potential streams, as described in (3.4). Thus, if the division of power is not allowable for a certain MS, it will no longer compete within this stage. Only $\lfloor R/2 \rfloor$ MSs obtain the highest capacity by using (3.3), with a maximum of two antennas per MS ($M_k = 2$). Lastly, all of the $\lfloor R/2 \rfloor$ selected stations from the current stage then compete with the candidates resulting from the previous stage (Ω). Hence, a new list of candidates is formed, and Ω is updated with a certain combination which meets the condition of (2.6) and ensures the maximum sum rate as provided by (3.10).

The algorithm advances successively to each of the following stages, where the allowable number of antennas is equal to the stage level, $M_k =$ (stage level), and only $\lfloor R/$(stage level)$\rfloor$ MS(s) are selected. Subsequently, the selected stations compete with those on the updated candidate list (Ω) from the previous stage only. The final stage, stage R, yields the final list of candidates, which shows the MS(s) that have been selected to transmit and the antenna indexes to which they have access.

3.3.2 Best Channels Based on Spatial Gains and Noise Enhancement Effects

In this algorithm, for the calculation of power allocation vectors and the user capacity in Figure 3.2, both the numerator and denominator of SNR in (3.10) are considered. Therefore, when noise enhancement exists, additional processing in calculating the SNR on spatial streams following post-processing and more feedback information, i.e., information about $\overrightarrow{\mathbf{p}}_k$ being sent to MSs, could be utilized in order to increase the algorithm selection accuracy, so as to maximize the actual sum rate.

In this method, because of the dependence between C_k and $\hat{n}_{kx}^2$ ($x \in \{1, \cdots, M_k\}$)

as presented in (3.10), the water-filling of $\overrightarrow{\mathbf{p}}_k$ for user k is not completely independent of other users, because $\hat{\mathbf{n}}_k^2$ depends on $\mathbf{U}_l$ and $\mathbf{\Lambda}_l$ with $l \neq k$, i.e., global CSI. Therefore, the calculation of $\hat{n}_{kj}^2$ precedes water-filling to find $\overrightarrow{\mathbf{p}}_k$, thus obtaining C_k. This is not a substantial computation increase, but it requires feedback to the MSs concerning $\overrightarrow{\mathbf{p}}_k$. This algorithm benefits from being divided into stages of differing complexity. In order to reduce the search space, the algorithm includes the scheduling/admission incorporating noise enhancement effects only in certain stages, referred to as vital stages. For all other stages, the algorithm with only a spatial gain decision is considered, which provides a less complex design.

3.3.3 Simulation Results

In this section, analytical and simulation results are presented in order to investigate the performance of the proposed antenna selection and power allocation algorithms. The two algorithms proposed: (i) Best channels (BCs) based on spatial gains, and (ii) BCs based on spatial gains and noise enhancement effects, are identified below as BC-SpG and BC-SpG/NE, respectively. A single BS is deployed with four receiving antennas ($R = 4$), and all $\ddot{K}$ users in the system are equipped with the same number of $\ddot{M}$ antennas ($\ddot{M}_1 = \ddot{M}_2 = \cdots = \ddot{M}_{\ddot{K}} = \ddot{M}$), where in most of the simulations $\ddot{K} = 5$ and $\ddot{M} = 4$.

Table 3.1 compares the BC-SpG/NE algorithm with a brute force exhaustive search in terms of statistics for the best antenna number configurations. In the table, the first row shows the combination (1,1,1,1), meaning that a total of four MSs are selected to maximize the sum rate, and that each station is assigned one spatial stream. The only other statistically significant combination is shown in the second row (2,1,1) with three active users, one with two spatial streams, and two MSs with one spatial stream each. From this table, it is clear that the (1,1,1,1) combination dominates overall. Hence, the algorithm BC-SpG/NE would consider stage one to

be the vital stage, i.e., when BC-SpG/NE is executed there is a high frequency of correctly selecting the optimum combination in the first stage.

Figure 3.3 shows the semi-analytical results for the total system sum rate as a function of SNR (E/N). This analysis investigates BC-SpG with and without a consideration of noise enhancement, as shown in Figure 3.3 by a dashed and solid black line, respectively. The performance of the latter scheme is close to the downlink

Table 3.1: Percentages of combination occurrence.

Combinations	Algorithms	
	Brute Force	BC-SpG/NE
1,1,1,1	98.42 %	99.71 %
2,1,1	1.58 %	0.17 %
2,2	0	0
3,1	0	0.07 %
4	0	0.05 %

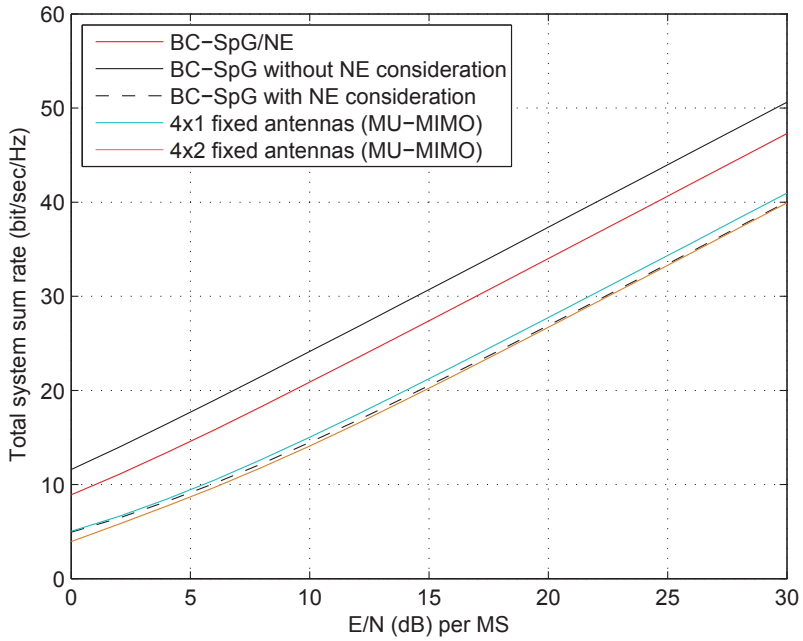

Figure 3.3: A sum rate comparison between antenna selection versus user selection methods for a MU-MIMO model.

performance; it is not affected by the noise enhancement problem and is presented as a benchmark. This figure also illustrates the performance of the BC-SpG/NE selection method (shown by a red line) when the algorithm is run with only stage one as the vital stage, with minimal degradation relative to the exhaustive search. In addition, the performance of two brute force algorithms is included for comparison, where the same number of MSs are selected with fixed (not optimized) antenna(s). As can be seen in the figure, a performance drop of $\sim$ 10bps/Hz occurs when noise enhancement (uplink transmission) is incorporated into simulations and calculations for the sum rates in the BC-SpG algorithms (solid versus dashed black lines). An analysis of the BC-SpG which considers noise enhancement shows that its performance is between the two benchmark results with fixed antennas. This means that the BC-SpG has a slight advantage due to its flexibility in assigning the spatial streams. The BC-SpG/NE algorithm is able to compensate for the capacity drop, with an improvement of 5dB over either the BC-SpG or the systems with fixed antennas.

Next, the complexity of the algorithms is analyzed, by comparing the complexity of both proposed scheduling schemes with that of the brute force search algorithm. The complexity is measured in terms of antenna combinations that are processed to arrive at the combination resulting in the highest total sum rate. Assuming that $\ddot{K} \geq R$ and $\ddot{M} = R$, the BC-SpG algorithm processes:

$$\binom{\ddot{K}}{R} + \sum_{\varsigma=2}^{R} \left(\binom{R-\varsigma+2}{\lfloor R/\varsigma \rfloor} + \sum_{\hat{\varsigma}=1}^{\lfloor R/\varsigma \rfloor} \binom{\lfloor R/\varsigma \rfloor}{\hat{\varsigma}} \binom{R-\varsigma\hat{\varsigma}+2}{R-\varsigma\hat{\varsigma}} + 1 \right) \tag{3.12}$$

combinations, where ς denotes the stage count. If stage one is considered to be the vital stage for BC-SpG/NE, as illustrated in Figure 3.3, then its complexity (in terms of antenna combinations to process) is given by:

$$R\ddot{M}\binom{\ddot{K}}{R} + \sum_{\varsigma=2}^{R} \left(\binom{R-\varsigma+2}{\lfloor R/\varsigma \rfloor} + \sum_{\hat{\varsigma}=1}^{\lfloor R/\varsigma \rfloor} \binom{\lfloor R/\varsigma \rfloor}{\hat{\varsigma}} \binom{R-\varsigma\hat{\varsigma}+2}{R-\varsigma\hat{\varsigma}} + 1 \right) \tag{3.13}$$

where both(3.12) and (3.13) express the worst case complexity.

Figure 3.4 illustrates the number of combinations processed by the BC-SpG and BC-SpG/NE algorithms (indicated by black and red lines, respectively), based on (3.12) and (3.13) as a function of $\ddot{K}$. For comparison purposes, the complexity of the brute

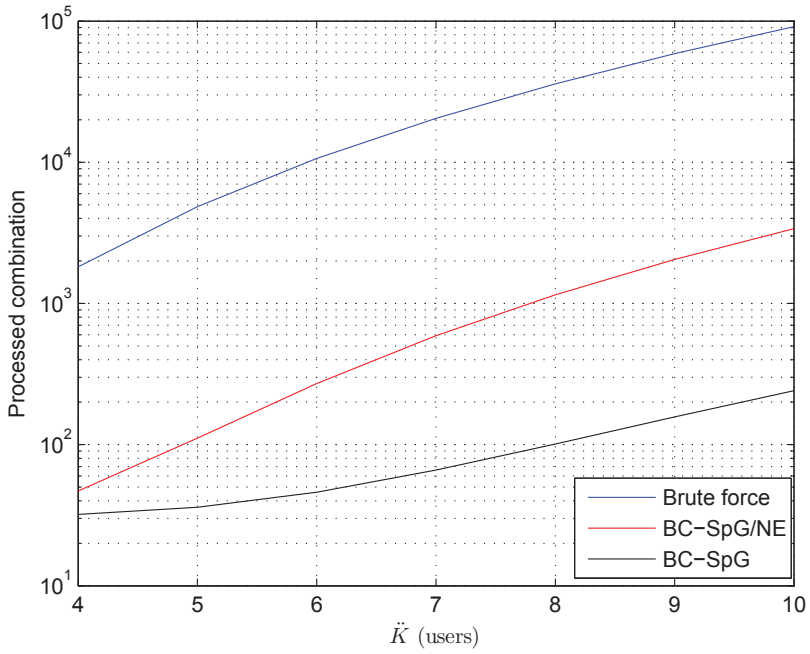

Figure 3.4: Comparison of complexity.

force search algorithm is plotted with a blue line as a benchmark; here the brute force algorithm would have to go through $\binom{KM}{R}$ different combinations in order to maximize the system capacity. From the figure, it can be seen that BC-SpG is the least complex algorithm, however it does not achieve a high total system sum rate, as shown in Figure 3.3. The BC-SpG/NE algorithm has a marginal increase in complexity, especially at low $\ddot{K}$ values, but it provides an improved total sum rate. Finally, the brute force algorithm performs a far greater number of processed combinations, which makes it an impractical solution in real-time applications.

3.4 Fair Rate Load-Adaptive Algorithm

This section deals with a more complex problem of user/antenna selection, by considering the CSI and buffer behavior jointly. The cost function in the decision process adopts an approach similar to that presented in [53] and [54], by utilizing the buffer state information, including the buffer size, the maximum delay time and arrival rate, and the weighted capacities of admitted users. Specifically, this section focuses on the weighted buffer size, referred to as g_k for the kth MS. As shown in Figure 3.1, every MS has its own buffer with L_k stored bit(s). Thus the weighted buffer ratio can be expressed as:

$$g_k = \frac{L_k}{\sum_{i=1}^{\ddot{K}} L_i} \tag{3.14}$$

To ensure fairness among users and to give preference based on the amount of queued data in addition to the CSI, the central controller/scheduler optimizes the weighted sum rate of (3.10) based on (3.14), as follows:

$$\max_{\Omega} \sum_{k \in \Omega} g_k C_k \tag{3.15}$$

If MS k transmits a portion of it buffered then L_k will decrease. As a result, g_k will also decrease when MS k go back to compete for the following time slot, which gives it less priority as it had cleared few of it data, and higher priority to those who have more stored data. This algorithm follows the same stages as the algorithms BC-SpG and BC-SpG/NE presented in the previous section, but calculates the weighted capacity according to (3.15), as opposed to using the sum of individual terms as in (3.11).

3.4.1 Simulation Results

In this section, the performance of the fair rate load-adaptive algorithm (FRLA) is analyzed. The same simulation setup is used as in Section 3.3.3, where a common

BS is equipped with four antennas. The number of competing MSs varies, as noted for the different simulations; whereas the number of antennas available at the MSs is always fixed at two.

Figures 3.5, 3.6 and 3.7 show the current buffer size, the standard deviation of all buffer sizes, and the sum dispatch rate versus the time slots (packet durations), respectively. The two algorithms that are under investigation in these simulations are the BC-SpG/NE (with no buffer consideration) and the FRLA, shown in red and green, respectively. In addition, the performance of a load-adaptive (LA) algorithm, where antenna selection is based purely on the buffer weight, is included for comparison and plotted with a blue line. The simulation results, which are averaged over a thousand runs, consider $\ddot{K} = 10$ MSs equipped with $\ddot{M} = 2$ antennas. For each scheduling scheme, Figure 3.5 plots the maximum, mean and minimum buffer sizes

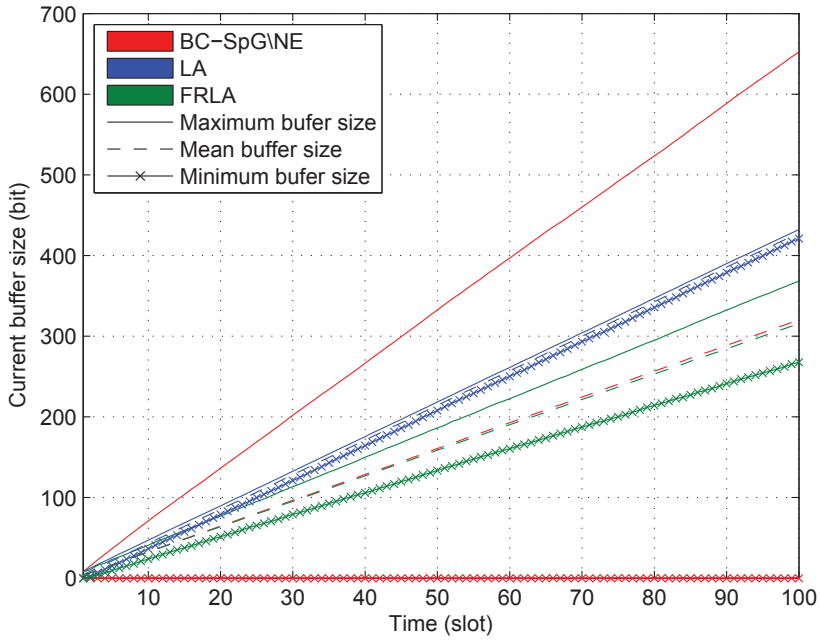

Figure 3.5: Comparison of different algorithms in terms of current buffer size, at $\ddot{K} = 10$.

for all MSs; these are represented as solid, dashed and starred lines, respectively.

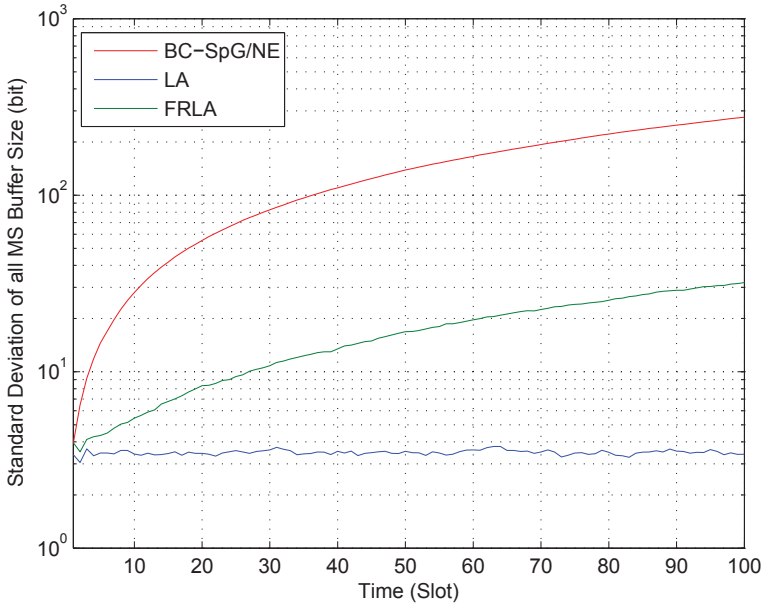

Figure 3.6: Comparison of different algorithms in terms of buffer size standard deviation, at $\ddot{K} = 10$.

Figures 3.5 and 3.6 show that the BC-SpG/NE scheme has the greatest variability in terms of buffer size. This variability is due to the unfairness of this selection approach, as the MSs with the best channel conditions cause buffer overruns for users with channel conditions that are worse (though still acceptable for transmission). The LA algorithm addresses the buffer overrun problem by allocating access to the channel based on the buffer size, ensuring full utilization of the buffer as a resource among all MSs. However, the LA scheme would significantly reduce the system dispatch rate, as shown in Figure 3.7. For the three algorithms tested, Figure 3.7 shows that FRLA has the highest dispatch rate. In particular, it outperforms the BC-SpG/NE algorithm, i.e., channel utilization is better than with BC-SpG/NE. Figure 3.5 also demonstrates that the FRLA algorithm has good buffer behavior.

Figures 3.8, 3.9 and 3.10 show simulations similar to those presented in Figures 3.5

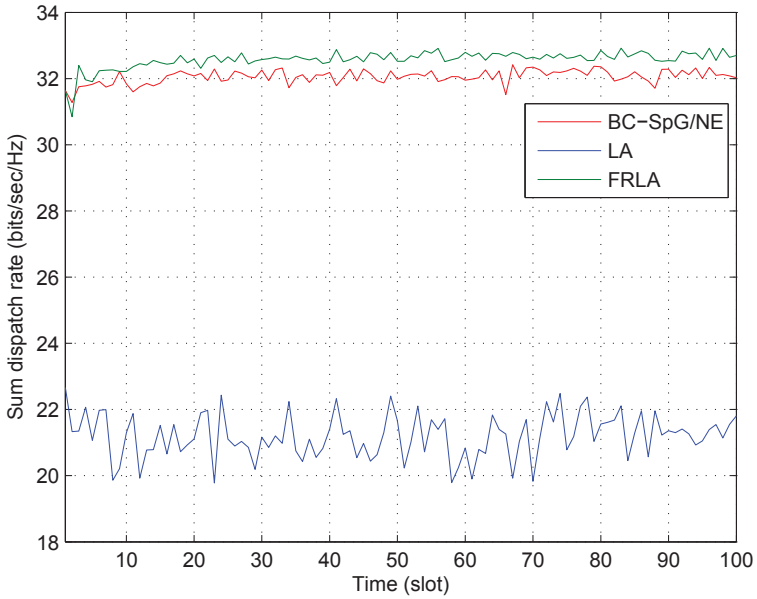

Figure 3.7: Comparison of different algorithms in terms of total system dispatch rate, at $\hat{K} = 10$.

to 3.7, but with a reduced number of MSs. Here $\ddot{K} = 5$, while all other attributes are kept the same, in order to analyze the effects of user density. Figure 3.8 suggests that the FRLA scheme achieves the best results, whereas for the BC-SpG/NE and LA algorithms the buffer size continues to increase linearly. Because the FRLA scheme always favors MSs that have good CSI conditions and a high volume of cashed data, this scheme is able to keep up with the arrival rates. This helps with the management of buffer content, so as to avoid any overflows that may occur with the BC-SpG/NE and LA schemes.

Hence, for a low- or high-density user environment, the FRLA scheduler exhibited the best performance. It had a higher dispatch rate under all conditions, as compared with the BC-SpG/NE algorithm, and better buffer behavior than the LA algorithm.

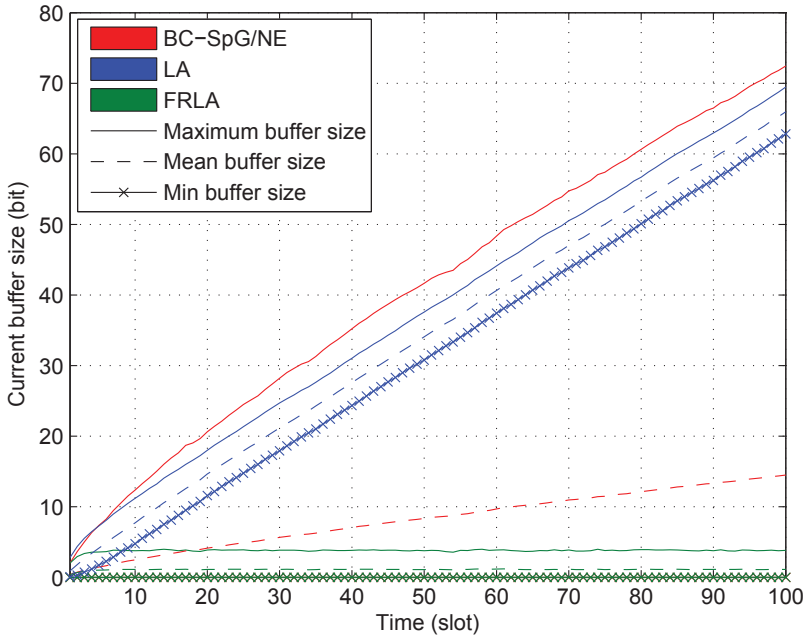

Figure 3.8: Comparison of different algorithms in terms of current buffer size, at $\ddot{K} = 5$.

3.5 Summary

A design and performance analysis of resource allocation and scheduling algorithms on the uplink has been presented for a MU-MIMO transmission strategy that employs beamforming and power allocation, utilizing local CSIT at the MSs and ZF post-processing at the BS using global CSI. Through first analyzing the noise enhancement at the receiver side, the SNR on the spatial channels was derived for such a system and used in further analyses of the total sum rate calculations. The statistical results presented demonstrate that with the approach of searching through the limited antenna sets when optimizing the sum rate, there is not much performance degradation in comparison to the results of exhaustive search solutions. The analysis and results validate the efficiency of the joint resource allocation and scheduling strategy proposed with a ZF receiver for a single-cell environment.

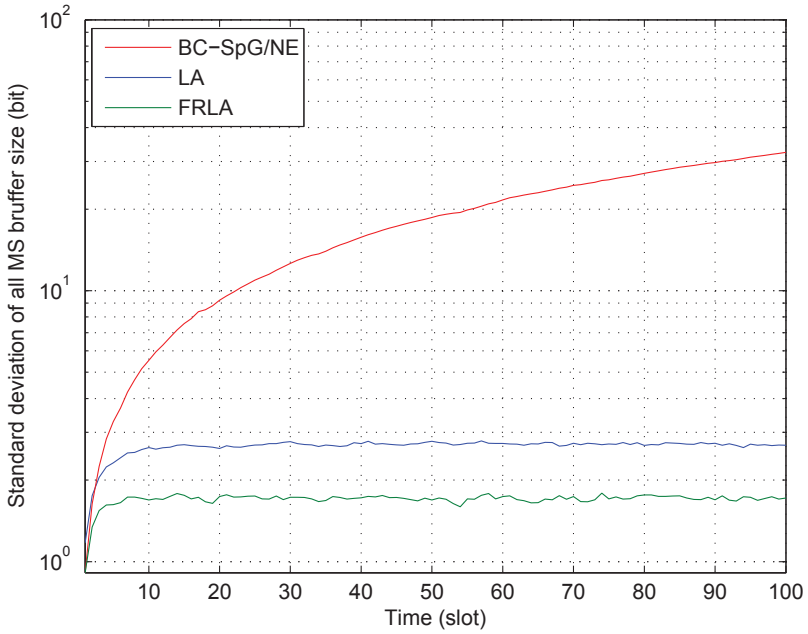

Figure 3.9: Comparison of different algorithms in terms of buffer size standard deviation, at $\ddot{K} = 5$.

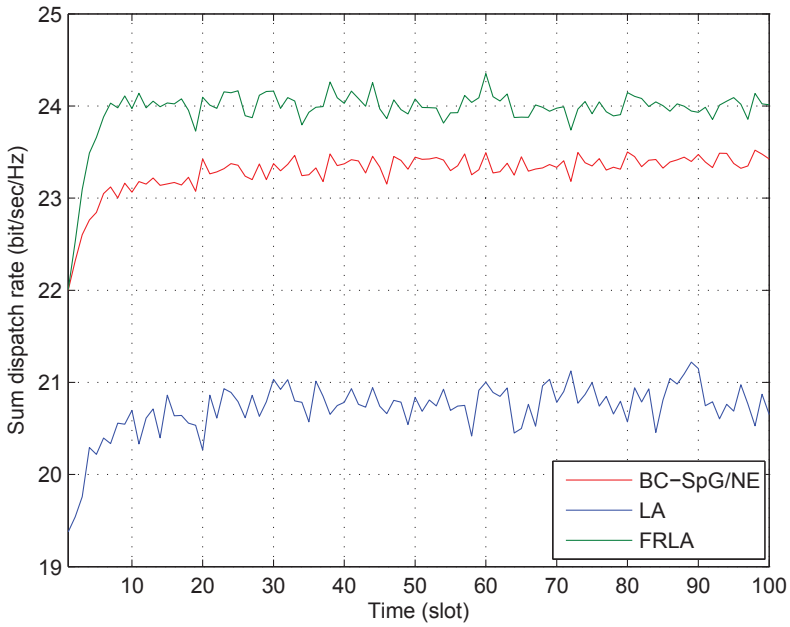

Figure 3.10: Comparison of different algorithms in terms of total system dispatch rate, at $\ddot{K} = 5$.

Chapter 4

Spatial Coordination and Cooperative Reception in a Double-Cell Environment

In the previous chapters, the MU-MIMO system has been investigated within a single-cell environment. In this chapter, the focus is on the operation of the MU-SIMO system in a double-cell system model, where two BSs with multiple antennas serve a number of MSs with single antennas simultaneously in the same frequency band. The general case of a multi-cell MU-MIMO system is considered in Chapter 5. In such systems, it is necessary to account for two types of interference: (i) intra-cell interference, and (ii) inter-cell interference (ICI). Intra-cell interference can be dealt with at the BSs by employing ZF multiuser decoders that mitigate noise enhancement effects, as described in previous chapters. To address problems related to ICI, this dissertation develops spatial coordination algorithms that reduce the impact of ICI. Specifically, in this chapter an interference-aware scheduling scheme is designed and integrated with cooperative reception (CR), where some data are decoded by combining signals from both BSs. In addition, for better control of the interference, a

second scheme is also presented that employs a successive interference canceler (SIC).

The chapter is organized into five sections. Section 4.1 explains the underlying multi-cell system model. In Section 4.2, derivations are presented for the capacity analysis. The multi-cell spatial coordination algorithm is developed in Section 4.3, while the corresponding simulations and analytical results are discussed in Section 4.4. Finally, a summary of the chapter is provided in Section 4.5.

4.1 A Double-Cell System Model

The network under consideration is illustrated in Figure 4.1. There are K active MSs in the area, serviced by $B = 2$ BSs. Each BS is equipped with an array of R receiving antennas, allowing it to be associated with up to R MSs, while each MS has a single antenna. All active MSs transmit their signals (s_k) to the corresponding BS in the same time slot, using the same bandwidth, where k is the global index assigned to the active MS ($k \in \{1, 2, .., K\}$).

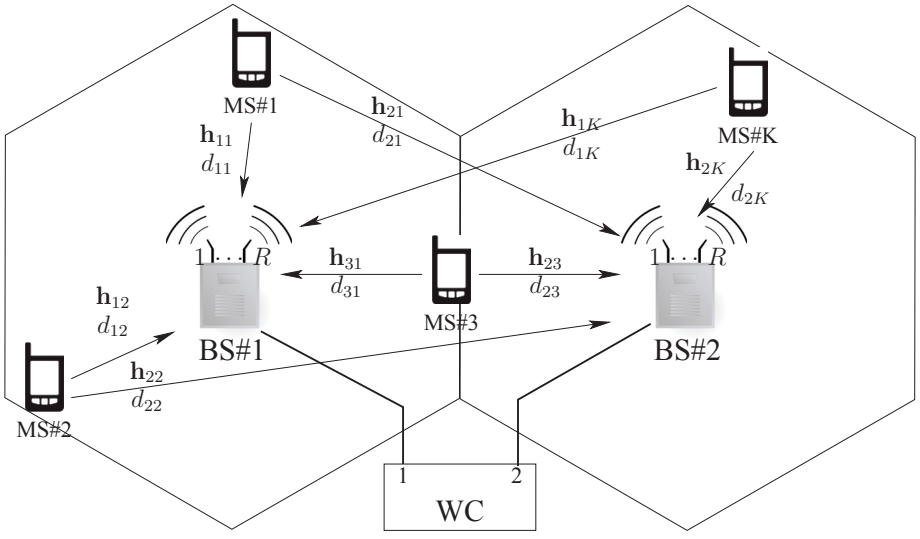

Figure 4.1: The two-cell MU-MIMO model.

From the MS antenna, flat fading channel gains to each accessible BS are assumed. The channels are represented by matrices (column vector) $\mathbf{h}_{bk}$ with $R \times 1$ dimensions, where b is the BS identifier ($b \in \{1, 2, .., B\}$; although in this chapter $B = 2$, general notation is employed, because some of the formulas will be reused in the next chapter). Assuming Rayleigh fading, elements of the channel matrices are i.i.d., zero-mean complex Gaussian RVs with a unit variance ($h_{bk}(i, j) \sim \mathcal{CN}(0, 1)$). Because there are multiple BSs in the system, in this model it is necessary to consider the deterministic attenuation of signals with distance. henceforth, the signal received at BS b is expressed as:

$$\mathbf{y}_b = \sum_{\forall k \in \Omega_b} D_{bk}\mathbf{h}_{bk}\sqrt{p_k}s_k + \sum_{\forall \hat{k} \notin \Omega_b} D_{b\hat{k}}\mathbf{h}_{b\hat{k}}\sqrt{p_{\hat{k}}}s_{\hat{k}} + \mathbf{n} \tag{4.1}$$

where $\hat{k}$ identifies the MSs that are assigned to other cells and cause the ICI, and p_k represents the power at the transmitter used by the kth MS. The data set Ω_b holds all the MS indexes that are assigned by the scheduler to access BS b. D_{bk} represents macro-scale signal attenuation, where the path loss coefficient between MS k and BS b is defined as $D_{bk} = 1/d_{bk}^{\alpha}$, and d_{bk} is the distance between MS k and BS b ($d_{bk} > 0$). Furthermore, $\alpha = 2$ is considered for ground wave propagation [55]. A simple power allocation is applied, where the power invested by MS k depends upon the distance traveled, so as to achieve a targeted SNR, $p_k = SNR \cdot d_{bk}^{2\alpha} \mid k \in \Omega_b$. The first summation term in (4.1) represents the information intended for the bth BS, while the second term of the equation represents all of the ICI affecting the bth BS. Complex AWGN is represented by elements of the matrix $\mathbf{n}$ with the dimensions $R \times 1$.

4.2 A Two-Layer Decoder

This chapter proposes a two-layer decoding mechanism. The first step is performed at the BS, immediately after the signal is received. This process is responsible for decoupling multiuser transmissions by applying the ZF approach; henceforth, the intra-cell interference is resolved. In the second step, for the MSs assigned to be handled by a single BS, after being processed by the decoding matrix, the resulting signal is passed through a maximum likelihood decoder (MLD) to retrieve the original data through hard-decision decoding. In the case of MSs that are handled by multiple BSs, after being processed by the decoding matrices at different BSs, the signals representing the same data are fed back to the WC to be processed by a diversity decoder. The WC employs maximal-ratio combining (MRC), to combine the multiple signals received into a single signal before passing it to the MLD. To improve the performance of MRC, another decoding approach is also proposed, where MRC is aided by SIC (MRC-SIC) to reduce the effects of ICI.

4.2.1 ZF Detection at the BS

The ZF is utilized to separate the mixed signals, based on the acquisition of CSI at the receiver. In order to retrieve the original signal sent by MS k from (4.1), the decoder of BS b multiplies $\mathbf{y}_b$ in (4.1) by $\mathbf{T}_{bk}$ as follows:

$$\begin{aligned}\hat{s}_k &= \mathbf{T}_{bk} D_{bk} \mathbf{h}_{bk} \sqrt{p_k} s_k \\ &+ \mathbf{T}_{bk} \left(\textstyle\sum_{\forall \bar{k} \in \Omega_b, \bar{k} \neq k} D_{bk} \mathbf{h}_{bk} \sqrt{p_k} s_k \right) \\ &+ \mathbf{T}_{bk} \left(\textstyle\sum_{\forall \hat{k} \notin \Omega_b} D_{b\hat{k}} \mathbf{h}_{b\hat{k}} \sqrt{p_{\hat{k}}} s_{\hat{k}} \right) + \mathbf{T}_{bk} \mathbf{n}\end{aligned} \tag{4.2}$$

Here $\mathbf{T}_{bk}$ is the multiuser ZF decoding matrix described in (2.4), with size $1 \times R$. It satisfies:

$$\begin{aligned}\mathbf{T}_{bk} \mathbf{h}_{bk} &= 1 \\ \mathbf{T}_{bk} \mathbf{h}_{b\bar{k}} &= 0\end{aligned} \tag{4.3}$$

where indices $\bar{k}$ refer to the MSs assigned to the bth BS, excluding MS k, and they cause intra-cell interference. As a result, (4.2) can be rewritten as:

$$\hat{s}_k = D_{bk}\sqrt{p_k}s_k + \mathbf{T}_{bk}\left(\sum_{\forall \hat{k} \notin \Omega_b} D_{b\hat{k}}\mathbf{h}_{b\hat{k}}\sqrt{p_{\hat{k}}}s_{\hat{k}}\right) + \mathbf{T}_{bk}\mathbf{n} \tag{4.4}$$

where the intra-cell interference is canceled at the cost of noise enhancement resulting from the multiplication by $\mathbf{T}_{bk}$ of ICI and AWGN. Therefore, the total system capacity achieved by MS k can be derived as follows:

$$C_{bk} = \log_2\left(1 + \frac{D_{bk}^2 p_k}{|\sigma_0^2 \mathbf{T}_{bk}\mathbf{T}_{bk}^{\mathcal{H}}| + \sum_{\forall \hat{k} \notin \Omega_b}\left|\mathbf{T}_{bk}\mathbf{h}_{b\hat{k}}D_{b\hat{k}}\sqrt{p_{\hat{k}}}\right|^2}\right) \tag{4.5}$$

where σ_0^2 and $^{\mathcal{H}}$ are the variance of the AWGN and the Hermitian operator, respectively.

4.2.2 Cooperative Reception at the WC

In certain scenarios, for MS distribution within the cells, it is preferable to disable a few MSs initially selected by the scheduler in a conventional one-to-one mapping of users or their spatial streams to the closest BSs, i.e., within the cell. This has the purpose of reassigning the vacated spatial streams to enhance the performance of "under-performing" MSs, and allowing the signals from these MSs to be handled by more than one BS. Thus, spatial decoding operations must be considered, in order to combine multiple replicas of the same signal efficiently. One of the best combining techniques is MRC, where multiple received signals, which represent the same data, are weighted with appropriately selected coefficients to improve the BER performance. This process can be carried out at the WC by sending the multiple versions of signals representing the same data from different BSs to the WC via the backhaul (wired) links. For MS signals received by more than one BS that are

processed with ZF decoding matrices for intra-cell interference removal, from (4.4), the combined received signal can be written as:

$$\begin{aligned}\hat{s}_k &= \textstyle\sum_{\forall b|k\in\Omega_b} w_{bk}\Big(D_{bk}\sqrt{p_k}s_k \\ &\quad +\mathbf{T}_{bk}\textstyle\sum_{\hat{k}\notin\Omega_b}\mathbf{h}_{b\hat{k}}D_{b\hat{k}}\sqrt{p_{\hat{k}}}s_{\hat{k}}+\mathbf{T}_{bk}\mathbf{n}\Big)\end{aligned} \tag{4.6}$$

where w_{bk} are weighting factors dependent on instantaneous SNRs, or rather SINRs, for different replicas of the same signal [23]. Here it is worth noting that assigning the kth MS to multiple BSs reduces the number of MSs contributing to ICI. The reason is that this MS then contributes to intra-cell interference at two BSs, which is canceled with ZF signal separation by using different decoding matrices for different BSs. The ICI level is therefore reduced for all signals received, at the expense of fewer connected MSs in the system, as compared to the situation where the MS is handled by only one BS. Therefore, from (4.6), the instantaneous signal-to-interference-to-noise ratio (SINR) can be expressed as:

$$SINR_k = \frac{p_k\left|\sum_{\forall b|k\in\Omega_b} w_{bk}D_{bi}\right|^2}{E\left[\left|\sum_{\forall b|k\in\Omega_b} w_{bk}\mathbf{T}_{bk}\mathbf{\Psi}_b\right|^2\right]} \tag{4.7}$$

where $\mathbf{\Psi}_b$ is a $R\times 1$ matrix representing the ICI and AWGN affecting BS b, and it is derived as:

$$\mathbf{\Psi}_b = \sum_{\hat{k}\notin\Omega_b}\mathbf{h}_{b\hat{k}}D_{b\hat{k}}\sqrt{p_{\hat{k}}}s_{\hat{k}}+\mathbf{n} \tag{4.8}$$

If, as in the present case, only two BSs are considered, the ICI level for both BSs can be considered to be balanced and independent, because a MS communicating with one BS interferes only with the other BS. Therefore, (4.7) can be simplified as follows:

$$SINR_k = \frac{p_k\left|\sum_{\forall b|k\in\Omega_b} w_{bk}D_{bk}\right|^2}{E\left[\sum_{\forall b|k\in\Omega_b}\left|w_{bk}\mathbf{T}_{bk}\mathbf{\Psi}_b\right|^2\right]} \tag{4.9}$$

Substituting $u_{bk} = w_{bk}\mathbf{T}_{bk}\mathbf{\Psi}_b$ in (4.9) yields:

$$SINR_k = \frac{p_k \left| \sum_{\forall b|k\in\Omega_b} u_{bk} \frac{D_{bk}}{\mathbf{T}_{bk}\mathbf{\Psi}_b} \right|^2}{E\left[\sum_{\forall b|k\in\Omega_b} |u_{bk}|^2 \right]} \tag{4.10}$$

The SINR reaches a maximum value if u^*_{bk} is set to $\frac{D_{bk}}{\mathbf{T}_{bi}\mathbf{\Psi}_b}$, where * stands for the complex conjugate operator. Therefore, for a signal sent from MS k to BS b, the MRC coefficient is:

$$w_{bk} = \frac{D_{bk}}{|\mathbf{T}_{bk}\mathbf{\Psi}_b|^2} \tag{4.11}$$

Substituting (4.11) in (4.9) allows the SINR to be rewritten as:

$$SINR_k = p_k \left(\sum_{\forall b|k\in\Omega_b} \frac{D^2_{bk}}{E\left[|\mathbf{T}_{bk}\mathbf{\Psi}_b|^2 \right]} \right) \tag{4.12}$$

As a result, the user data rate is:

$$C_k^{MRC} = \log_2 \left(1 + p_k \left(\sum_{\forall b|k\in\Omega_b} \frac{D^2_{bk}}{E\left[|\mathbf{T}_{bk}\mathbf{\Psi}_b|^2 \right]} \right) \right) \tag{4.13}$$

4.2.3 Cooperative Reception with Successive Interference Cancellation

The maximum achievable data rate in (4.13) is limited by the presence of ICI that affects the corresponding BSs. Henceforth, SIC is utilized in order to eliminate the ICI. However SIC is only applied on the MSs that are CR to limit the growth of system complexity. This can be done at the WC as shown in Figure 4.2, provided that the BSs forward both hard- and soft-decoded data to the WC [1, 56]. The hard-decoded data, shown as a dashed line, result from resolving the data related to MS antennas that are associated with only one BS. Hence, ZF post-processing is performed at the BS, followed by maximum likelihood estimation. The forwarded soft-decoded data

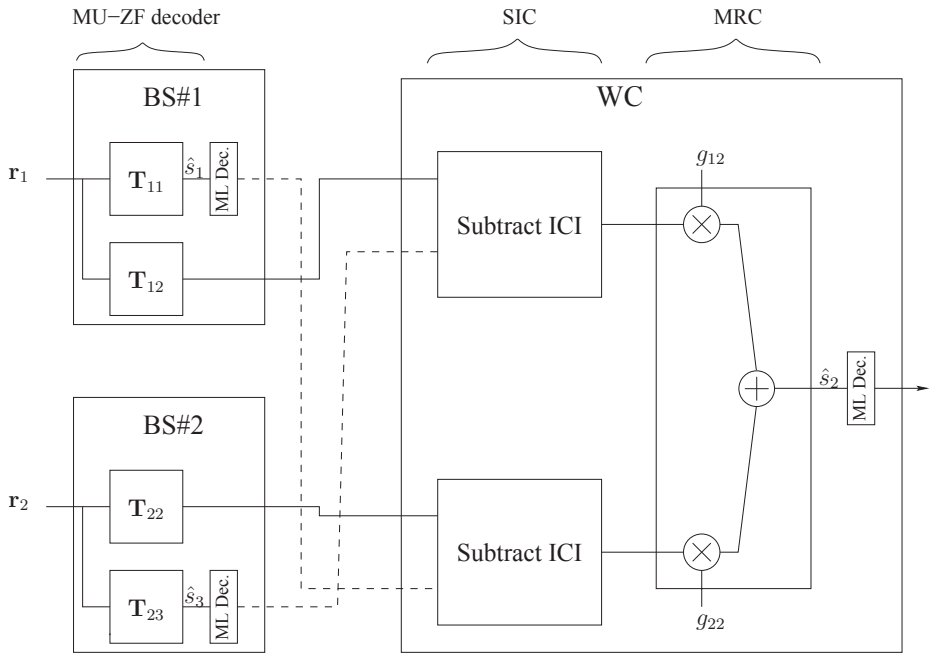

Figure 4.2: The MRC-SIC decoder.

represent the signals that are intended to be resolved at multiple BSs. As a result, the ZF process is only implemented on the received signal to deal with the intra-cell interference, and the processed data are then forwarded to the WC. The WC receives all of the information and, assuming full CSI knowledge, the centralized controller is able to subtract all of the ICI before combining the multiple signals with MRC. This permits (4.13) to be rewritten as:

$$C_k^{MRC-SIC} = \log_2 \left(1 + p_k \left(\sum_{\forall b | k \in \Omega_b} \frac{D_{bk}^2}{E\left[|\mathbf{T}_{bk}\mathbf{n}| \right]^2} \right) \right) \tag{4.14}$$

The power allocation assigned to the kth MS in (4.13) and (4.14) is adjusted to accommodate the multiple streams utilized. Therefore,

$$p_k = \frac{SNIR}{\left(\sum_{\forall b | k \in \Omega_b} D_{bk}^2 \right)} \tag{4.15}$$

4.3 A Multi-Cell Scheduling Algorithm

The aim of this algorithm is to maximize the total system sum rate by focusing on reducing the ICI, in accordance with the analysis in the previous section. This is done by temporarily disabling a number of selected MSs that are experiencing a high level of interference, and assigning the free streams to previously selected MSs, thus increasing the utilization of the CR approach. The scheduling process is carried out by the WC, with the assumption that it has full knowledge of the distances between the BSs and MSs (d_{bk}). This involves the long-term average of the received signal strength, referred to in the literature as the received signal strength indicator (RSSI). Figure 4.3 illustrates the general flow of the proposed algorithm, which proceeds in the following steps:

1. For every path between BS b and MS k, calculate its weight g_{bk}, where

$$g_{bk} = \frac{D_{bk}}{\sum_{\forall \hat{b} | \hat{b} \neq b} D_{\hat{b}k}} \tag{4.16}$$

The weighting scheme reflects the ratio between the attenuation coefficient for the described path and the summation of attenuation coefficients for the other paths with which MS k interferes. Therefore, the selection of MSs with high weighted values reflects either high sum rates for the specific MSs, or a low level of interference caused by them.

2. Select the highest R MSs based on their weights, and add their indexes in Ω_b.

3. For BS b, find

$$\min_{k}(d_{bk}) \; \forall k \in \Omega_b \tag{4.17}$$

$$\max_{\hat{k}}(d_{b\hat{k}}) \; \forall \hat{k} \in \Omega_{\hat{b}}, \hat{k} \notin \Omega_b | \hat{b} \neq b \tag{4.18}$$

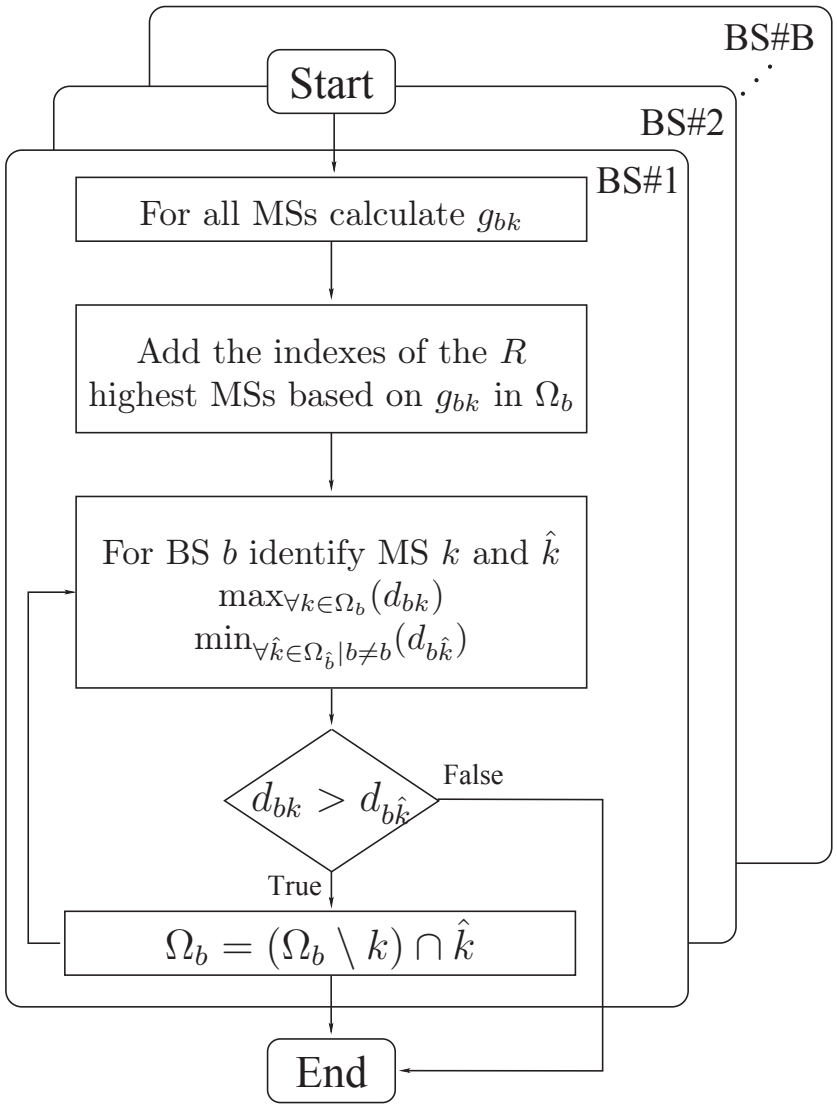

Figure 4.3: General flow of the spatial allocation algorithm for the multi-cell systems.

This step is not executed until step 2 has been performed for all B BSs, where all initial Ω_b are set.

4. If $d_{bk} < d_{b\hat{k}}$, then exit.

5. Remove k from Ω_b, replace it with $\hat{k}$, and go to step 3.

The last two steps address the situation where there is a MS (k) associated with a certain BS (b) positioned behind an interfering MS ($\hat{k}$) from another cell. The algorithm solves this problem by disabling k and replacing it with the interfering MS. This procedure thus reduces the global ICI level.

With regard to the trade-off between the total system sum rate and fairness among MSs, this algorithm neglects fairness in favor of increasing the system capacity. However, this proposed approach could be extended to solve this problem, by modifying the cost function (4.16) according to [53].

4.4 Simulation Results

In this section, analytical and simulation results are presented in order to investigate the performance of the proposed decoders and user selection algorithms for the two-cell uplink MU-SIMO model considered. The three decoders analyzed are: (i) ZF and MRC-SIC, with the assumption that noise enhancement does not affect the performance – this unrealistic model is used only as a benchmark; (ii) ZF and MRC-SIC based on (4.5) and (4.14); and (iii) ZF and MRC based on (4.5) and (4.13). In addition, two selection algorithms are considered: (i) the proposed algorithm from Figure 4.3 (identified as *Alg. 1*); and (ii) a simplified algorithm that is based on executing only the first two steps discussed in Section 4.3 (identified as *Alg. 2*). All simulations consider two BSs ($B = 2$) equipped with two antennas ($R = 2$). The $\ddot{K}$ MSs are uniformly distributed over a rectangular area of size 25×25 [normalized unit of space], and $\ddot{K} = 5$ unless otherwise noted. In addition, the BSs are positioned on a diagonal in the rectangular service area, and are equidistant from the center and the adjacent corners. Total system sum rate is evaluated as sum of capacities like in (4.5) and (4.14) or (4.15) averaged over random locations of MSs.

Figure 4.4 shows the semi-analytical results for the total system sum rate as a

function of SNR. For *Alg. 1* (with blue performance curves), the best performance is achieved when it is used with ZF and MRC-SIC without noise enhancement (solid blue line). The same algorithm with ZF and MRC-SIC decoders, with noise enhancement (dashed blue line), attains a similar performance at the expense of a longer convergence time to find the optimum parameters. When MRC is used without SIC, a drastic reduction ($\sim$ 5 bits/sec/Hz) in system performance is seen (dashed and dotted blue line). The performance of decoding strategies using *Alg. 2*, shown in Figure 4.4 by red lines, is always poorer than that of strategies using *Alg. 1*.

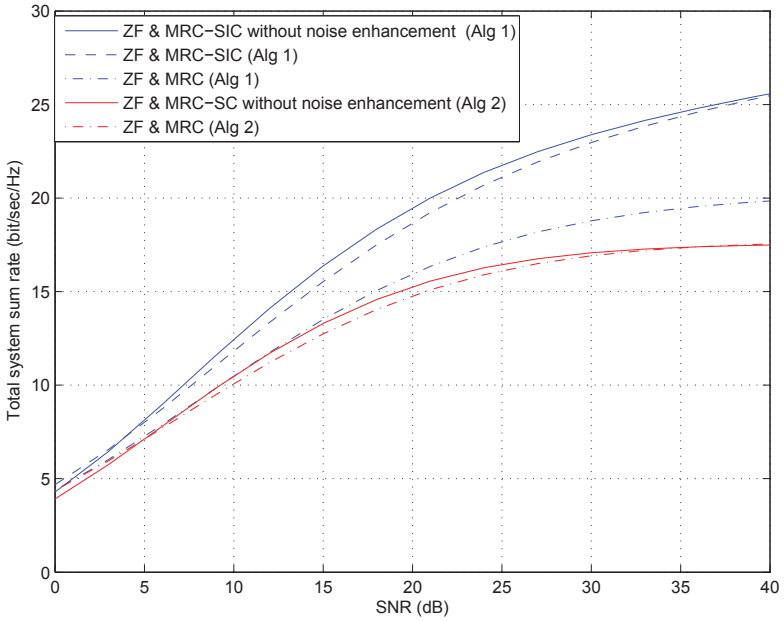

Figure 4.4: Comparison of total system sum rates plotted against the SNR.

Figure 4.5 presents results for total system sum rates as a function of $\ddot{K}$ evaluated at SNR=36 dB, as shown by blue and red performance curves for *Alg. 1* and *Alg. 2*, respectively. In this figure it can be seen that the plotted results exhibit an increase in total system sum rate with an increase in the number of available users. Because higher values of $\ddot{K}$ are associated with a greater number of choices, this increases

the probability of selecting users with good channel conditions. When $\ddot{K} = 2$, all simulations indicate the same performance; both algorithms result in the same selection, since 2 MSs are always selected. The greatest difference in performance occurs when $R \cdot B = \ddot{K} = 4$. This is due to the utilization of CR by *Alg. 1*, which employs the possibility of canceling one or two users to achieve a higher performance. With an increasing number of MSs, all of the curves indicate comparable results, with a decrease of ~ 2.5 bit/sec/Hz due to noise enhancement caused by the ZF decoding matrix.

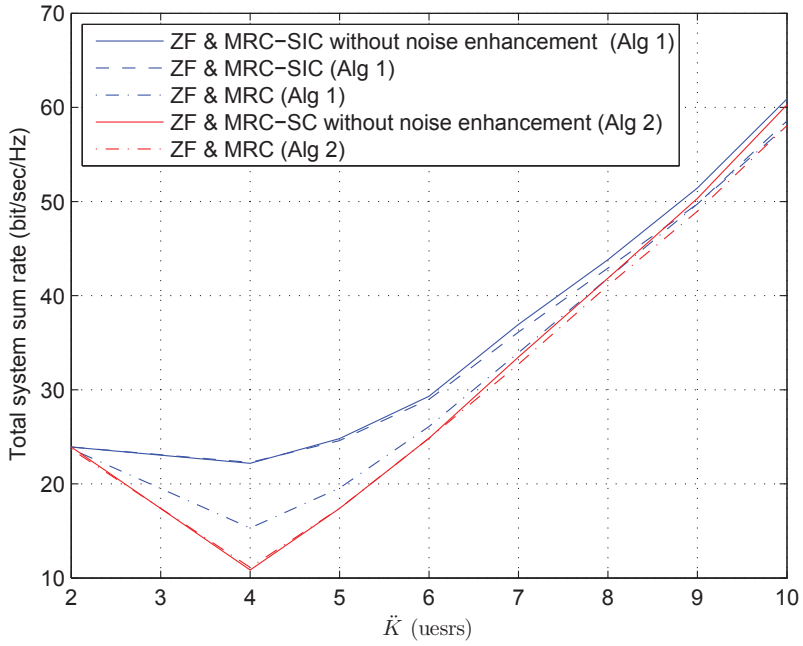

Figure 4.5: Comparison of total system sum rates plotted against MS density.

Figure 4.6 shows the total system sum rate performance when fixed power is applied to all transmissions, for the same setup as considered in Figure 4.4. For simplicity, the magnitude of the noise affecting all receivers is assumed to be 1 watt. From Figure 4.6, it can be seen that low performance is caused by noise enhancement,

although a slight improvement in system performance is achieved when SIC is utilized. Therefore, for systems that are restricted to fixed power, special consideration should be given to channel gains (CSI) when selecting the MS, so as to reduce noise enhancement caused by the ZF decoder.

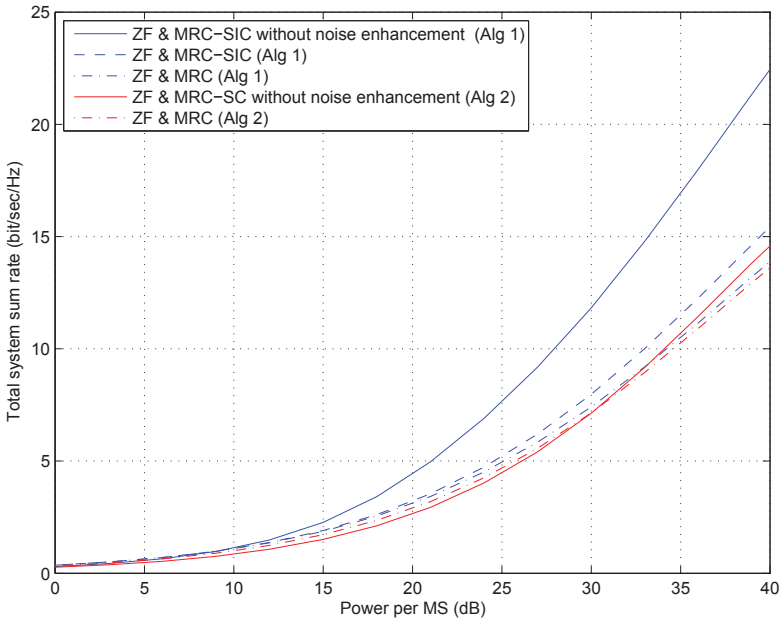

Figure 4.6: Comparison of total system sum rates plotted against power per MS.

4.5 Summary

A performance analysis of different decoding designs for two-cell uplink MU-SIMO is presented. First, investigations are conducted for sum rate performance using the ZF post-processing decoupling of spatial streams, which applies to MSs that are associated with a single BS. Secondly, the performance of MSs that are associated with multiple BSs is derived, where MRC or MRC-SIC is utilized to combine multiple replicas of a common signal. Moreover, a selection algorithm is designed to control

and limit the ICI level. The analysis and results demonstrate that a huge gain is achieved when applying the proposed antenna selection algorithm, with even better performance when SIC is deployed. However, further analysis should be carried out to consider channel gains in the selection algorithm with a higher density of users.

Chapter 5

Resource Management for Multi-Cell Networks

In the previous chapter, a system model was presented that is applicable to multi-cell networks, however only two-cell MU-SIMO systems were analyzed. On the one hand, intra-cell interference was dealt with by using a ZF canceler, as in the case of the single-cell systems. On the other hand, the impact of ICI was reduced by a CR method that improved the performance of the underlying two-cell system. However, as noted by this author in [41], these algorithms do not scale well when performing with a number of active MSs. Therefore, in this chapter, a more sophisticated RRM and scheduling algorithm is introduced for more general systems. The proposed algorithm utilizes spatial coordination together with a power allocation algorithm to deal with under-performing antennas/users. Due to its low complexity and fast convergence, Newton's method of optimization is employed to manage the transmission power levels [32].

The chapter is organized as follows: The generalized multi-cell system model is described in Section 5.1. The capacity formula and Newton's method derivations for the current system model are presented in Sections 5.2 and 5.3, respectively.

Section 5.4 introduces the proposed resource allocation algorithm, while Section 5.5 presents the simulation results. Finally, Section 5.6 concludes the chapter.

5.1 The Multi-Cell System Model

The multi-cell network model under study is illustrated in Figure 5.1, where the $\ddot{K}$ MSs are distributed randomly in the area serviced by B BSs. Each BS is equipped with an array of R receiving antennas, allowing it to be associated with up to R MSs, while each MS has $\ddot{M}_k$ antenna(s) ($\ddot{k} \in \{1, 2, .., \ddot{K}\}$ and $\ddot{M}_{\ddot{k}} \geq 1$). All BSs are connected via a reliable backbone to a centralized WC, where joint detection is

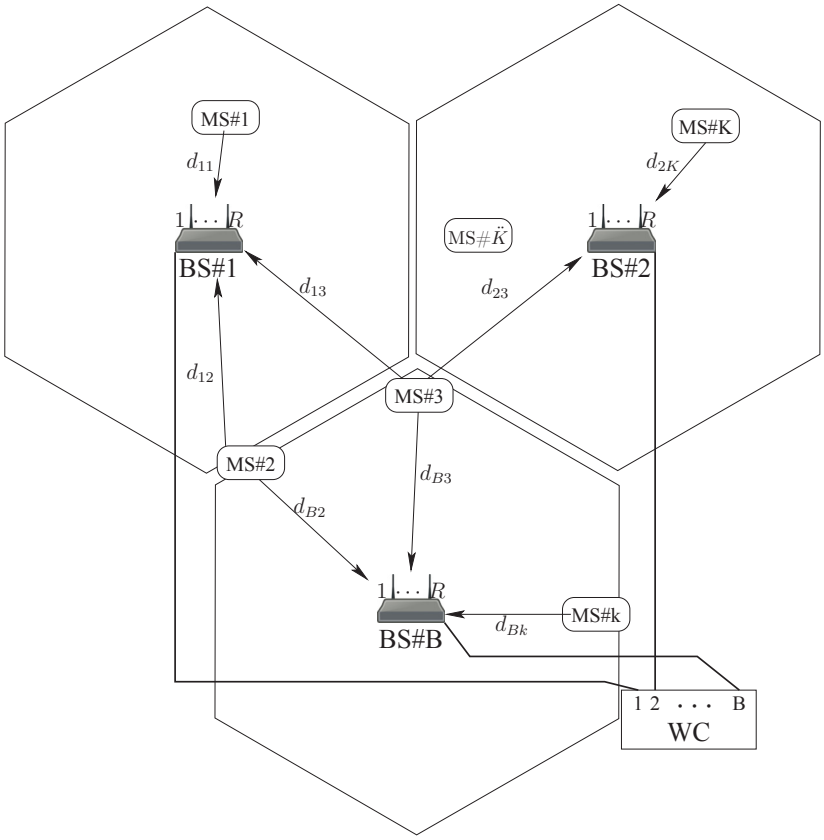

Figure 5.1: The uplink multi-cell MU-MIMO system model.

performed by using soft decisions from BSs for certain users. The power allocation is implemented at the WC, which requires knowledge of the global CSI, while the spatial coordination is done distributively, as it requires only the local CSI. The spatial coordination is performed based on the CSI for each antenna at a MS and the designated BS. Only K of $\ddot{K}$ MSs are permitted to transmit their signals ($s_{km},\ \mid m \in 1, \ldots, \ddot{M}_{\ddot{k}}$) to the corresponding BS in the same time slot using the same bandwidth, where s_{km} represents the scalar data sent from mth antenna of the kth user. This chapter breaks away from the conventional representation of the received data that uses column vector representations of the transmitted data and channel gain matrices, as in (2.1). Further analysis is accommodated by working with the scalar representations of transmitted data and column vectors $\mathbf{h}_{bkm}$ representing Rayleigh fading channels from the m antenna of the kth MSs to the bth BS. This approach benefits from the fact that $\mathbf{H}_{bk}\mathbf{s}_k = \sum_{m=1}^{M_k} \mathbf{h}_{bkm} s_{km}$. Henceforth, the received signal at BS b is derived as:

$$\begin{aligned} \mathbf{y}_b \ &= \textstyle\sum_{\forall k,m} a_{bkm}\sqrt{p_{km}} D_{bk}\mathbf{h}_{bkm}s_{km} \\ &\quad + \textstyle\sum_{\forall \hat{k},\hat{m}} q_{b\hat{k}\hat{m}}\sqrt{p_{\hat{k}\hat{m}}} D_{b\hat{k}}\mathbf{h}_{b\hat{k}\hat{m}}s_{\hat{k}\hat{m}} + \mathbf{n} \end{aligned} \tag{5.1}$$

where $\sum_{\forall k,m}$ are in fact double summations. This equation comprises three parts, with the first representing the transmitted signals selected for ZF post-processing at BS b. The second summation represents the ICI, which is the result of the signals that are intended for ZF post-processing at other BSs $\hat{b}$, where $\hat{b} \neq b$. The third term ($\mathbf{n}$) is a $R \times 1$ column vector representing circularly symmetric AWGN with a variance of σ_0^2 for each element.

In (5.1), p_{km} denotes the power allocated to the mth antenna of user k and D_{bk} is the deterministic signal attenuation normalized as $1/d_{bk}^{\alpha}$, where d_{bk} is the distance between BS b and user k and α is the propagation factor. The $\mathbf{h}_{bkm}$ is a column vector of size $R \times 1$ representing the Rayleigh fading channel(s) from the mth transmitting

antenna of user k to the array of antennas at the bth BS. a_{bkm} and $q_{b\hat{k}\hat{m}}$ are two indicator functions, such that a_{bkm} is defined as:

$$a_{bkm} = \begin{cases} 1 & \text{if } \{k, m\} \in \Omega_b \\ 0 & \text{otherwise} \end{cases} \tag{5.2}$$

where Ω_b is a set that holds all the antenna/user element indexes $\{k, m\}$ that are assigned to BS b, and $q_{b\hat{k}\hat{m}}$ indexes users contributing to ICI:

$$q_{b\hat{k}\hat{m}} = \begin{cases} 1 & \text{if } \{\hat{k}, \hat{m}\} \in \Omega_{\hat{b}}, \forall \hat{b} \neq b \\ 0 & \text{otherwise} \end{cases} \tag{5.3}$$

5.2 Capacity Analysis

This section rederives the formulas presented in (4.5) and (4.13), generalizing them for the system model with multiple antennas at the MSs and multiple BSs, that is investigated in this chapter. Consideration is still given to the two-layer decoding process described originally in Section 4.2. The first layer implements the MU detection of all user signals, and is performed at the BS. The second layer implements diversity combining as a form of CR at the WC. These derivations for capacities of users being handled by a single BS or by multiple BSs are essential for implementing Newton's method for power allocation, which is used in this chapter as described in Section 5.3

5.2.1 Multiuser Transmissions

When multiple stations transmit to a common destination simultaneously using the same frequency band, each signal could interfere with the others, resulting in irretrievable data. Therefore, ZF is utilized to separate the mixed signals, based on acquiring CSI at the receiver. Thus, in order to retrieve the original signal sent by the mth

antenna of MS k, the decoder of BS b multiplies (5.1) by $\mathbf{T}_{bkm}$:

$$\begin{aligned}\bar{s}_{km} &= \mathbf{T}_{bkm} a_{bkm} \sqrt{p_{km}} D_{bk} \mathbf{h}_{bkm} s_{km} \\ &+ \mathbf{T}_{bkm} \left(\textstyle\sum_{\forall \bar{k},\bar{m}} a_{b\bar{k}\bar{m}} \sqrt{p_{\bar{k}\bar{m}}} D_{b\bar{k}} \mathbf{h}_{b\bar{k}\bar{m}} s_{\bar{k}\bar{m}} \right) \\ &+ \mathbf{T}_{bkm} \left(\textstyle\sum_{\forall \hat{k},\hat{m}} q_{b\hat{k}\hat{m}} \sqrt{p_{\hat{k}\hat{m}}} D_{b\hat{k}} \mathbf{h}_{b\hat{k}\hat{m}} s_{\hat{k}\hat{m}} \right) + \mathbf{T}_{bkm} \mathbf{n}\end{aligned} \tag{5.4}$$

where $\mathbf{T}_{bkm}$ is the multiuser ZF decoding matrix with size $1 \times R$. In order to recover data of interest and to cancel intra-cell interference:

$$\begin{aligned}\mathbf{T}_{bkm} \mathbf{h}_{bkm} &= 1 \\ \mathbf{T}_{bkm} \mathbf{h}_{b\bar{k}\bar{m}} &= 0\end{aligned} \tag{5.5}$$

where the diacritical mark ($^-$) refers to all antennas/users that are assigned to BS b, excluding the $\{k,m\}$ transmitter/antenna, i.e., all the transmissions that are causing intra-cell interference. In order to obtain a non-zero solution for $\mathbf{T}_{bkm}$ in (5.5), the following condition must be met: $\sum_{k,m} a_{bkm} \leq R$. As a result, (5.4) can be rewritten as:

$$\begin{aligned}\bar{s}_{km} &= a_{bkm} \sqrt{p_{km}} D_{bk} s_{km} \\ &+ \mathbf{T}_{bkm} \left(\textstyle\sum_{\forall \hat{k},\hat{m}} q_{b\hat{k}\hat{m}} \sqrt{p_{\hat{k}\hat{m}}} D_{b\hat{k}} \mathbf{h}_{b\hat{k}\hat{m}} s_{\hat{k}\hat{m}} \right) \\ &+ \mathbf{T}_{bkm} \mathbf{n}\end{aligned} \tag{5.6}$$

Henceforth, the MAI (actually the ICI) affecting all resolved signals at BS b is denoted as:

$$\mathbf{\Psi}_b = \sum_{\forall \hat{k},\hat{m}} q_{b\hat{k}\hat{m}} \sqrt{p_{\hat{k}\hat{m}}} D_{b\hat{k}} \mathbf{h}_{b\hat{k}\hat{m}} s_{\hat{k}\hat{m}} + \mathbf{n} \tag{5.7}$$

The variance of the enhanced noise and interference affecting the signal transmitted by the mth antenna of the kth MS is given by:

$$\begin{aligned}\mathrm{Var}(\mathbf{T}_{bkm} \mathbf{\Psi}_b) &= \mathrm{E}[\mathbf{T}_{bkm} \mathbf{n} \mathbf{n}^{\mathcal{H}} \mathbf{T}_{bkm}^{\mathcal{H}}] + \mathrm{E}[|\mathbf{T}_{bkm} \textstyle\sum_{\forall \hat{k},\hat{m}} q_{b\hat{k}\hat{m}} \sqrt{p_{\hat{k}\hat{m}}} D_{b\hat{k}} \mathbf{h}_{b\hat{k}\hat{m}} s_{\hat{k}\hat{m}}|^2] \\ &= |\mathbf{T}_{bkm} \mathbf{T}_{bkm}^{\mathcal{H}}| \sigma_0^2 + \textstyle\sum_{\forall \hat{k},\hat{m}} |\mathbf{T}_{bkm} q_{b\hat{k}\hat{m}} \sqrt{p_{\hat{k}\hat{m}}} D_{b\hat{k}} \mathbf{h}_{b\hat{k}\hat{m}}|^2\end{aligned} \tag{5.8}$$

Therefore, the capacity of the link between the mth BS and the antenna/user indicated by $(k\,m)$ is:

$$C_{bkm} = \log_2\left(1 + \frac{a_{bkm} D_{bk}^2 p_{km}}{|\sigma_0^2 \mathbf{T}_{bkm} \mathbf{T}_{bkm}^{\mathcal{H}}| + \sum_{\forall \hat{k},\hat{m}} |\mathbf{T}_{bkm} q_{b\hat{k}\hat{m}} \sqrt{p_{\hat{k}\hat{m}}} D_{b\hat{k}} \mathbf{h}_{b\hat{k}\hat{m}}|^2}\right) \tag{5.9}$$

5.2.2 Cooperative Reception

In certain MS position scenarios, one antenna/MS could be assigned to multiple BSs in a single time slot. Therefore, a special decoding operation must be considered to combine multiple replicas of the same signal efficiently. To this end, CR is applied with diversity combining, where the multiple received signals are weighted with an appropriately chosen coefficient before a decision is made for improving the reliability of the user's data. This process is performed at the WC, after forwarding of the soft decoded data from the ZF post-processing that is done at the BSs. Thus, from (5.6), the combined received signals from the multiple BSs can be written as:

$$\begin{aligned} \bar{s}_{km} &= \textstyle\sum_{\forall b} w_{bkm} \left(a_{bkm} \sqrt{p_{km}} D_{bk} s_{km} \right. \\ &\quad \left. + \mathbf{T}_{bkm} \textstyle\sum_{\hat{k}\hat{m}} q_{b\hat{k}\hat{m}} \sqrt{p_{\hat{k}\hat{m}}} D_{b\hat{k}} \mathbf{h}_{b\hat{k}\hat{m}} s_{\hat{k}\hat{m}} + \mathbf{T}_{bkm} \mathbf{n}\right) \\ &= \sqrt{p_{km}} s_{km} \textstyle\sum_{\forall b} \left(w_{bkm} a_{bkm} D_{bk}\right) \\ &\quad + \textstyle\sum_b w_{bkm} \mathbf{T}_{bkm} \Psi_b \end{aligned} \tag{5.10}$$

where w_{bkm} is the combining weighted coefficient for the signal from BS b. Therefore, from (5.10), the SINR is expressed as:

$$SINR_{km} = \frac{p_k \left|\sum_{\forall b} w_{bkm} D_{bk}\right|^2}{\mathrm{E}[\left|\sum_{\forall b} w_{bkm} \mathbf{T}_{bkm} \Psi_b\right|^2]} \tag{5.11}$$

where the variance of the combined enhanced noise and interference is given by:

$$\begin{aligned}
&\mathrm{Var}(\textstyle\sum_{\forall b} w_{bkm}\mathbf{T}_{bkm}\mathbf{\Psi}_b)\\
&= \textstyle\sum_{\forall b} w_{bkm}^2 \mathrm{E}[\mathbf{T}_{bkm}\mathbf{n}\mathbf{n}^{\mathcal{H}}\mathbf{T}_{bkm}^{\mathcal{H}}] + \mathrm{E}[|\sum_{\forall b} w_{bkm}\mathbf{T}_{bkm}\sum_{\forall \hat{k},\hat{m}} a_{b\hat{k}m}\sqrt{p_{\hat{k}\hat{m}}}D_{b\hat{k}}\mathbf{h}_{b\hat{k}\hat{m}}|^2]\\
&= \textstyle\sum_{\forall b} w_{bkm}^2\sigma_0^2|\mathbf{T}_{bkm}\mathbf{T}_{bkm}^{\mathcal{H}}| + \sum_{\forall \hat{k},\hat{m}} p_{\hat{k}\hat{m}}|\sum_{\forall b} w_{bkm}\mathbf{T}_{bkm}q_{b\hat{k}\hat{m}}D_{b\hat{k}}\mathbf{h}_{b\hat{k}\hat{m}}|^2\\
&= V_{km}
\end{aligned} \tag{5.12}$$

Hence, applying (5.12) in (5.11) yields:

$$SINR_{km} = \frac{p_k\left|\sum_{\forall b} w_{bkm}D_{bk}\right|^2}{\sum_{\forall b} w_{bkm}^2\sigma_0^2|\mathbf{T}_{bkm}\mathbf{T}_{bkm}^{\mathcal{H}}| + \sum_{\forall \hat{k},\hat{m}} p_{\hat{k}\hat{m}}|\sum_{\forall b} w_{bkm}\mathbf{T}_{bkm}q_{b\hat{k}\hat{m}}D_{b\hat{k}}\mathbf{h}_{b\hat{k}\hat{m}}|^2} \tag{5.13}$$

As a result, after decoding at the WC through signal combining, the user data rate is:

$$C_{km} = \log_2\left(1 + \frac{p_k\left|\sum_{\forall b} w_{bkm}a_{bkm}D_{bk}\right|^2}{\sum_{\forall b} w_{bkm}^2 a_{bkm}\sigma_0^2|\mathbf{T}_{bkm}\mathbf{T}_{bkm}^{\mathcal{H}}| + \sum_{\forall \hat{k},\hat{m}} p_{\hat{k}\hat{m}}|\sum_{\forall b} w_{bkm}\mathbf{T}_{bkm}a_{bkm}q_{b\hat{k}\hat{m}}D_{b\hat{k}}\mathbf{h}_{b\hat{k}\hat{m}}|^2}\right) \tag{5.14}$$

Assuming equal gain combining CR, the combining coefficients $w_{bkm} = 1$. In order to simplify the presentation, these coefficients are not considered further in this chapter. A comparison of (5.9) with (5.14) shows that the latter is a more general equation. Therefore, (5.14) could be used to calculate the total system sum rate as:

$$C_{total} = \sum_{\forall k,m} C_{km} \tag{5.15}$$

5.3 Power Allocation

In this section, Newton's optimization method is utilized for power allocation in order to maximize the total system sum rate, as in (5.15), where the power vector variable represents the invested power for all transmitting antennas from all active MSs. For a given assignment of users/antennas to the BS(s), this method uses an iterative search

to find the power allocation vector $\mathbf{P}$ to optimize C_{total}, as follows:

$$\mathbf{P}_{i+1} = \mathbf{P}_i - [\nabla^2 C_{total}(\mathbf{P}_i)]^{-1} \nabla C_{total}(\mathbf{P}_i) \tag{5.16}$$

where $\nabla C_{total}(\mathbf{P}_i)$ and $\nabla^2 C_{total}(\mathbf{P}_i)$ are the gradient and the Hessian matrices, respectively. $\mathbf{P}_i$ is a column vector, with elements $\{p_{11}, p_{12}, \ldots, p_{KM_K}\}$ representing the power assigned to potentially active users/antennas. As usual, i denotes the iteration index as Newton's method attempts to converge toward power vector/allocation $\mathbf{P}$, as the stationary (min or max) point for the total sum rate C_{total}. The gradient matrix elements are given by:

$$\nabla C_{total} = \Big[\frac{\partial C_{total}}{\partial p_{11}} \frac{\partial C_{total}}{\partial p_{12}} \cdots \frac{\partial C_{total}}{\partial p_{KM}}\Big]' \tag{5.17}$$

where $(')$ represents the matrix transpose operator. Each element in (5.17) can be expressed as:

$$\frac{\partial C_{total}}{\partial p_{km}} = \frac{\partial C_{km}}{\partial p_{km}} + \frac{\partial\big(\sum_{\forall \hat{k},\hat{m}} C_{\hat{k}\hat{m}}\big)}{\partial p_{km}} \tag{5.18}$$

where the partial derivative term is separated into two parts. The first part, which considers taking the derivative with respect to p_{km} over its own user/antenna (k, m) capacity C_{km}, is calculated as:

$$\frac{\partial C_{km}}{\partial p_{km}} = \frac{1}{\ln(2)} \frac{\big|\sum_{\forall b} a_{bkm} D_{bk}\big|^2}{V_{km} + p_{km}\big|\sum_{\forall b} a_{bkm} D_{bk}\big|^2} = A_{km} \tag{5.19}$$

In (5.18), the second part represents capacity affected by ICI transmissions:

$$\begin{aligned} &\frac{\partial\big(\sum_{\forall \hat{k},\hat{m}} C_{\hat{k}\hat{m}}\big)}{\partial p_{km}} \\ &\qquad = -\frac{1}{\ln(2)} \sum\nolimits_{\forall \hat{k},\hat{m}} \frac{p_{\hat{k}\hat{m}}\big|\sum_{\forall \hat{b}} a_{\hat{b}\hat{k}\hat{m}} D_{\hat{b}\hat{k}}\big|^2 \frac{\partial V_{\hat{k}\hat{m}}}{\partial p_{km}}}{(V_{\hat{k}\hat{m}}^2 + p_{\hat{k}\hat{m}}\big|\sum_{\forall \hat{b}} a_{\hat{b}\hat{k}\hat{m}} D_{\hat{b}\hat{k}}\big|^2 V_{\hat{k}\hat{m}})} \\ &\qquad = B_{km} \end{aligned} \tag{5.20}$$

where $\ln(X)$ is the natural logarithm of X, and $\frac{\partial V_{\hat{k}\hat{m}}}{\partial p_{km}}$ is defined as:

$$\frac{\partial V_{\hat{k}\hat{m}}}{\partial p_{km}} = |\sum\nolimits_{\hat{b}} a_{\hat{b}\hat{k}\hat{m}} q_{\hat{b}km} D_{\hat{b}k} \mathbf{T}_{\hat{b}\hat{k}\hat{m}} \mathbf{h}_{\hat{b}km}|^2 \tag{5.21}$$

In (5.18), only two terms are included when calculating the derivative, as the derivative with respect to p_{km} of the capacity cost function due to intra-cell interference is always equal to zero $\left(\frac{\partial C_{\bar{k}\bar{m}}}{\partial p_{km}} = 0\right)$, where $\{k, m\}, \{\bar{k}, \bar{m}\} \in \Omega_b$. This is due to the fact that the intra-cell interference is canceled by the ZF post-processing approach.

For the Hessian matrix:

$$\nabla^2 C_{total} = \begin{bmatrix} \frac{\partial^2 C_{total}}{\partial p_{11}^2} & \frac{\partial^2 C_{total}}{\partial p_{11}\partial p_{12}} & \cdots & \frac{\partial^2 C_{total}}{\partial p_{11}\partial p_{KM}} \\ \frac{\partial^2 C_{total}}{\partial p_{12}\partial p_{11}} & \frac{\partial^2 C_{total}}{\partial^2 p_{12}} & \cdots & \frac{\partial^2 C_{total}}{\partial p_{12}\partial p_{KM}} \\ \vdots & \vdots & \ddots & \vdots \\ \frac{\partial^2 C_{total}}{\partial p_{KM}\partial p_{11}} & \frac{\partial^2 C_{total}}{\partial p_{KM}\partial p_{12}} & \cdots & \frac{\partial^2 C_{total}}{\partial^2 p_{KM}} \end{bmatrix} \tag{5.22}$$

equations are first derived for the second order partial derivatives identified as the diagonal elements, where:

$$\frac{\partial^2 C_{total}}{\partial p_{km}^2} = \frac{\partial^2 C_{km}}{\partial p_{km}^2} + \frac{\partial^2 (\sum_{\forall \hat{k},\hat{m}} C_{\hat{k}\hat{m}})}{\partial p_{km}^2} \tag{5.23}$$

Similarly to (5.18), (5.23) is divided into two partial derivatives. The first part, which takes the second order derivative with respect to the targeted power invested by antenna m of MS k (p_{km}) for its own contribution to the total sum rate, is given by:

$$\frac{\partial^2 C_{km}}{\partial p_{km}^2} = \frac{\partial A_{km}}{\partial p_{km}} = -\frac{1}{\ln(2)} \frac{\left|\sum_{\forall b} a_{bkm} D_{bk}\right|^4}{(V_{km} + p_{km}\left|\sum_{\forall b} a_{bkm} D_{bk}\right|^2)^2} \tag{5.24}$$

The second part of (5.23) is the partial derivative for the contribution to the total sum rate of the MSs that cause ICI with respect to $\{k, m\}$:

$$\begin{aligned} &\frac{\partial^2 (\sum_{\forall \hat{k},\hat{m}} C_{\hat{k}\hat{m}})}{\partial p_{km}^2} \\ &= \frac{\partial B_{km}}{\partial p_{km}} = \frac{1}{\ln(2)} \sum\nolimits_{\forall \hat{k},\hat{m}} \frac{p_{\hat{k}\hat{m}}\left|\sum_{\forall \hat{b}} a_{\hat{b}\hat{k}\hat{m}} D_{\hat{b}\hat{k}}\right|^2 \left(\frac{\partial V_{\hat{k}\hat{m}}}{\partial p_{km}}\right)^2 (2V_{\hat{k}\hat{m}} + p_{\hat{k}\hat{m}}\left|\sum_{\forall \hat{b}} a_{\hat{b}\hat{k}\hat{m}} D_{\hat{b}\hat{k}}\right|^2)}{(V_{\hat{k}\hat{m}}^2 + p_{\hat{k}\hat{m}}\left|\sum_{\forall \hat{b}} a_{\hat{b}\hat{k}\hat{m}} D_{\hat{b}\hat{k}}\right|^2 V_{\hat{k}\hat{m}})^2} \end{aligned} \tag{5.25}$$

The result arrived at in (5.25) can be compacted by taking the derivative of the denominator of (5.20) only, where the derivative of the numerator is zero. This is due to the fact that $\frac{\partial^2 V_{\hat{k}\hat{m}}}{\partial {p_{km}}^2} = 0$.

Equations are next derived for the non-diagonal elements of (5.22) that illustrate the mixed second partial derivatives. They are expressed as:

$$\frac{\partial^2 C_{total}}{\partial p_{km}\partial p_{\dot{k}\dot{m}}} = \frac{\partial^2 C_{km}}{\partial p_{km}\partial p_{\dot{k}\dot{m}}} + \frac{\partial^2 C_{\dot{k}\dot{m}}}{\partial p_{km}\partial p_{\dot{k}\dot{m}}} + \frac{\partial^2 \left(\sum_{\forall \hat{k},\hat{m}} C_{\hat{k}\hat{m}}\right)}{\partial p_{km}\partial p_{\dot{k}\dot{m}}} \tag{5.26}$$

assuming that $\{\dot{k},\dot{m}\} \in \Omega_{\dot{b}}$ and $\{\hat{k},\hat{m}\} \notin (\Omega_b \cup \Omega_{\dot{b}})$. The first part of (5.26) is the mixed partial derivative over C_{km}, where:

$$\frac{\partial^2 C_{km}}{\partial p_{km}\partial p_{\dot{k}\dot{m}}} = \begin{cases} -\frac{1}{\ln(2)} \frac{\left|\sum_{\forall b} a_{bkm} D_{bk}\right|^2 \left(\frac{\partial V_{km}}{\partial p_{\dot{k}\dot{m}}}\right)}{(V_{km} + p_{km}\left|\sum_{\forall b} a_{bkm} D_{bk}\right|^2)^2} & \text{if } \{\dot{k},\dot{m}\} \notin \Omega_b \\ 0 & \text{if } \{\dot{k},\dot{m}\} \in \Omega_b \end{cases} \tag{5.27}$$

The second part of (5.26) is responsible for taking the derivative of $C_{\dot{k}\dot{m}}$ with respect to the mixed partial variables p_{km} and $p_{\dot{k}\dot{m}}$. The derivative would have the same results and conditions, according to Schwarz's theorem. Hence, (5.27) becomes:

$$\frac{\partial^2 C_{\dot{k}\dot{m}}}{\partial p_{km}\partial p_{\dot{k}\dot{m}}} = \begin{cases} -\frac{1}{\ln(2)} \frac{\left|\sum_{\forall \dot{b}} a_{\dot{b}\dot{k}\dot{m}} D_{\dot{k}\dot{m}}\right|^2 \left(\frac{\partial V_{\dot{k}\dot{m}}}{\partial p_{km}}\right)}{(V_{\dot{k}\dot{m}} + p_{\dot{k}\dot{m}}\left|\sum_{\forall \dot{b}} a_{\dot{b}\dot{k}\dot{m}} D_{\dot{k}\dot{m}}\right|^2)^2} & \text{if } \{\dot{k},\dot{m}\} \notin \Omega_b \\ 0 & \text{if } \{\dot{k},\dot{m}\} \in \Omega_b \end{cases} \tag{5.28}$$

Finally, the last part of (5.26) derives the second derivative for the performance of the active antennas/users that are not assigned to BS b and $\dot{b}$ $\{\hat{k},\hat{m} \notin (\Omega_b \cup \Omega_{\dot{b}})\}$:

$$\frac{\partial^2 C_{\hat{k}\hat{m}}}{\partial p_{km}\partial p_{\dot{k}\dot{m}}} = \frac{1}{\ln(2)} \frac{p_{\hat{k}\hat{m}}\left|\sum_{\forall \hat{b}} a_{\hat{b}\hat{k}\hat{m}} D_{\hat{b}\hat{k}}\right|^2 \left(\frac{\partial V_{\hat{k}\hat{m}}}{\partial p_{km}}\right)\left(\frac{\partial V_{\hat{k}\hat{m}}}{\partial p_{\dot{k}\dot{m}}}\right)(2V_{\hat{k}\hat{m}} + p_{\hat{k}\hat{m}}\left|\sum_{\forall \hat{b}} a_{\hat{b}\hat{k}\hat{m}} D_{\hat{b}\hat{k}}\right|^2)}{(V^2_{\hat{k}\hat{m}} + p_{\hat{k}\hat{m}}\left|\sum_{\forall \hat{b}} a_{\hat{b}\hat{k}\hat{m}} D_{\hat{b}\hat{k}}\right|^2 V_{\hat{k}\hat{m}})^2} \tag{5.29}$$

To summarize, in this method (5.17) and (5.22) are substituted into (5.16), and the procedure is iterated until p_{km} values converge.

5.3.1 Power Optimization Results

Figure 5.2 analyzes the convergence of Newton's method, with iterative steps being modified versions of (5.16) and the corresponding analysis in Section 5.3. Specifically, the total sum rate calculated according to (5.15) based on (5.9) and (5.14) is examined

as a function of the iterative index i. The impact of the choice of the initial p_{km} values (the "initial guess") is also considered. In the simulations, there are three BSs, where each BS has three antennas. In addition, ten MSs ($\ddot{K} = 10$) are randomly distributed, and each MS is equipped with three antennas ($\ddot{M} = 3$). The objective function (C_{total} in (5.15)) is not concave or uni-modal with respect to $\mathbf{P}$, therefore, implementing Newton's method for C_{total} based on the direction proposed in (5.16) does not necessarily result in an optimized solution (the global maximum). Equation (5.16) was modified by adjusting the iteration steps for maximizing the cost function in (5.15), with the original step being controlled by the varying $[|\nabla^2 C_{total}(\mathbf{P}_i)|^{-1}]$. With these modified steps, it was ensured that improved convergence was achieved. First, it was decided to replace (5.16) in the modified iterative search with:

$$\mathbf{P}_{i+1} = \mathbf{P}_i + |\nabla^2 C_{total}(\mathbf{P}_i)|^{-1} \nabla C_{total}(\mathbf{P}_i) \tag{5.30}$$

The convergence results for this iterative search are illustrated in Fig. 5.2, where the curves corresponding to an initial power (p_0) for all active antennas of 0 or p_{max} are shown in green or blue, respectively. (p_{max} is the maximum power for any antenna in the system, with $p_{max} = 30dB$). The non-diagonal elements for $\nabla^2 C_{total}$ in (5.30) are set to zero and discarded. This is done to reduce the complexity when calculating the inverse, without affecting the performance of the method. In the second modified search, (5.16) was replaced with:

$$\mathbf{P}_{i+1} = \mathbf{P}_i + |\nabla^2 C_{total}(\mathbf{P}_i)^{-1}| \nabla C_{total}(\mathbf{P}_i) \tag{5.31}$$

Here all of the elements of the Hessian matrix are included. The results for this search procedure are shown in pink in Fig. 5.2, where the initial guess for the transmission power is set to $p_{min} = 0$. A comparison of the performance of the different search procedures plotted in green and pink shows that (5.30) converges somewhat more slowly but to a higher value, for the same initial conditions. Setting p_0 to p_{max}

for (5.30), indicated in blue, results in faster convergence, with minimal performance improvement for the first few iterations. Therefore, (5.30) with $p_0 = p_{max}$ is employed in all other simulations in this chapter, when Newton's method is used to allocate power for different possible combinations of antennas/users.

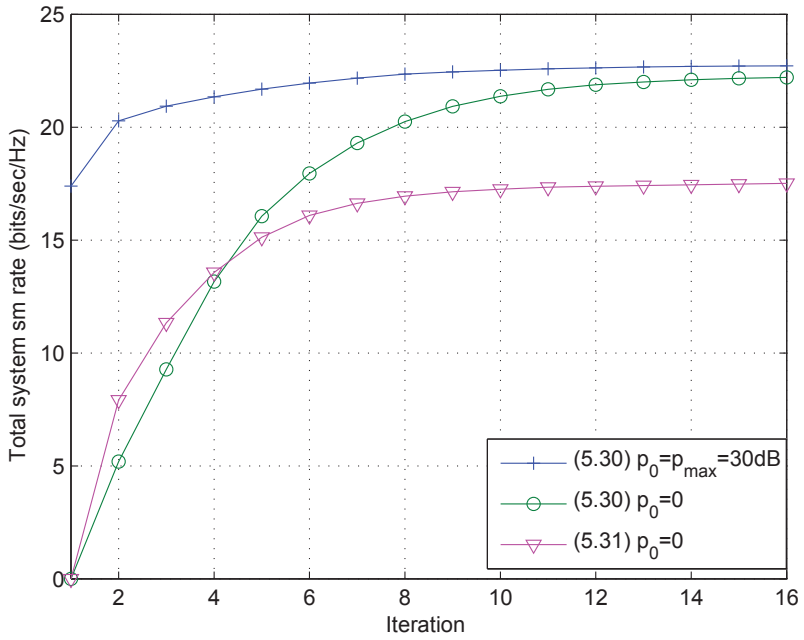

Figure 5.2: Convergence of modified Newton's method, for power allocation maximizing the total sum rate.

5.4 Radio Resource Management

The proposed resource allocation for the system under study in this chapter proceeds in three stages, and is summarized in Figure 5.3. The first two stages, highlighted in red and green, select the initial combinations of at most ($K = B \times R$) users/antennas as potential active transmitters, based on the channel conditions (including both deterministic signal attenuation and Rayleigh fading gains). It is stipulated that these

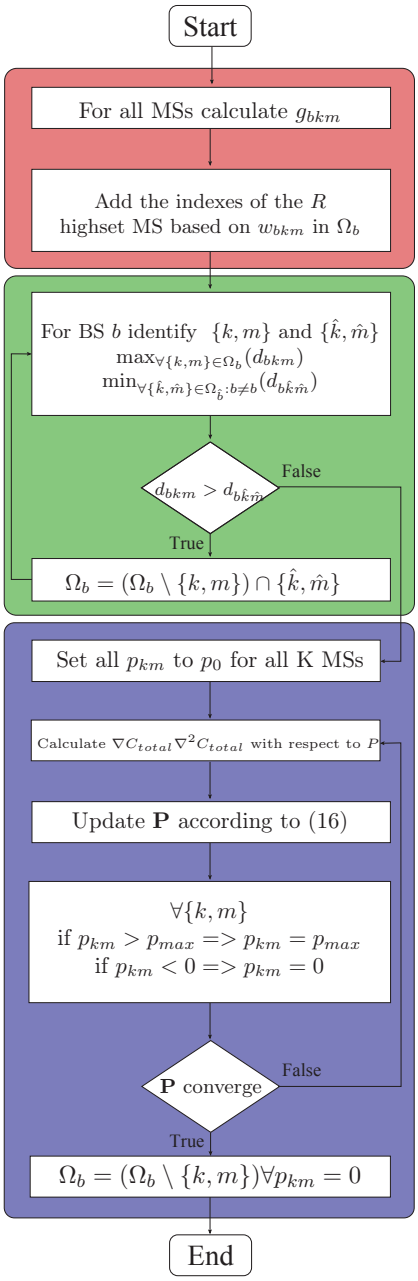

Figure 5.3: The proposed RRM algorithm.

combinations are the most likely to result in a maximum total system sum rate. The last stage, highlighted in blue, improves the total system sum rate in (5.15) by using power allocations for a given set of users/antennas from the initial selection. This is

achieved by employing the modified Newton's optimization method presented in the previous section, in order to find the best transmitting power per active antenna, so as to increase the total system capacity.

The procedures included in the red and green areas of Fig. 5.3 represent the user/antenna spatial coordination that allocates the available $(B \times R)$ spatial streams to the MSs, using a simplified, efficient approach. To this end, the spatial coordination is divided into two stages. The first stage, shown in the red area of Fig. 5.3, could be implemented independently for every BS, and would include the following steps:

1. The weight function g_{bkm} for every potentially active antenna is calculated, where
$$g_{bkm} = \frac{D_{bkm} h_{bkm}}{\sum_{\forall \hat{b} | \hat{b} \neq b} D_{\hat{b}km} h_{\hat{b}km}} \tag{5.32}$$

2. Based on the highest values calculated in (5.32), R transmitters are selected for each BS, and their indexes $\{k, m\}$ are added to the initial set of active antennas (Ω_b).

3. After the initial set of active users/antennas (Ω_b) is established, the information can either be distributed among the BSs, or sent directly to the WC for further processing.

In the first stage, there is a finite probability that multiple BSs could select a common user/antenna. When this happens, such users/antennas are considered for CR.

The second stage of the algorithm, represented by the green area in Fig. 5.3, is responsible for removing from set Ω_b users/antennas that would have a low capacity due to ICI. This stage could have distributed implementation, and could be executed at every BS instead of relying on the WC. The algorithm proceeds as follows:

4. Find the $\{k, m\}$ for BS b that has the weakest signal strength based on the attenuation factor.

5. Find the $\{\hat{k}, \hat{m}\}$ that has the highest interference level for the spatial streams associated with BS b.

6. If user $\hat{k}$ is closer than k to BS b, then remove $\{k, m\}$ from Ω_b, substitute $\{\hat{k}, \hat{m}\}$, and return to step 4.

Therefore, the users/antennas that are selected by more then one BS are flagged, and their soft decoded information is forwarded to the WC for diversity combining.

The third stage, shown in the blue area of Fig. 5.3, utilizes the iterative modification of Newton's method to find power allocation vectors optimizing the total sum rate for the initial selection of users/antennas, with two main objectives. The first objective is to maximize the total system sum rate, based on adjusting the power for all users/antennas that are included in all Ω_b. The second objective is to deactivate temporarily the users/antennas that are degrading the overall system performance, by setting their power to zero. This stage has the following steps:

7. For all $\{k, m\}$ selected from the previous stages, set the power to an initial value $\mathbf{P}_0$. Based on an examination of a few initial power vector values, it was found that setting the value to the maximum available power is to be recommended.

8. Calculate ∇C_{total} and $\nabla^2 C_{toatl}$, based on (5.17) and (5.22), respectively.

9. For the ith iteration, find P_{i+1} as shown in (5.30).

10. The resulting optimized power values for all $\{k, m\}$ potentially active transmitters are examined. If they exceed the power range, they are then set to the boundaries.

11. If the objective function does not converge, go to step 8.

12. The users/antennas exceeding the minimum boundary are temporarily suppressed and removed from the sets of active users/antennas.

5.5 Simulation Results

In this section, analytical and simulation results are presented in order to investigate the performance of the proposed resource management algorithms for the multi-cell MU-MIMO model considered. The performance of three algorithms is evaluated. The first algorithm (referred to in the figures and tables as Alg. 1) implements the entire scheduling scheme as presented in Figure 5.3. The second algorithm (Alg. 2) considers two stages only, omitting the second stage (represented by the green area in Fig. 5.3). In addition, a third scheduling algorithm (Alg. 3) is implemented, where all of the decisions and resource management are performed at the WC. It should also be noted that CR is not implemented in Alg. 3, so that it can be used as a benchmark for the first two scheduling algorithms.

In all simulations, three BSs ($B = 3$) and $\ddot{K}$ randomly distributed MSs are placed in a 25×25 area. The BSs are equally spaced from each other and from the center of the area. The BSs are always equipped with 3 antennas ($R = 3$), while at the MSs the number of antennas varies in different simulations, as noted in the presentation of the results/figures. The simulation results are always averaged over a thousand realizations of channel conditions and different MS positions, unless otherwise stated.

Table 5.1 shows the percentage of common assignments of selected users/antennas

Table 5.1: Percentage occurrence of similar combinations.

	$\ddot{M} = 1$	$\ddot{M} = 2$	$\ddot{M} = 3$
Alg. 1 vs Alg. 2	65%	31 %	49%
Alg. 1 vs Alg. 3	2.5%	30.5 %	49%
Alg. 2 vs Alg. 3	49%	98 %	100%

to particular BS combinations, for all three algorithms. The columns present the results for three different cases, based on the number of available antennas at the MSs. Increasing the number of antennas while keeping the number of MSs fixed ($\ddot{K} = 10$)

increases the number of possible user/antenna combination choices. From the table it can be seen that reducing the number of antennas results in higher discrepancies in the selection of common combinations of users/antennas. This is due to the fact that higher numbers of antennas provide a greater number of available combinations, which in turn reduces the occurrence of CR, leading to minimum variation between the algorithms. For this reason, the focus is first on evaluating the three algorithms when a low number of antennas is used at the MSs.

Fig. 5.4, compares the three algorithms in terms of convergence in finding the

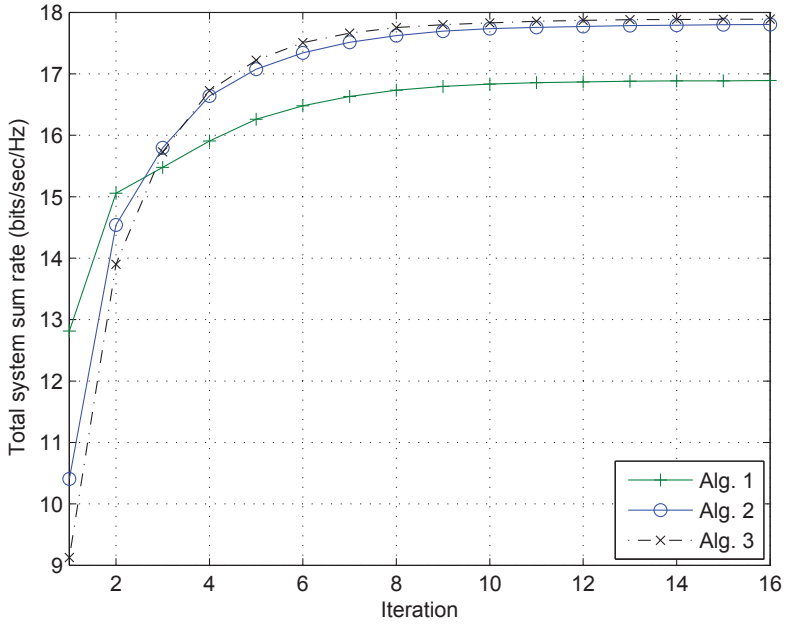

Figure 5.4: The convergence rate of different scheduling schemes.

maximum total sum rate, where $\ddot{K} = 10$ and $\ddot{M} = 1$. The results for algorithms 1, 2 and 3 are plotted in green, blue and black, respectively. Although Alg. 1 exhibits the highest total sum rate for the first few iterations, the total sum rate levels off at a low value. Alg. 2 and 3 have very similar results, with the former converging faster. This means that if the power is not optimized for allocation among the transmitting

antennas, then Alg. 1 is preferable. However, Alg. 2 could yield a better performance when Newton's method is applied.

Figures 5.5 and 5.6 present the total system sum rate and power savings versus the

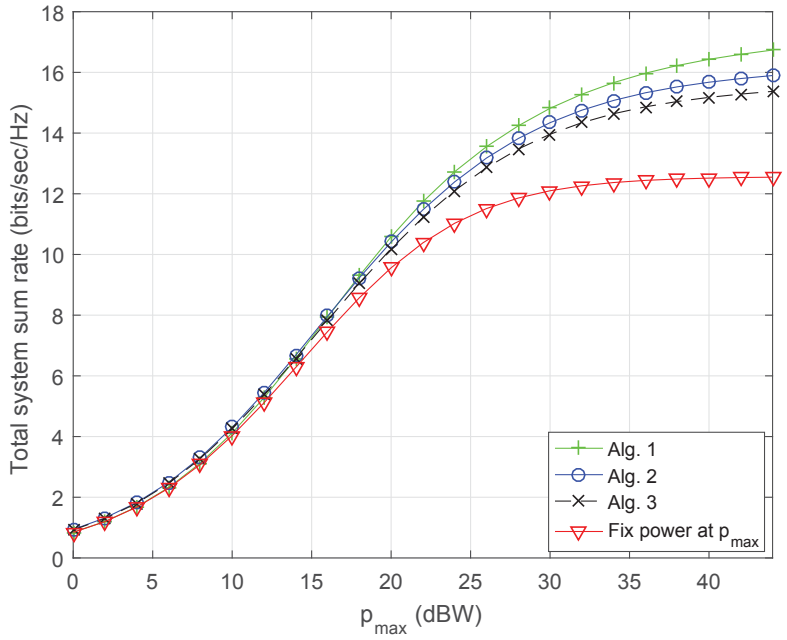

Figure 5.5: The total system sum rate for different antenna selection approaches, with $\ddot{K} = 10$ $\ddot{M} = 1$.

maximum available transmission power, for ten randomly distributed MSs ($\ddot{K} = 10$) and one antenna per MS ($\ddot{M} = 1$). The power savings are determined in relation to the maximum power in the system. The results for algorithms 1, 2 and 3 are plotted in green, blue and black, respectively. In addition, a fourth system is implemented, shown in red, which illustrates the performance of a system that does not utilize a power allocation method; hence, maximum power is always used at all transmitters. Figure 5.5 shows that Alg. 1 has the best total sum rate performance when compared to all the other algorithms, and Figure 5.6 corroborates that Alg. 1 yields the greatest power savings. This is due to the fact that at a low $\ddot{M}$, there are few antennas from which to select, which reduces the advantage of performing spatial coordination.

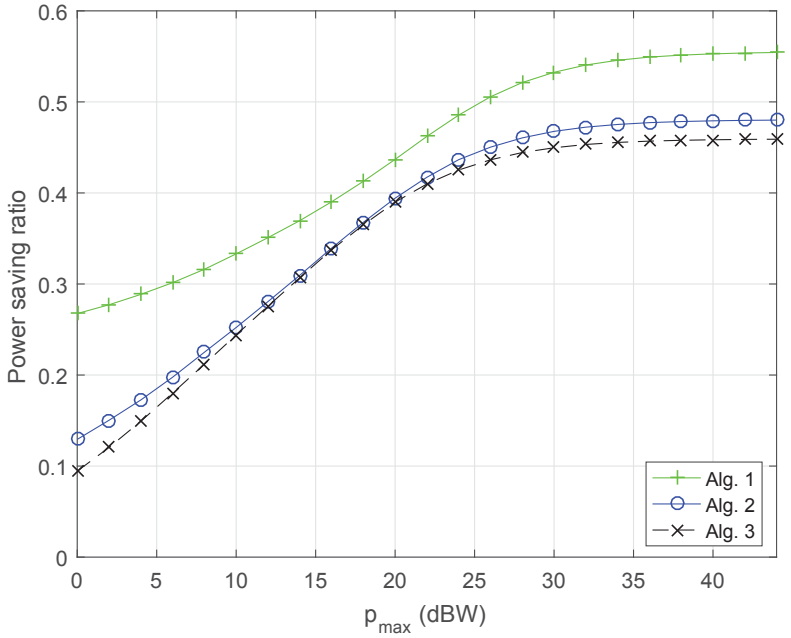

Figure 5.6: Power savings as compared with the fixed power approach, for $\ddot{K} = 10$ $\ddot{M} = 1$.

This is addressed by utilizing the proposed joint algorithm (Alg. 3) which focuses on reducing the number of users that are overpowered by ICI, noise enhancement and partial CR. In Alg. 2, the use of CR is lower than in Alg. 1, and CR is not implemented in Alg. 3. Hence, when the performance of Alg. 3 is compared to that of Alg. 1, an improvement of $\sim 10\%$ is seen in the total system sum rate, and 170% in power savings.

Next, Figs. 5.7 and 5.8 present the results for capacity and power savings, for simulations with ten MSs equipped with two antennas ($\ddot{M} = 2$) each. It can be seen from Fig. 5.7 that when an extra antenna is added to each MS, all of the proposed algorithms have a similar total sum rate performance, which exceeds that of the fixed power system. Figure 5.8 shows that all of the proposed algorithms achieve power savings, in comparison to the system with fixed power. Moreover, Alg. 1 provides the greatest power savings of all algorithms. This is achieved due to the increased

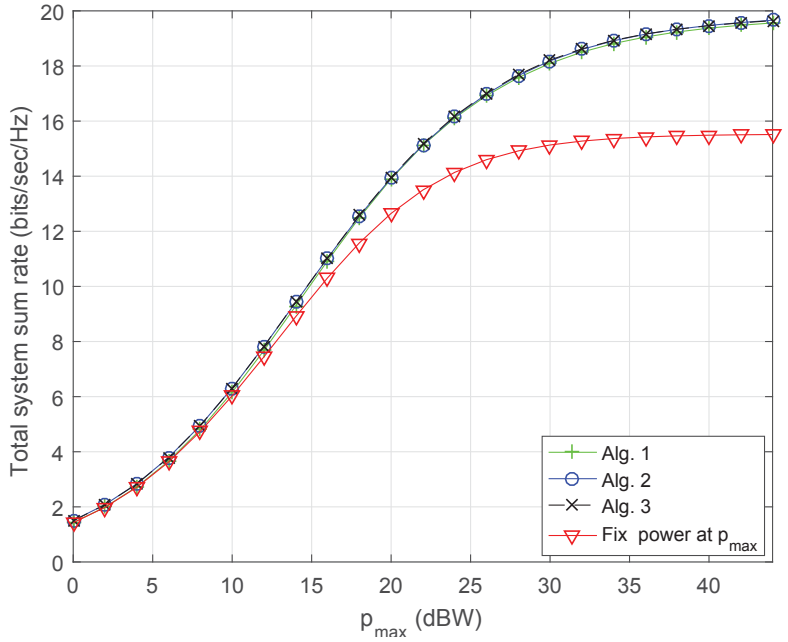

Figure 5.7: The total system sum rate for different antenna selection approaches, with $\ddot{K} = 10$ $\ddot{M} = 2$.

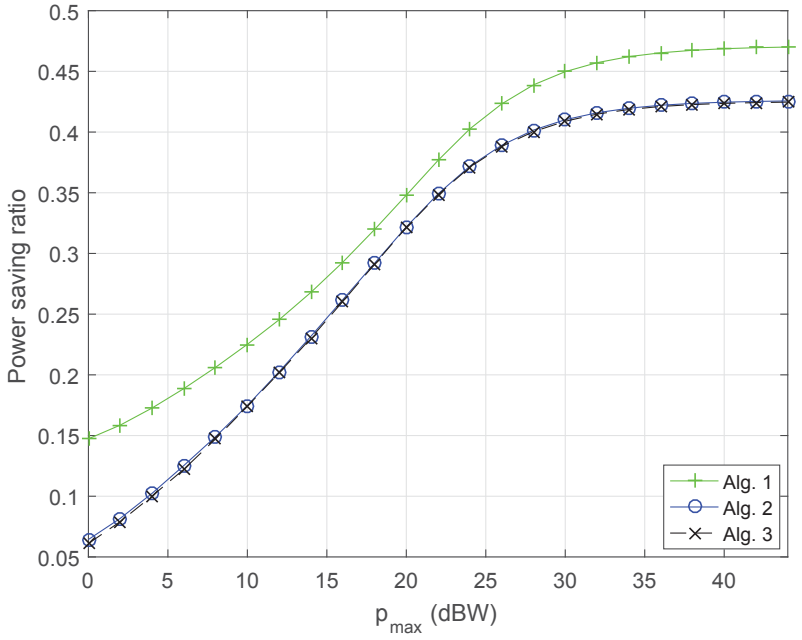

Figure 5.8: Power savings as compared with the fixed power approach, for $\ddot{K} = 10$ $\ddot{M} = 2$.

chance of selecting an antenna with transmissions to be received by multiple BSs, which in turn reduces the number of transmitting users. Without CR, this would reduce the total sum rate, which is not the case here. It is important to emphasize that reducing the number of transmitters did not reduce the total system data rate, not only because of CR, but also because of the deployment of power allocation.

Finally, Figs. 5.9 and 5.10 present the results for the total system sum rate and power savings, with three antennas ($\ddot{M} = 3$) deployed per MS. A comparison of

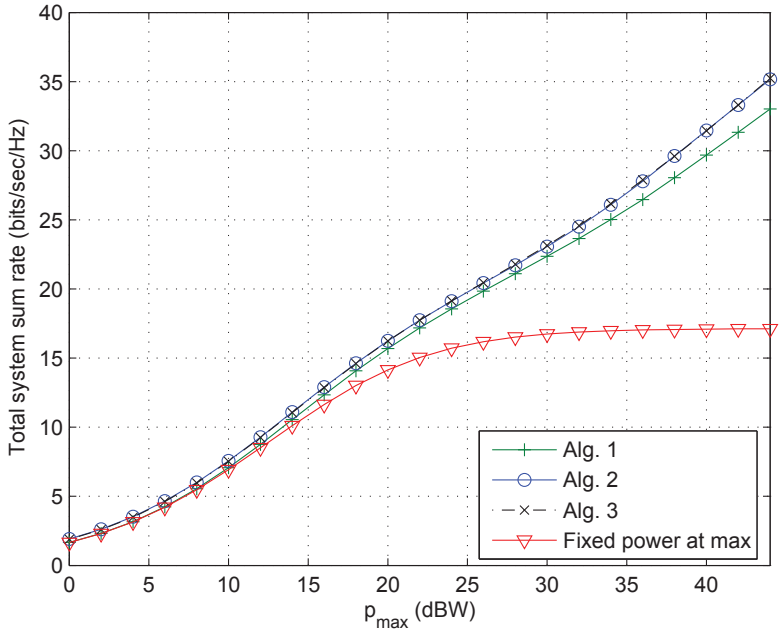

Figure 5.9: The total system sum rate for different antenna selection approaches, with $\ddot{K} = 10$ $\ddot{M} = 3$.

the total sum rate performance of systems using the proposed power optimization with that of the system using fixed power, as seen in Fig. 5.9, shows that their performance increases linearly with an increase in maximum available power. In contrast, the performance of the system with fixed power stabilizes at a constant value after reaching a power of $25dB$. This is due to the low number of active

antennas in the latter system that are degrading the total sum rate performance. In the proposed schemes, such situations are avoided by deploying Newton's method to deactivate those transmissions temporarily. With regard to the systems that utilize Newton's method as part of the scheduling algorithm, Fig. 5.9 shows very similar results for the performance of Alg. 2 and Alg. 3. This is because, as demonstrated in Table 5.1, both methods yield an identical selection of user/antenna combinations at $\ddot{M} = 3$.

Figure 5.10 shows the power savings gained by the three proposed algorithms in comparison to the scheduling algorithm that assigns fixed power to all active users/antennas. From the figure, all three algorithms are able to provide power savings of 67% at high power levels, in comparison to the fixed power scheme. However, Alg. 1 exhibits greater power savings than the other two algorithms; at a low p_{max}

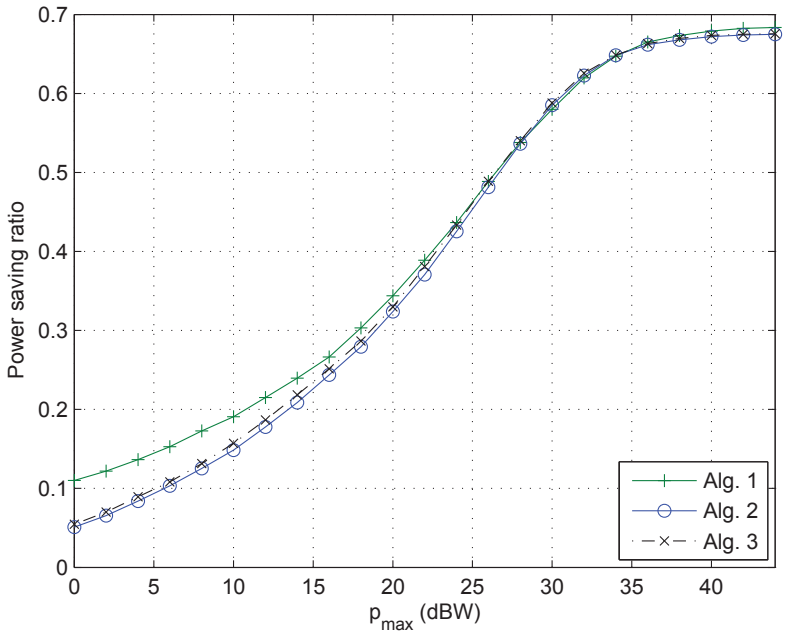

Figure 5.10: Power savings as compared with the fixed power approach, for $\ddot{K} = 10$ $\ddot{M} = 3$.

value, Alg. 1 yields 50% more power savings than Alg. 2 or 3.

Table 5.2 indicates how many combinations of users/antennas the algorithms need to examine, which reflects the complexity of these algorithms. The two columns labeled BS and WC show the complexity for the indicated hosts, whereas the last column presents the total system complexity. The complexity associated with New-

Table 5.2: Algorithm complexity

	BS	WC	Total
Alg. 1	$\binom{KM}{R} + R$	None	$B(\binom{KM}{R} + R)$
Alg. 2	$\binom{KM}{R}$	None	$B(\binom{KM}{R})$
Alg. 3	None	$\frac{(KM)!}{(KM-RB)!R!}$	$\frac{(KM)!}{(KM-RB)!R!}$

ton's method is not included here, as all three algorithms are equally affected by this approach. However, the power optimization method in Alg. 1 requires fewer calculations because it makes greater use of CR. Alg. 1 and 2 are performed at each BS independently, therefore, the total system complexity is scaled only by B. However, the scheduling operations of Alg. 3 (at different BSs) are dependent upon one another, hence, the scheduling is performed at a centralized location, the WC. This results in a greater number of combinations to be analyzed, and a less efficient system.

Figure 5.11 shows the semi-analytical results for the average bit error rate (BER) as a function of the maximum available power at the transmitter. This analysis considers implementing the same system model presented earlier, but with the addition of an iterative interference canceler (IIC) processed at the WC for all received signals. The solid and dotted lines represent the system models with and without the IIC, respectively, for all system models. With fixed power, BER performance would converge at a high power per antenna to BER 10^{-1}; this value is improved to 10^{-2} when the IIC is utilized in this system. The two proposed algorithms, Alg. 1 and Alg. 2, can achieve a BER performance comparable to that of the fixed power system without the great complexity added by the IIC. Performance is significantly improved

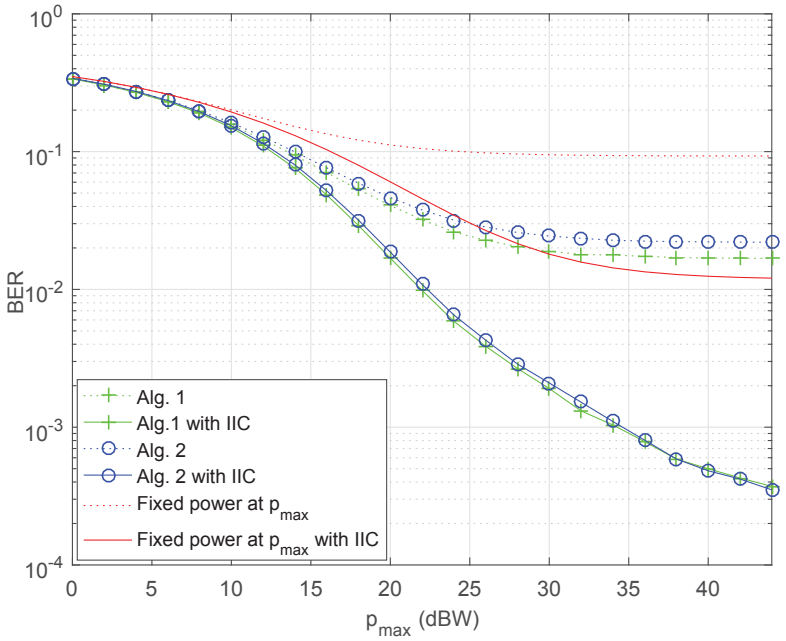

Figure 5.11: BER performance versus maximum available power.

when the IIC is integrated with the two proposed algorithms. A comparison of Alg. 1 and Alg. 2 shows that they have a very similar performance when the IIC is used, however Alg. 1 performs slightly better than Alg. 2 when the IIC is not used.

In conclusion, Alg. 1 exhibited good performance results at all levels of antenna density. The simulation results show that Alg. 1 always provided the greatest transmission power savings, while total system capacity decreased marginally at high $\ddot{M}$ values. Furthermore, the proposed schemes provide a less complex approach, with a performance that equals or even exceeds that of the IIC-based scheme with equal power allocation. In terms of BER performance, all of the proposed algorithms achieved similar results, which can be improved if the IIC is employed.

5.6 Summary

In this chapter, the design and performance analysis of a joint scheduling algorithm and power allocation were presented for uplink MU-MIMO transmissions in a multi-cell topology. The ZF method was used to resolve and cancel completely the intra-cell interference. The CR approach and Newton's method were adopted for the system at hand and applied in the proposed scheduling algorithms in order to reduce the impact of ICI. Newton's method of optimization assisted in the allocation of power among all transmit antennas, with certain power constraints. In addition, the simulation results illustrated that the proposed algorithms scale well with increasing density of antennas/users, resulting in high performance and good power savings. The complexity of the proposed algorithms was also characterized.

Chapter 6

Conclusions and Future Work

The primary objective of this dissertation was to design and implement radio resource management algorithms for the uplink transmission in MU-MIMO systems, with the aim of improving the total system data rate. In this chapter, the dissertation contributions and conclusions are presented in Section 6.1, followed by suggestions for future work related to this field in Section 6.2.

6.1 Dissertation Contributions and Summary

The following are the main contributions of this work:

1. An analysis of ZF-based detection methods is performed for MU-MIMO systems on the uplink in single-cell and multi-cell settings. Because the proposed systems do not require additional processing at the MSs, system complexity is reduced. In addition, a spatial allocation algorithm is integrated into the MU-MIMO system to demonstrate the advantage of performing radio resource and interference management. Specifically, the effects of noise enhancement intrinsic to ZF-type processing are controlled. The systems implemented achieve better sum rate and

BER performance than is the case with conventional systems, as corroborated in the simulations.

2. Three advanced spatial allocation algorithms are proposed for a single-cell environment. The first two algorithms are based on a rate-adaptive approach; the second algorithm adopts a more complex solution to achieve a higher total system sum rate, by including noise enhancement effects as a decision factor. The third algorithm, which is a hybrid rate- and load-adaptive algorithm, provides better buffer management and a higher dispatch rate. Moreover, the water-filling principle for power allocation is employed with all three algorithms to distribute power along the spatial streams, in order to optimize the total sum rate. In particular, in the power allocation and antenna selection strategies, effects are incorporated that are specific to the different signal processing in the detection algorithms.

3. Development and analysis are presented for a proposed uplink MU-MIMO multi-cell system with ZF detection coordinated among the BSs. This is achieved by adopting the CR method and applying it to a limited number of MSs. As a result, a two-layer decoder is introduced, where the first layer performs the MU detection for all signals received at the BS. The second layer implements the diversity combining method at the WC only for signals that are intended to be received via cooperation of the BSs. This helps to reduce the global ICI level, while still maintaining low system complexity. Finally, SIC is integrated with the CR method to reduce ICI effects for signals that are processed jointly, with the objective of attaining higher system capacity.

4. A distributed radio resource management algorithm, which incorporates spatial coordination and a power allocation method, is presented for a multi-cell MU-MIMO system. The antenna selection algorithm utilizes the CR method, where

multiple BSs can select and decode from common transmitting antennas. In addition, Newton's method is employed to help reduce the ICI by (i) allocating an optimum power value to each transmitting user, and (ii) disabling antennas which contribute excessively to interference effects.

The main chapters of this dissertation can be summarized as follows:

Chapter 2 proposes two ZF decoders to perform MU detection for the uplink transmissions in a MU-MIMO system. The two decoders are comprised of ZF as a stand-alone, and ZF integrated with SVD. While neither model requires any MU processing on the MS side, the BS is required to have full CSI in order to perform the spatial de-multiplexing. This work proposes a solution to overcome problems in inverting the matrix ζ_k, which is necessary in order to find a suitable decoder for ZF-SVD. This problem does not occur on the downlink, and the proposed solution is unique to this dissertation. Specifically, the columns of the underlying matrix are manipulated to create a square matrix that is invertible, without affecting the operation or the performance of the system.

A spatial coordination algorithm is developed where the centralized scheduler decides when an antenna should be active or temporarily disabled, based on channel gains. In addition, the scheduler limits the number of active transmitting users, to comply with ZF requirements. When the ZF and ZF-SVD approaches are tested in simulations, the results show no improvement over conventional systems such as the SU-MIMO. However, when the MU-MIMO system is integrated with a spatial coordination algorithm, a saving of 1 dB is achieved at BER $10^{-}3$. In addition, the simulation results show an increase in the total system sum rate.

Chapter 3 introduces three advanced spatial coordination algorithms, where the MU detection performed for all three algorithms is based on the ZF-SVD. When assigning spatial (parallel) channels, the proposed algorithms take into consideration the dependency among the utilized channel gains. Here it was not possible to benefit

from the large body of work concerning resource allocation for OFDMA, as this problem does not occur in OFDMA systems. This is because in OFDMA, each signal is transmitted in a dedicated band without affecting subcarrier gains. The algorithms are divided into multiple stages, where each stage considers a limited number of antennas per MS and analyzes the corresponding effects. The first proposed algorithm (BC-SpG) is the least complex, as it only considers the spatial gains in its decisions; while the second algorithm (BC-SpG/NE) is a more intelligent scheduler that considers channel gains and noise enhancement when selecting the transmitting antennas. The third algorithm (FRLA) integrates the BC-SpG/NE and a load-adaptive algorithm to achieve better control of the MS buffers. In addition, specialized water-filling algorithms are applied for all of the systems developed, in order to allocate the power for all active antennas.

The initial semi-analytical result shows a degradation in system performance when basic ZF detection algorithms are deployed on the uplink, as compared with downlink transmissions. This is due to noise enhancement in ZF uplink detection in MU-MIMO systems, which does not occur in downlink transmissions. The deployment of BC-SpG/NE yields a significant increase in performance, due to the incorporation of noise enhancement effects in the process of selecting antennas in the first stage. The division of the selection process into stages also results in reduced algorithm complexity. The buffer states are analyzed subsequently in the proposed MU-MIMO system with randomly arriving packets. The simulation results show that the FRLA algorithm yields the highest performance in terms of total system throughput. Finally, the proposed algorithm is compared with a brute-force approach for selecting the antennas, in order to illustrate the complexity of the different schemes.

Chapter 4 focuses on developing a system model that is applicable to multi-cell MU-MIMO, with the aim of reducing ICI effects with minimum complexity. This chapter begins by investigating the performance of a double-cell system and creating

a two-layer decoder. The first layer, that affects all MSs, performs MU detection to cancel intra-cell interference fully; this is applied at the BS level. The second layer is executed only on a few received signals, that are intended to be cooperatively received by multiple BSs through the WC. Specifically, the WC performs diversity combining of signals from different BSs, handling common users that do not have reliable reception in the first stage. The inclusion of CR assists in controlling the ICI level for all signals received. Furthermore, the diversity combining method is integrated with the SIC algorithm to achieve further reduction of the ICI.

A spatial coordination algorithm is proposed, which allows multiple BSs to select a common transmitting antenna to utilize the CR method. In addition, the algorithm is designed to be interference-aware, where the scheduler selects the antennas/users that have good channel gains and cause minimum interference effects. The simulation results show good capacity improvement in comparison to other systems that do not utilize the CR method.

Chapter 5 advances the development of the radio resource management algorithm proposed in Chapter 4. This is accomplished by integrating into the scheme from Chapter 4 (i) an optimization algorithm to improve antenna selection, and (ii) an iterative power allocation mechanism. The optimization algorithm employed is Newton's method, which has the advantage of relatively low computational complexity and fast convergence times, as illustrated in [32]. This chapter investigates the best direction function which complements the optimization of the original cost function, and also considers the best initial values that can be used to achieve faster convergence and to avoid local minima. This approach improves the scheduling algorithm by temporarily deactivating a few transmitting antennas that contribute excessively to interference, and by working with MSs that have good channel gains in order to improve the total system sum rate.

Two algorithms are proposed with different levels of cooperative reception and corresponding complexity for distributing different CSI and data over the backhaul links. The simulation results indicate a tradeoff between total system capacity and power savings, however both proposed algorithms show an improvement in performance and complexity in comparison with a competing algorithm.

6.2 Suggested Future Work

In this section, the following related topics are suggested for future research:

1. Imperfect CSI Knowledge

This work depends on the assumption of global CSI availability at the BSs for successful calculation of the ZF decoding matrixes. In addition, instantaneous knowledge of global CSI is considered at the scheduler to ensure proper evaluation of competing MSs and to make decisions based on the spatial gains. However, in real-world applications these assumption are difficult to fulfill due to imperfect estimation of the CSI and continuous changes in channel conditions. Therefore, research is required in order to understand the effects of delay and partial channel estimation.

2. Massive MIMO systems

Massive MIMO systems with a very large number of antennas at the BSs are currently being studied as a potential future solution for wireless transmissions. From a theoretical point of view, the bandwidth efficiency can be increased simply by increasing the array of antennas at the BSs. The proposed work can be implemented in such applications, however, extensive research is required to test the scalability of the algorithms presented here when applied to a massive MIMO model. In addition, interference effects must be carefully investigated,

as ICI levels can be expected to increase substantially due to the large number of transmissions occurring within a multi-cell system.

3. Full Duplex Transmission

This thesis focuses on designing uplink cross-layer resource allocation algorithms. The implemented work is also applicable to the downlink transmission, because the performance of the downlink transmission is mainly dependent upon channel gains. However, special consideration must be given to full duplex mode in terms of performance deterioration due to self-interference and co-channel interference (where the uplink affects the downlink transmission).

4. Creating a Hybrid MU Detector for a Multi-Cell Topology

In a multi-cell environment it was necessary to use ZF as a stand-alone decoder. The ZF-SVD decoding was not used due to the fact that MS signals are received at multiple BSs, and joint channels were not considered from the MSs to multiple BSs. As a result, it was not possible to benefit from performance gains with ZF-SVD decoding at low SNR values. Thus, a hybrid decoder could be investigated that uses both ZF and ZF-SVD, based on the principles developed in Chapter 2.

5. A Resource Allocation Algorithm that Considers Noise Enhancement for Multi-Cell Networks

Due to time limitations, the BC-SpG/NE algorithm proposed in Chapter 3 was not applied to multi-cell environments. The direct application of earlier results could yield improved performance at the expense of high system complexity. Some time could be invested in studying the problem, with the aim of finding a feasible algorithm with minimized complexity. Achieving this would assist in controlling noise enhancement resulting from the MU decoder.

6. Considering Discrete Capacity Performance

In the testing of the results, capacity was presented as a real continuous value based on the Shannon theorem. This is an accepted method in the research field, which helps to give an indication of system performance. However, in real network environments modulation techniques are used, where the data rate achieved is based on a targeted BER and the resulting SNR value. Hence, the proposed system could be tested in a real environment, in order to evaluate the data rate in a discrete manner.

7. Analyzing the MIMO-OFDM Problem

This work focuses on radio resource management and noise enhancement for MU-MIMO models with a single carrier. Most modern wireless communication systems utilize OFDM, such as LTE and IEEE 802.11ac, which is based on the multi-carrier modulation. Thus, this work could be extended to perform radio resource control and optimization for MIMO-OFDM systems that require the inclusion of additional parameters such as subcarrier allocation.

Bibliography

[1] D. Tse and P. Viswanath, *Fundamentals of Wireless Communication*. New York, NY, USA: Cambridge University Press, 2005.

[2] D. Bliss, K. Forsythe, and A. Chan, "MIMO wireless communication," *Linconlan Laboratory Journal*, vol. 15, no. 1, pp. 97–126, 2005.

[3] S. Kumagai and F. Adachi, "Joint Tx/Rx signal processing for uplink distributed antenna network using single-carrier MU-MIMO," in *2015 10th Int. Conf. on Inform., Commun. and Signal Process. (ICICS)*, Singapore, Dec 2015, pp. 1–5.

[4] C. Lim, T. Yoo, B. Clerckx, B. Lee, and B. Shim, "Recent trend of multiuser MIMO in LTE-advanced," *IEEE Commun. Mag.*, vol. 51, no. 3, pp. 127–135, 2013.

[5] Z. Ding, S. Dasgupta, and R. Lopez, "Interference cancellation and blind equalization for linear multi-user systems," in *Proc. IEEE Int. Conf. Acoust. Speech Signal Process., ICASSP '00*, vol. 1, Istanbul, 2000, pp. 145–148.

[6] *IEEE 802.11ac*, IEEE 802.11acTM-2013 Std., 2013.

[7] *LTE*, 3GPP R8 Std., 2008.

[8] R. Liao, B. Bellalta, M. Oliver, and Z. Niu, "MU-MIMO MAC protocols for wireless local area networks: A survey," *IEEE Commun. Surveys Tutorials*, vol. 18, no. 1, pp. 162–183, 2016.

[9] M. Jankiraman, *Space-Time Codes and MIMO Systems*, ser. The Artech house universal personal communications series. Artech House, Incorporated, 2004.

[10] B. Vucetic and J. Yuan, *Space-Time Coding*. Wiley, 2003.

[11] F. R. P. Cavalcanti and S. Andersson, Eds., *Optimizing Wireless Communication Systems*. Springer Publishing, 2009.

[12] K.-h. Lee and C.-k. Kim, "User scheduling for MU-MIMO transmission with active CSI feedback," *EURASIP J. on Wireless Commun. and Networking*, vol. 2015, no. 1, pp. 1–12, 2015. [Online]. Available: http://dx.doi.org/10.1186/s13638-015-0331-4

[13] B. G. Lee, D. Park, and H. Seo, *Wireless Communications Resource Management*. Wiley Publishing, 2008.

[14] L. Choi and R. Murch, "A transmit preprocessing technique for multiuser MIMO systems using a decomposition approach," *IEEE Trans. Wireless Commun.*, vol. 3, no. 1, pp. 20–24, 2004.

[15] W. Liu, L. L. Yang, and L. Hanzo, "SVD-assisted multiuser transmitter and multiuser detector design for MIMO systems," *IEEE Trans. Veh. Technol.*, vol. 58, no. 2, pp. 1016–1021, 2009.

[16] S. Serbetli and A. Yener, "Transceiver optimization for multiuser MIMO systems," *IEEE Trans. Signal Process.*, vol. 52, no. 1, pp. 214–226, 2004.

[17] D. Nguyen and T. Le-Ngoc, Eds., *Wireless Coordinated Multicell Systems: Architectures and Precoding Designs*. SpringerBriefs Publishing, 2014.

[18] L. Venturino, A. Zappone, C. Risi, and S. Buzzi, "Energy-efficient scheduling and power allocation in downlink OFDMA networks with base station coordination," *IEEE Trans. Wireless Commun.*, vol. 14, no. 1, pp. 1–14, Jan 2015.

[19] H. Fattah and H. Alnuweiri, "A load adaptive subcarrier and bit allocation algorithm for non-real time services in an OFDMA system," in *6th Int. Symp. Wireless Communication Systems, ISWCS 2009*, Tuscany, Sept 2009, pp. 642–646.

[20] R. Bujalance, G. Goťmez, D. Morales-Jimeťnez, F. Blaťnquez-Casado, and J. Entrambasaguas, "Performance evaluation of cross-layer scheduling algorithms over MIMO-OFDM," in *5th Int. Conf. Broadband and Biomedical Communications, IB2Com 2010*, Malaga, Dec 2010, pp. 1–5.

[21] D. Choi, D. Lee, and J. H. Lee, "Resource allocation for CoMP with multiuser MIMO-OFDMA," *IEEE Trans on Veh. Technology*, vol. 60, no. 9, pp. 4626–4632, Nov 2011.

[22] E. Yaacoub and Z. Dawy, "A survey on uplink resource allocation in OFDMA wireless networks," *IEEE Commun. Surveys Tutorials*, vol. 14, no. 2, pp. 322–337, Second 2012.

[23] A. Goldsmith, *Wireless Communications*. Cambridge University Press, 2005.

[24] Y.-F. Chen and J.-W. Chen, "A fast subcarrier, bit, and power allocation algorithm for multiuser OFDM-based systems," *IEEE Trans. Veh. Technol.*, vol. 57, no. 2, pp. 873–881, March 2008.

[25] N.-D. Dào and Y. Sun, "User-selection algorithms for multiuser precoding," *IEEE Trans. Veh. Technol.*, Sept 2010.

[26] G. Wunder and C. Zhou, "Queueing analysis for the OFDMA downlink: Throughput regions, delay and exponential backlog bounds," *IEEE Trans. Wireless Commun.*, vol. 8, no. 2, pp. 871–881, Feb 2009.

[27] "Lightweight AP (LAP) registration to a wireless LAN controller (WLC)," Cisco Systems, Inc, Tech. Rep., Sep 2008. [Online]. Available: http://www.cisco.com/c/en/us/support/docs/wireless-mobility/wireless-lan-wlan/70333-lap-registration.pdf

[28] C. Choi, L. Scalia, T. Biermann, and S. Mizuta, "Coordinated multipoint multiuser-MIMO transmissions over backhaul-constrained mobile access networks," in *Personal Indoor and Mobile Radio Commun. (PIMRC), 2011 IEEE 22nd Int. Symp. on*, Toronto, Sept 2011, pp. 1336–1340.

[29] R. Irmer, H. Droste, P. Marsch, M. Grieger, G. Fettweis, G. Fettweis, S. Brueck, H.-P. Mayer, L. Thiele, and V. Jungnickel, "Coordinated multipoint: Concepts, performance, and field trial results," *IEEE Commun. Mag.*, pp. 102–111, 2011.

[30] "Combating interference: MU-MIMO, CoMP, and HetNet," Mitsubishi Electric Research Laboratories, Tech. Rep., Sep 2012.

[31] W. Yu, T. Kwon, and C. Shin, "Multicell coordination via joint scheduling, beamforming and power spectrum adaptation," in *INFOCOM, 2011 Proc. IEEE*, Shanghai, April 2011, pp. 2570–2578.

[32] W. Yu, T. Kwon, and C. Shin, "Joint scheduling and dynamic power spectrum optimization for wireless multicell networks," in *Info. Sci. and Systems (CISS), 2010 44th Annual Conf. on*, Princeton, NJ, March 2010, pp. 1–6.

[33] X. Xu, H. Zhand, and Q. Wang, "Inter-cell interference mitigation for mobile communication system," *Advances in Veh. Networking Technologies*, p. 358, April 2011.

[34] J. Tang, D. K. C. So, E. Alsusa, K. A. Hamdi, and A. Shojaeifard, "Energy efficiency optimization with interference alignment in multi-cell MIMO interfering broadcast channels," *IEEE Trans. Commun.*, vol. 63, no. 7, pp. 2486–2499, July 2015.

[35] J. Niu, D. Lee, T. Su, G. Y. Li, Z. Tang, and Y. Fu, "Multi-cell cooperative scheduling for uplink SC-FDMA systems," in *Personal Indoor and Mobile Radio Commun. (PIMRC), 2013 IEEE 24th Int. Symp. on*, London, Sept 2013, pp. 1582–1586.

[36] B. Gui and L. Cimini, "Bit loading algorithms for cooperative OFDM systems," in *IEEE Military Communications Conf. 2007. MILCOM 2007*, Orlando, FL, Oct 2007, pp. 1–7.

[37] B. O. Lee, O.-S. Shin, and K.-B. Lee, "Uplink user selection scheme for multiuser MIMO systems in a multicell environment," in *IEEE Int. Conf. Commun., 2010. ICC 2010*, Cape Town, May 2010, pp. 1–6.

[38] A. Alyahya and J. Ilow, "Zero-forcing assisted spatial stream allocation in uplink multiuser MIMO systems," in *2015 IEEE 28th Canadian Conf. on Elect. and Comput. Eng. (CCECE)*, Halfiax, May 2015, pp. 1030–1035.

[39] A. Alyahya and J. Ilow, "Spatial stream scheduling in uplink multiuser MIMO systems with zero-forcing post-processing," in *2015 IEEE 14th Canadian Workshop on Inform. Theory (CWIT)*, St. John's, July 2015, pp. 101–105.

[40] A. Alyahya and J. Ilow, "Uplink scheduling in multi-cell MU-MIMO systems with ZF post-processing and diversity combining," in *2015 IEEE 14th Canadian Workshop on Inform. Theory (CWIT)*, St. John's, July 2015, pp. 83–87.

[41] A. Alyahya and J. Ilow, "Short paper : radio resource and interference management in uplink multi-cell MU-MIMO systems with ZF post-processing," in *2015 IEEE Veh. Technology Conf. (VTC Fall)*, Boston, MA, Sept 2015.

[42] A. Alyahya and J. Ilow, "Spatial coordination and resource management for uplink MU-MIMO systems," in *In preparation*.

[43] A. Alyahya and J. Ilow, "Multi-cell coordination of radio resouces in MU-MIMO systems with ZF post-processing," in *Computer comminucatins, submitted in July 2016*.

[44] F. Xiong, *Digital Modulation Techniques*, ser. Artech House telecommunications library. Artech House, 2000.

[45] J. Linnartz, *Narrowband land-mobile radio networks*. Artech House, 1993.

[46] S. Alamouti, "A simple transmit diversity technique for wireless communications," *IEEE J. Sel. Areas Commun.*, vol. 16, no. 8, pp. 1451–1458, 1998.

[47] D. Gesbert, M. Kountouris, R. W. Heath, C.-B. Chae, and T. Sälzer, "Shifting the MIMO paradigm - from single-user to multiuser communications," *IEEE Signal Proc. Mag.*, no. 9, pp. 36–46, 2007.

[48] E. Lee and D. Messerschmitt, *Digital Communications*. Kluwer Academic Publishers, 1992.

[49] H. Li, "On the performance of multicell MU-MIMO uplink transmission scheme based on SVD," in *2nd Int Conf. on Future Comput. and Commun. (ICFCC)*, vol. 2, Wuhan, 2010, pp. V2–183–V2–186.

[50] J. Litva and T. K. Lo, *Digital Beamforming in Wireless Communications*, 1st ed. Norwood, MA, USA: Artech House, Inc., 1996.

[51] "Linear processing for multiple antennas: Beam-steering," 2007, course notes for EE 7950, Alberta University.

[52] D. K. Borah, R. A. Kennedy, and I. Fijalkow, "Effects of colored noise on the performance of linear equalizers," in *Acoustics, Speech, and Signal Processing, 1999. Proceedings., 1999 IEEE International Conference on*, vol. 5, Phoenix, AZ, 1999, pp. 2479–2482 vol.5.

[53] M. Torabzadeh and W. Ajib, "Packet scheduling and fairness for multiuser MIMO systems," *IEEE Trans. Veh. Technol.*, vol. 59, no. 3, pp. 1330–1340, March 2010.

[54] C.-X. Zhong and L.-X. Yang, "Cross-layer scheduling and dynamic resource allocation for downlink multiuser MIMO systems with limited feedback," in *Int. Workshop Cross Layer Design, 2007. IWCLD '07*, Jinan, Sept 2007, pp. 1–4.

[55] A. Alyahya and J. Ilow, "Power allocation in cooperative space-time coded wireless relay networks," in *Veh. Tech. Conference (VTC Fall), 2012 IEEE*, Quebec City, Sept 2012, pp. 1–5.

[56] L. Zhou and W. Yu, "Uplink multicell processing with limited backhaul via per-base-station successive interference cancellation," *IEEE J. on Sel. Areas Commun.*, vol. 31, no. 10, pp. 1981–1993, October 2013.